Titre: Title:	Reliable Cognitive Ultra Wideband Communication Systems Under Coexistence Constraints
Auteur: Author:	Farshad Sarabchi
Date:	2014
Type:	Mémoire ou thèse / Dissertation or Thesis
Référence: Citation:	Sarabchi, F. (2014). Reliable Cognitive Ultra Wideband Communication Systems Under Coexistence Constraints [Thèse de doctorat, École Polytechnique de Montréal]. PolyPublie. https://publications.polymtl.ca/1550/

UNIVERSITÉ DE MONTRÉAL

RELIABLE COGNITIVE ULTRA WIDEBAND COMMUNICATION SYSTEMS UNDER COEXISTENCE CONSTRAINTS

FARSHAD SARABCHI
DÉPARTEMENT DE GÉNIE ÉLECTRIQUE
ÉCOLE POLYTECHNIQUE DE MONTRÉAL

THÈSE PRÉSENTÉE EN VUE DE L'OBTENTION
DU DIPLÔME DE PHILOSOPHIÆ DOCTOR
(GÉNIE ÉLECTRIQUE)
AOÛT 2014

UNIVERSITÉ DE MONTRÉAL

ÉCOLE POLYTECHNIQUE DE MONTRÉAL

Cette thèse intitulée :

RELIABLE COGNITIVE ULTRA WIDEBAND COMMUNICATION SYSTEMS UNDER COEXISTENCE CONSTRAINTS

présentée par : SARABCHI Farshad
en vue de l'obtention du diplôme de : Philosophiæ Doctor
a été dûment acceptée par le jury d'examen constitué de :

M. WU Ke, Ph.D., président
M. NERGUIZIAN Chahé, Ph.D., membre et directeur de recherche
M. CARDINAL Christian, Ph.D., membre
M. TATU Serioja, Ph.D., membre

DEDICATION

To my wife
for her endless love and support.

ACKNOWLEDGMENTS

Many people has contributed to the completion of this dissertation and I would like to convey my sincere gratitude to all of them. First and foremost, I would like to take this opportunity to express my gratitude to my supervisor, Professor Chahé Nerguizian, for providing the constant encouragement, supervision and support in overcoming the challenges I faced during my Ph.D. studies. His optimistic look into life and positive thinking always motivated me. I would also like to thank the members of my thesis jury, Prof. Ke Wu and Prof. Christian Cardinal from École Polytechnique de Montréal and Prof. Serioja Tatu from National Institute of Scientific Research (INRS), for the time and effort they have put forth and the feedback they have provided.

I am also thankful to all my colleagues at the Poly-Grames Research Center at the École Polytechnique de Montréal, for creating a pleasant and stimulating environment for research. It will be a long list of all my friends in Montreal to whom I owe for always being there for me. However, particularly, I will always be indebted to Mani Tousi who was always willing to help, support and give his best suggestions.

I would like to thank my parents for their unconditional love, continual support and encouragement throughout my entire life. I am deeply indebted to them for every success I have ever achieved. I would like to send a heartfelt acknowledgement to my Family-in-law for the support and love I received from them.

Last but not least, my heart full of profound feeling of gratitude and appreciation goes to the wonderful woman of my life, Shabnam, my wife and my best friend. She gave me support and help, discussed ideas and prevented several wrong turns. Truly, I could not have done it without her.

RÉSUMÉ

La croissance rapide des systèmes de communication sans fil et la rareté du spectre ont motivé les industries et les fournisseurs ouvrant dans le domaine de communication sans fil de développer des stratégies et des technologies de communication qui peuvent utiliser efficacement les ressources spectrales. La réutilisation pacifique du spectre sous-licence et sous-utilisé peut être une solution prometteuse pour certaines initiatives en cours telles que la communication mobile à haut débit, la communication machine-à-machine, et la connectivité WiFi. Un des plus gros facteurs qui empêche l'approche de cette réutilisation de fréquences est l'effet d'environnements bruyants sur les dispositifs coexistent dans la même bande de fréquence. Par conséquent, la demande pour une stratégie de coexistence pacifique entre les utilisateurs du spectre, des défis et des questions techniques qu'elle engêndre, motive notre recherche. Il est à noter que dans cette thèse, nous considérons un système pratique appelé MB-OFDM UWB (en anglais multiband orthogonal frequency division multiplexing ultra wideband) pour donner un aperçu pratique de ce concept.

Pour atteindre cet objectif, d'abord nous examinons le problème d'interférence des utilisateurs secondaires sur les utilisateurs principaux. A cet effet, tenant compte d'un système secondaire OFDM, nous proposons des méthodes de mise en forme du spectre pour les applications de transmission à antennes simples et multiples. Nous présentons une technique débit-efficace nommé "enhanced active interference cancellation (E-AIC)" qui est en effet capable de créer des encoches ayant des caractéristiques flexibles. Afin de résoudre le problème de dépassement du spectre causé pas la technique classique-AIC, nous utilisons une approche multi-contraintes qui à son tour cause un problème multi-contrainte de minimisation (en anglais multi-constraint minimization problem, MCMP). Cependant, un nouvel algorithme itératif basé sur la technique SVD (en anglais singular value decomposition) est proposé, permettant ainsi de réduire la complexité de la solution de MCMP. Les résultats de simulation obtenus montrent que la technique E-AIC proposée fournit de meilleures performances en termes de suppression des lobes latéraux avec 0 dB de dépassement, moins de complexité de calcul et moins de perte de débit par rapport aux méthodes AIC précédentes. Quant aux antennes multiples, nous proposons deux nouvelles techniques AIC, qui utilisent l'idée principale des approches de sélection d'antennes d'émission (en anglais transmit antenna selection, TAS). Bien que les résultats montrent que les deux techniques permettent la création d'encoche identique, la technique per-tone TAS-AIC a la plus grande efficacité spectrale.

Après avoir obtenu une emission sans interférence pour le système MB-OFDM UWB, nous analysons, modélisons et atténuons le bruit impulsif au récepteur MB-OFDM UWB. Pour ce

faire, d'abord, nous proposons un cadre analytique qui décrit les principales caractéristiques d'interférence d'un système à ultra large bande et saut temporel (en anglais time-hopping UWB, TH-UWB) niveau de ces paramètres de signalisation. Les résultats montrent que la distribution d'interférence dépend fortement aux paramètres de saut temporel du système TH-UWB. Afin de modéliser le signal d'interférence TH-UWB, les distributions gaussienne généralisée et symmetric-α-stable (SαS) sont adoptées, dans lesquelles les paramètres sont estimés en utilisant la méthode du maximum de vraisemblance et une technique de type de régression basée sur la fonction caractéristique, respectivement. En outre, nous analysons la performance exacte d'un système MB-OFDM altéré par un système TH-UWB dans un cadre général. La comparaison de la performance analytique, la simulation empirique et les résultats d'approximation montre que les deux méthodes d'approximation sont valables pour tous les rapports interférence sur bruit (en anglais interference to noise ratio, INR), alors que SαS fournit une approximation plus précise pour une grande valeur de INR.

Ensuite, nous présentons une technique d'atténuation des interférences impulsives pour les systèmes de communication OFDM qui sont robustes et fiables sur des canaux câblés et sans fil. En effet, selon la simplicité et l'efficacité de la technique de suppression de non-linéarité, nous proposons une version améliorée de la technique de suppression pour faire face aux effets nuisibles de sa caractéristique non-linéaire. Par conséquent, une technique d'annulation d'interférence itérative sérielle est proposée pour reconstruire ICI (en anglais intercarrier interference) et soustraire du signal reçu dans le domaine fréquentiel. Afin d'améliorer les performances de la technique de réduction d'interférences proposée, nous présentons une nouvelle technique pour trier les sous-porteuses reçues selon la contribution des résultats de l'interférence. Les résultats de simulation montrent que l'amélioration proposée dans la méthode de suppression, diminue l'erreur de manière significative.

ABSTRACT

The rapid growth of wireless communication systems along with the radio spectrum's scarcity and regulatory considerations have put the onus on the wireless industries and service providers to develop wireless communication strategies and technologies that can efficiently utilize the spectral resources. Hence, peaceful reuse of underutilized licensed radio frequencies (by secondary users) can be a promising solution for some ongoing initiatives such as mobile broadband, machine to machine applications and WiFi connectivity. One of the biggest factor that prevents the spectrum reusing approach to effectively address the spectrum scarcity, is noisy environments result from coexistence of different devices in the same frequency band. Therefore, the request for a peaceful coexistence strategy between spectrum users which leads to various challenges and technical issues, motivates our research. It is worth noting that, in this thesis, we consider a practical system called multiband orthogonal frequency division multiplexing ultra wideband (MB-OFDM UWB) as an underlay system to provide a practical insight into this concept. However, all the obtained results and contributions are applicable to other OFDM-based communication systems.

Towards this goal, we first investigate the problem of the interference from secondary users to the primary users. For this purpose, considering an OFDM-based secondary communication system, we propose spectrum shaping methods for single and multiple transmit antennas applications. For single antenna scenario, we present a throughput-efficient enhanced active interference cancellation (E-AIC) technique which is indeed capable of creating notches with flexible characteristics. In order to address the spectrum overshoot problem of conventional-AIC techniques, we employed a multi-constraint approach which leads to a multi-constraint minimization problem (MCMP). Hence, a novel iterative singular value decomposition (SVD) based algorithm is proposed to reduce the complexity of the MCMP's solution. The obtained simulation results show that the proposed enhanced-AIC technique provides higher performance in terms of sidelobes suppression with 0 dB overshoot, less computational complexity and less throughput-loss compared to previous constrained-AIC methods. For multiple transmit antennas, we propose two novel AIC techniques employing main ideas behind bulk and per-tone transmit antenna selection (TAS) approaches. Simulation results show that although both techniques provide identical notch creation, the per-tone TAS-AIC technique has higher spectral efficiency.

After securing a non-interfering transmission for the MB-OFDM UWB system, we stepped towards analyzing, modeling and mitigating the interference from other systems on the receiver of the MB-OFDM UWB system. As a practical scenario we consider an inter-network

interference (INI) from a time-hopping ultra-wideband (TH-UWB) to a MB-OFDM UWB systems which indeed has an impulsive nature. To do so, first, we provide an analytical framework which describes key features of the TH-UWB interference in the context of its time-hopping signaling parameters. The obtained results show that the interference distribution highly depends on the time-hopping parameters of the TH-UWB system. In order to model the INI interference signal, the generalized Gaussian (GG) and the Symmetric-α-Stable (SαS) distributions are adopted, where their parameters are estimated employing the maximum likelihood and a characteristic function-based regression-type techniques, respectively. Furthermore, we present an exact performance of a MB-OFDM system impaired by a TH-UWB system in a general framework. The comparison of the analytical performance, the empirical simulation and the approximation results show that both approximation methods are valid for low interference-to-noise-ratio (INR), while SαS provides a more accurate approximation for high INR.

Then, we aim at presenting an impulsive interference mitigation technique for robust and reliable OFDM-based communication systems over wired and wireless channels. According to simplicity and efficiency of the blanking nonlinearity method, we indeed propose an enhanced version of the blanking technique to address the detrimental effects of its nonlinear characteristic. Hence, an iterative serial interference cancellation technique is proposed to reconstruct intercarrier interference and subtract from received signal in frequency domain. Toward improving the performance of the proposed interference mitigation technique, we present a new ordering metric to sort received subcarriers according to the contribution of the intercarrier interference results from nonlinear characteristic of the blanking. Simulation results show that the proposed enhancement in blanking method significantly decreases the level of error floors.

TABLE OF CONTENTS

DEDICATION iii

ACKNOWLEDGMENTS iv

RÉSUMÉ v

ABSTRACT vii

TABLE OF CONTENTS ix

LIST OF FIGURES xii

LIST OF APPENDICES xv

LIST OF ABREVIATIONS AND NOTATIONS xvi

CHAPTER 1 INTRODUCTION 1
- 1.1 UWB Technology 3
- 1.2 Unlicensed Spectrum Sharing Challenges 3
- 1.3 Spectrum Shaping and sidelobe suppression 6
- 1.4 Non-Gaussian Interference Analysis 8
  - 1.4.1 Interference in UWB networks 9
  - 1.4.2 Mathematical Descriptions of Non-Gaussian Noise 9
- 1.5 Non-Gaussian Interference Cancellation 12
- 1.6 Motivations, Objectives, Contributions and Organization of the Thesis 15
  - 1.6.1 Motivations and Objectives 15
  - 1.6.2 Contributions and Organization of the Thesis 15

CHAPTER 2 ARTICLE 1: ENHANCED ACTIVE INTERFERENCE CANCELLATION TECHNIQUE FOR OFDM-BASED COGNITIVE RADIO: SINGLE & MULTIPLE TRANSMIT ANTENNAS APPLICATIONS 19
- 2.1 Abstract 19
- 2.2 Introduction 19
- 2.3 System Model 22
- 2.4 Enhanced AIC for SISO System 24

2.5 Enhanced AIC for MIMO System . . . 28
2.5.1 Bulk TAS-AIC Technique . . . 29
2.5.2 Pre-tone TAS-AIC Technique . . . 32
2.6 Simulation Results . . . 33
2.6.1 Enhancement in terms of Overshoot Reduction and Channel Consideration . . . 34
2.6.2 Enhancement in terms of Notch Characteristics . . . 36
2.6.3 E-AIC for CR System with Multiple Transmit Antennas . . . 39
2.7 Conclusion . . . 42

CHAPTER 3 Article 2: IMPACT OF TH-UWB INTERFERENCE SIGNALS ON MB-OFDM UWB SYSTEMS: INTERFERENCE MODELING AND PERFORMANCE ANALYSIS . . . 44
3.1 abstract . . . 44
3.2 Introduction . . . 45
3.3 System Model . . . 47
3.3.1 MB-OFDM UWB Signal Model . . . 47
3.3.2 TH-UWB Signal Model . . . 47
3.3.3 Receiver Processing and Channel Models . . . 48
3.4 Interference Analysis and Modeling . . . 50
3.4.1 Interference characterization . . . 51
3.4.2 Interference Modeling . . . 53
3.4.3 Simulation Results for Interference Modeling . . . 58
3.5 Performance Analysis . . . 63
3.6 Numerical and Simulation Results . . . 66
3.7 Conclusion . . . 70

CHAPTER 4 ARTICLE 3: IMPULSIVE NOISE MITIGATION FOR OFDM-BASED SYSTEMS USING ENHANCED BLANKING NONLINEARITY . . . 71
4.1 abstract . . . 71
4.2 Introduction . . . 71
4.3 System Model . . . 74
4.3.1 Impulsive Noise Model . . . 75
4.3.2 Blanking Nonlinearity . . . 76
4.4 Frequency Domain Interference Canceller . . . 77
4.4.1 Iterative Parallel Interference Cancellation (IPIC) . . . 78
4.4.2 Iterative Serial Interference Cancellation (ISIC) . . . 79

4.5 Simulation Results 82
4.6 Conclusion 86

CHAPTER 5 GENERAL DISCUSSION 88

CHAPTER 6 CONCLUSIONS AND FUTURE WORKS 91
6.1 Conclusions 91
6.2 Future Works 93

REFERENCES 95

APPENDICES 102

LIST OF FIGURES

Figure 1.1 The potential interferences between secondary and primary users . . . 5
Figure 1.2 FCC spectral mask for indoor and outdoor UWB systems [2]. 6
Figure 1.3 Frequency band plan of MB-OFDM UWB systems [7]. 7
Figure 1.4 Symmetric α-stable probability density functions which can be used to model different empirical data samples, from high impulsive $\alpha = 0.5$ to low impulsive $\alpha = 1.5$ as well as zero and non-zero skewness parameter, β. 11
Figure 1.5 Generalized Gaussian distribution probability density functions where $\sigma^2 = 1$ and $\mu = 0$. 13
Figure 2.1 The main concept behind the AIC method (a) spectral leakage results in from active subcarriers within the null band and (b) the frame structure of the conventional AIC. 23
Figure 2.2 The frame structure of the proposed enhanced AIC technique for single antenna applications. 25
Figure 2.3 The frame structure of the proposed bulk TAS-AIC technique, the AIC tones are sent from i^{th} transmit antenna. 30
Figure 2.4 The frame structure of the proposed per-one TAS-AIC technique, the AIC tones are distributed over subcarriers with the weakest desired channel among all transmit antennas. 32
Figure 2.5 Comparison of the multi- and single-constraint approaches given $N_{Null} = 20$ and $N_{PT} = 6$. 34
Figure 2.6 Effect of power spectrum thresholds on the depth of the created notch, given $N_{Null} = 20$ and $N_{PT} = 6$ 35
Figure 2.7 Performance of the conventional and the enhanced AIC techniques in presence of the fading channel. 36
Figure 2.8 Power spectrum of the output OFDM signal using the E-AIC methods for different value of m, given $N_{Null} = 20$ 37
Figure 2.9 Capability of creating flexible notches (a) The trade-off between the notch depth and the notch width and (b) variation of the depth of the created notch as a function of number of null tones. 38
Figure 2.10 Power spectrum of a OFDM-based CR system using the bulk and the per-tone TAS-AIC techniques for different N_{PT}. 40

Figure 2.11 The depth of the created notch versus the number of transmit antennas for different N_{PT}. 40
Figure 2.12 Throughput loss of the proposed methods versus number of transmit antennas, SNR = 20. 41
Figure 3.1 System Model. 48
Figure 3.2 The symbol structure of a TH-UWB signal. 49
Figure 3.3 Different symbol structures of (a) a MB-OFDM symbol covers multiple TH-UWB frames (b) one TH-UWB frame overlaps with multiple MB-OFDM symbols. 51
Figure 3.4 The symbol structure of (a) a MB-OFDM signal and a TH-UWB signal with $N_{burst} = 8$ and $N_{cbp} = 4$, (b) TH-UWB signals with $N_{cbp} = 4$ and $N_{burst} = \{32, 64\}$ and (c) TH-UWB signals with $N_{burst} = 8$ and $N_{cbp} = \{16, 32\}$. 53
Figure 3.5 Empirical TH-UWB interference signal's pdf plotted with the Gaussian distribution for different time-hoping parameters corresponding to different scenarios. 54
Figure 3.6 A comparison of the pdf and cdf of the interference plus noise signal with GGD and SαS distributions (a) and (b) for INR = 0dB, (c) and (d) for INR = 20dB, respectively. 59
Figure 3.7 Shaping parameter versus interference signal's time-hopping parameters in order to study the effect of the TH-UWB's signaling parameters on the impulsive behaviour of the interference signal (a) p, vs. N_{burst} and (b) p, vs. N_{cpb} for SIR = 10 dB and SNR = 30 dB. 60
Figure 3.8 A comparison of the empirical interference plus noise signal's pdf with GG and SαS distributions considering different interference channel (a) the AWGN, (b) the residential environment with NLOS link and (c) the open outdoor environment with LOS scenario. $N_{cpb} = 32$, $N_{burst} = 32$. 62
Figure 3.9 BER versus SNR for MB-OFDM UWB system impaired by a TH-UWB signal. Lines, markers and solid lines represent empirical, exact and approximation simulation results, respectively. $N_{cpb} = 32$, $N_{burst} = 32$. . 67
Figure 3.10 BER versus SNR for different interference channel, $N_{cpb} = 16$, $N_{burst} = 16$ and SIR = 10 dB. 67
Figure 3.11 BER versus SNR for MB-OFDM UWB system impaired by a TH-UWB signal. Lines and markers represent empirical and SαS approximation simulation results, respectively. 69

Figure 3.12 BER versus $\{N_{cpb}, N_{burst}\}$ for MB-OFDM UWB system impaired by a TH-UWB signal. SNR = 25 dB and SIR = 10 dB. 69
Figure 4.1 Block diagram of an OFDM system with impulsive noise canceller . . . 77
Figure 4.2 Block diagram of an OFDM receiver with the blanking and the IPIC block. 78
Figure 4.3 Block diagram of an OFDM receiver with the blanking and the proposed ISIC block. 79
Figure 4.4 Real part of (a) the transmitted and the received modulated symbols, (b) the inter-carrier interference, (c) the two proposed ordering metrics. 80
Figure 4.5 Performance comparison of B-OFDM and PIC-OFDM with proposed ISIC-OFDM considering p = 0.8. 83
Figure 4.6 BER vs. threshold of PIC-OFDM and ISIC-OFDM for various number of iterations, considering p = 0.8. 84
Figure 4.7 Performance comparison of B-OFDM and PIC-OFDM with ISIC-OFDM for various impulsive noises. 85
Figure 4.8 BER vs. threshold of ISIC-OFDM for various noise environment. 86

LIST OF APENDICES

Appendix A NOISE AND ICI VARIANCES CALCULATION 102

LIST OF ABREVIATIONS AND NOTATIONS

Abbreviations

AIC	Active Interference Cancellation
AST	Adaptive symbol transition
AWGN	Additive White Gaussian Noise
BER	Bit Error Rate
BG	Bernoulli-Gaussian
BPPM	Binary Pulse Position Modulation
BPSK	Binary Phase Shift Keying
C - AIC	Conventional Active Interference Cancellation
CCI	Co-Channel Interference
cdf	Characteristic Distribution Function
CM	Channel Model
CR	Cognitive Radio
DFT	Discrete Fourier Transform
DS	Direct-Sequence
DS-UWB	Direct-Sequence Ultra-Wideband
E-AIC	Enhanced Active Interference Cancellation
ECMA	European Computer Manufacturers Association
ED	Euclidean
FCC	Federal Communications Commission
FF	Frequency-Flat
FFT	Fast Fourier Transform
GA	Gaussian Approximation
GCQ	Gauss-Chebyshev Quadrature
GG	generalized Gaussian
GGD	Generalized Gaussian Distribution
GLM	Gaussian-Laplacian Mixture
GMN	Gaussian Mixture Noise
ICI	Inter-Carrier Interference
IEEE	Institute of Electrical and Electronic Engineers
IFFT	Inverse Fast Fourier Transform
i.i.d.	Independent, Identically Distributed
INI	Inter-Network Interference

INR	Interference-to-Noise-Ratio
IPN	Interference-Plus-Noise
IR	Impulse Radio
ISIC	Iterative Successive Inter-carrier Interference Cancellation
ISM	Industrial, Scientific and Medical
LOS	Line-of-Sight
MB-OFDM	Multi-Band Orthogonal Frequency Division Multiplexing
MCMP	Multi-Constrained Minimization Problem
MCS	Multiple-choice sequences
MGF	Moment Generating Function
MIMO	Multi Input Multi Output
MISO	Multi Input Single Output
ML	Maximum-Likelihood
M-PAM	M-ary Pulse Amplitude Modulation
M-PSK	M-ary Phase Shift Keying
M-QAM	M-ary Quadrature Amplitude Modulation
MRC	Maximum-Ratio Combining
MUI	Multiple User Interference
NB	Narrowband
NBI	Narrowband Interference
NLOS	Non-Line-of-Sight
NT	null tones
OFDM	Orthogonal Frequency Division Multiplexing
OSIC	Ordered Successive Interference Cancellation
PAM	Pulse Amplitude Modulation
pdf	Probability Density Function
PIC	Parallel Inter-carrier Interference Cancellation
PLC	Power Line Communication
PSD	Power Spectral Density
PT	protection tones
QAM	Quadrature Amplitude Modulation
QPSK	Quaternary Phase Shift Keying
SU	Primary User
SW	Subcarrier weighting
SBL	Sparse Bayesian learning
SC	Single-Carrier

SCMP	Single-Constrained Minimization Problem
SIC	Inter-carrier Interference Cancellation
SINR	Signal -to-Interference plus Noise Ratio
SIR	Signal-to-Interference Ratio
SNR	Signal-to–Noise Ratio
SRRC	Square-Root Raised Cosine
SVD	Singular value decomposition
SU	Secondary User
TAS	Transmit Antenna Selection
TFC	Time-Frequency Code
TG	Task Groups
TH-UWB	Time-Hopping Ultra-Wideband
UNII	Unlicensed National Information Infrastructure
UWB	Ultra-Wideband
WiMAX	Worldwide Interoperability for Microwave Access
WLAN	Wireless Local Area Network
WMAN	Wireless Metropolitan Area Network
WPAN	Wireless Personal Area Network

Notation

$\mathbf{X}$	Matrices or Frequency-domain vectors
$\mathbf{x}$	Vectors
$(\cdot)^*$	Complex conjugate
$[\cdot]^T$	Transpose
$[\cdot]^H$	Hermitian transpose
$\otimes$	Convolution operator
$\lfloor \cdot \rfloor$	Floor function
$\lceil \cdot \rceil$	Ceiling function
$\|.\|$	Absolute value of a complex number
$\|\| \cdot \|\|$	The ℓ_2 vector norm
$\det(\cdot)$	Matrix determinant
diag($\mathbf{x}$)	The main diagonal elements of the matrix $\mathbf{X}$
off-diag($\mathbf{x}$)	The off diagonal elements of the matrix $\mathbf{X}$
$\Re\{\cdot\}$	The real part of a complex number
$\Im\{\cdot\}$	The imaginary part of a complex number
$\mathbb{E}(\cdot)$	Statistical expectation
$\Pr\{\cdot\}$	The probability of an event
$Q(x)$	Gaussian Q-function, $Q(x) \triangleq \frac{1}{2\pi} \int_0^\infty e^{-t^2/2} \mathrm{d}t$
$\Gamma(x)$	Gamma function, $\Gamma(x) \triangleq \int_x^\infty e^{-t} t^{x-1} \mathrm{d}t$

CHAPTER 1

INTRODUCTION

The rapid growth of wireless communication systems has made the radio spectrum a precious resource and allocation the spectrum tremendously difficult. Therefore, spectrum assignment is of great importance for wireless industries and service providers. The primary method of spectrum allocation is to issue a license for a specific application (primary user, PU), which provides the primary user with an exclusive access to a part of the radio spectrum. Thus, if the primary user switches to an idle mode, the radio spectrum which is permanently assigned to this user, remains unused. In fact, it leads to inefficient radio spectrum utilization. Since, large parts of the radio spectrum have been allocated for an exclusive usage of licensed users, for future applications, telecommunication industries and regulation bodies face a spectrum scarcity problem. Hence, the efficient utilization and sharing the highest possible of the available radio spectrum is one of the major issues to be solved due to the presence of different types of wireless devices that requires innovative technologies.

In order to increase the spectrum usage efficiency, another spectrum allocation method is a peaceful reuse of underutilized licensed radio frequencies by secondary users (SU) without generating harmful interference to primary users. In fact, secondary users may share unlicensed spectrum according to certain technical regulations which allow the peaceful coexistence of primary and secondary users. Therefore, unlicensed spectrum allocation methods enable more efficient spectrum utilization by allowing different users to share the spectral resources. Consequently, both academia and industry have been motivated to improve the employment method of radio spectrum with a particular interest in unlicensed reuse of already licensed spectrum in order to increase spectrum efficiency.

There are two main methods for implementing the unlicensed spectrum sharing approach which are underlay and overlay access to the radio spectrum. In the underlay approach, a secondary user may share a licensed radio frequency band with active primary users as long as it does not interfere with them. The underlay spectrum utilization has been successfully exploited by some of the Federal Communication Commission (FCC) regulations such as the Unlicensed National Information Infrastructure (UNII) radio band, Industrial, Scientific and Medical (ISM) radio band and Ultra-WideBand (UWB). The UNII radio band in 5 GHz range is introduced by Part 15.401 to 15.407 of the FCC in 1997 as license-free bands for wireless LAN applications [1]. The ISM band was proposed for industrial, scientific and medical purposes only, however, in recent years it has been used for short-range wireless com-

munication in the 915 MHz, 2.450 GHz, and 5.800 GHz bands [2]. In February 2002, FCC issued first report and order [3] which authorized the commercial and unlicensed deployment of a wide range of radio spectrum for UWB systems. In order to prevent an inference from UWB to other legacy wireless devices, FCC specified a radio spectral mask for both indoor and outdoor applications of UWB in the USA. On the other hand, in overlay mode, a secondary user may utilize a free part of licensed spectrum which is not used by licensed users. Cognitive radio technology [4] is one of the promising solutions to the problem of overlay unlicensed spectrum utilization to opportunistically use the radio spectrum without interfering with licensed users as well as minimizing the spectral congestion via spectrum sharing. It is one of the promising solutions to the problem of unlicensed spectrum utilization as well as minimizing the spectral congestion via spectrum sharing. More information about the CR approach can be found in [5].

Besides higher spectrum efficiency, acceptable system performance and reliability are critical for successful deployment of unlicensed utilization of radio spectrum. Therefore, the proposed systems for unlicensed reuse of radio spectrum must take into account the peaceful coexistence between primary and secondary users as well as secondary users themselves. To do so, secondary users have to be equipped with specific signal processing techniques which not only guarantee limited amount of interference to primary users but also assure a reliable communication in presence of interference signals.

This thesis mainly focuses on the coexistence issues in spectrum sharing paradigm. According to the huge bandwidth of UWB as an underlay system, coexistence issues are one of the main challenges of this technology. Hence in this thesis, in order to implement proposed signal processing algorithms in a practical application, a Multiband Orthogonal Frequency Division Multiplexing (MB-OFDM) UWB system is considered. Specifically, two different spectrum sharing challenges in a MB-OFDM UWB system are investigated. First problem is to mitigate a potential interference from MB-OFDM UWB systems to primary wireless communication systems working in the same frequency band. The other problem is the performance enhancement of MB-OFDM UWB systems in presence of non-Gaussian interference signal. To do so, first, we propose signal processing algorithms in order to control the interference from MB-OFDM UWB system into legacy narrowband wireless communication systems. Second, we provide a comprehensive analysis of the effects of Impulse Radio UWB (IR-UWB) interference on the performance of a MB-OFDM UWB system to model the inter-network interference between MB-OFDM UWB and IR-UWB systems. Finally, a robust receiver is proposed for a MB-OFDM UWB system in presence of the non-Gaussian noise.

This chapter presents an introduction to several main topics discussed throughout this

thesis. In section 1.1 an overview of UWB technology as well as some previous and recent developments in the UWB field are given. In section 1.2, we elaborate on the current status of unlicensed spectrum sharing challenges specifically related to the coexistence of UWB systems and legacy communication systems or other UWB technologies. The most recent works related to the main three parts of this thesis including spectrum shaping, interference analysis and interference cancellation are explained in 1.3, 1.4 and 1.5, respectively. Finally in section 1.6, we present the dissertation's motivations, objectives, contributions and organizations.

1.1 UWB Technology

In the late 1800's, Marconi used short pulse spark-gap signals with ultrawide bandwidth for sending and receiving Morse codes [6]. In fact, due to technical difficulties of the ultrawide operational bandwidth of short pulses, communication industries was not inclined to invest on this technology and other communication systems such as narrowband bandwidths systems drew their interest. However, in the 1960s, UWB system revived in different application such as military radar. In the 1970s, UWB communications became center of interests as carrier-free communication systems. This trend continued in the early 2000s when the commercial use of UWB systems faced political and regulatory obstacles. Finally in 2002, FCC released new regulations allowing the unlicensed operation of UWB systems in the 3.1-10.6 GHz band.

Subsequent to FCC's regulations, IEEE established two task groups (TGs), called TG3a [7] and TG4a [8], under IEEE 802.15 wireless personal area networks (WPANs) working group, for high data-rate communication applications and low data-rate localization and positioning applications, respectively. Among several received proposals for high data-rate applications, TG3a task group narrowed down the proposals to two: multi-band orthogonal frequency division multiplexing [9] and Direct-Sequence UWB (DS-UWB) [10]. However, neither of these proposals was able to achieve the majority vote. Consequently, in 2006 TG3a abandoned the standardization efforts and let marketplace decide the ultimate winner. Later in 2009, MB-OFDM UWB proposal was adopted by the European Computer Manufacturers Association (ECMA) [11]. In task group TG4a, however, a single proposal was chosen which is based on impulse Radio, namely time-hopping UWB (TH-UWB), technology [12].

1.2 Unlicensed Spectrum Sharing Challenges

Although unlicensed reuse of underutilized radio spectrum is one of the promising methods to increase the spectral efficiency of wireless communication systems in near future, the potential interference between secondary and primary users may turn this opportunity into a serious problem. In order to elaborate this fact, as shown in Fig. 1.1, a secondary

network in near vicinity of a primary network (with partial overlap in geographical coverage) is considered. The secondary network consists of devices which are connected to the notebook 1 sharing radio spectrum with other wireless devices in the primary network. While the secondary network shares spectrum with primary users using underlay approach, according to distance between devices, there may be some potential source of interference between secondary and primary users. For instance, the wireless headphone (SU-1) receives interference from the tablet (PU-5) and base station and like wise the wireless camera may interfere (SU-3) with the other tablet (PU-1). Therefore, one of the most important challenges in sharing radio spectrum between licensed and unlicensed devices is providing a reliable and spectrally efficient communication in presence of interference signals.

As mentioned before, in order to investigate the coexistence issues in spectrum sharing approaches, UWB systems which share the radio spectrum as an underlay system with other coexisting devices, including WLAN, various radars, and WiMax are considered in this thesis. Although FCC has been ordered a transmit power limitation on UWB systems (Fig. 1.2) in order to provide some level of protection for legacy wireless communication system, it has been studied [13, 14, 15, 16] that depending on the distance between UWB and primary users, all UWB technologies can turn into a potential source of interference for coexisting narrowband wireless systems which are located in near vicinity of them. Therefore, UWB transmitters must equip with specific signal processing techniques in order to suppress the potential interference to the legacy communication systems. As will be describes in Section 1.3, spectrum sharing is on of the promising signal processing techniques which has been proposed in literature in order to avoid any interference to narrowband systems.

On the other hand, as will be explained in more detail in Section 1.4, UWB systems may receive some interferences from other wireless communication systems as well. Narrowband wireless systems are the well-known source of interference for UWB devices which are widely investigated in the literature. The other potential source of interference is between UWB devices with different technologies which is due to the fact that there is no common standard available for UWB technologies (such as MB-OFDM and IR-UWB). According to the frequency overlap of MB-OFDM and IR-UWB systems, IEEE has raised concern that manufacturers have to consider the coexistence issue between different UWB technologies. In spite of the fact that the effect of the narrowband interference signals on the performance of UWB systems is widely studied, the effect of inter-network interference signals has to be investigated.

Finally, since a secondary user (i.e. UWB system) has to deliver a promised level of quality of service in presence of aforementioned interference signals, it has to be equipped with proper interference cancellation mechanisms. Although there exists a considerable body of literature

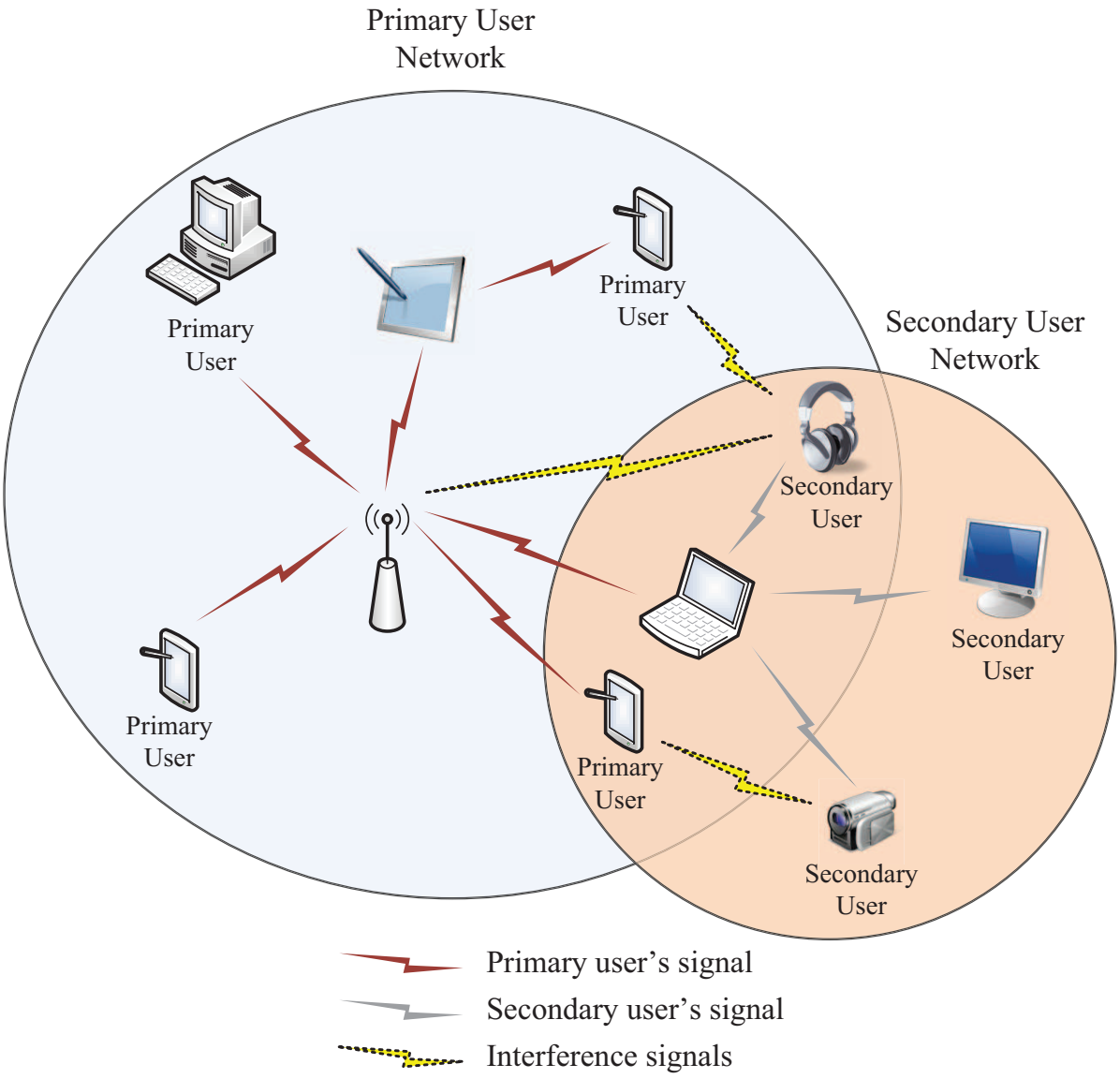

Figure 1.1 The potential interferences between secondary and primary users

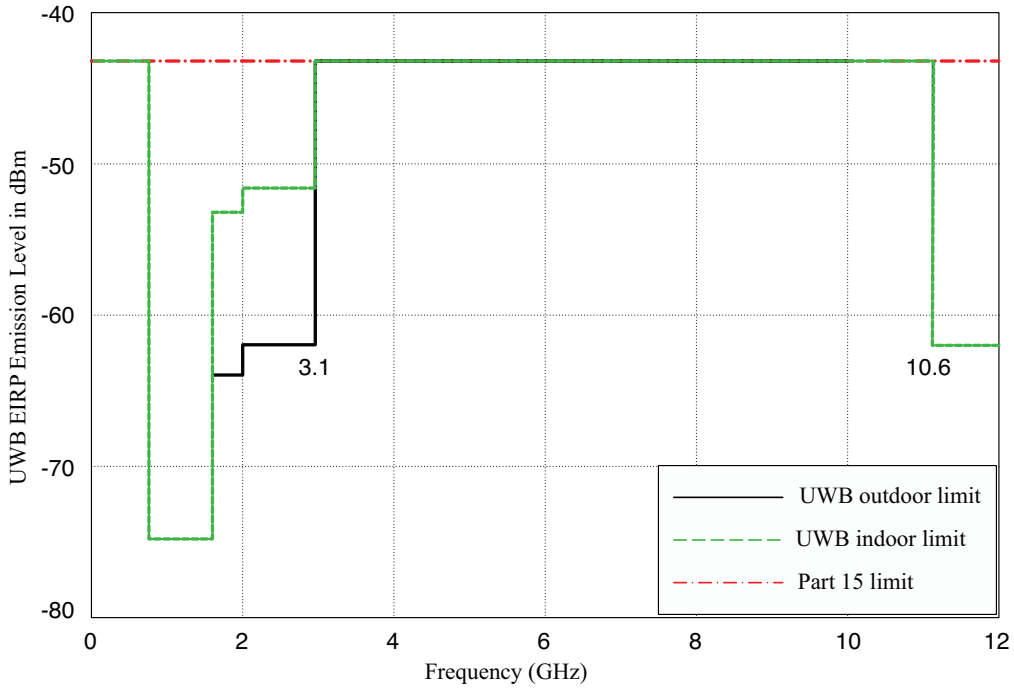

Figure 1.2 FCC spectral mask for indoor and outdoor UWB systems [2].

on interference mitigation for OFDM-based receivers in power line communication and co-channel interferences, impulsive noise cancellation in MB-OFDM UWB system in particular have received very little attention. We discuss relevant literature in Section 1.5.

1.3 Spectrum Shaping and sidelobe suppression

In cognitive radio, interference detection and avoidance are two independent steps that should be fulfilled in order to solve coexistence problem with legacy wireless communication systems. Therefore in order to have a peaceful UWB system, one can use the same techniques employed in the cognitive radio. According to the modulation techniques used in cognitive radio devices, there are several methods that have been presented in literatures for interference avoidance. Since, in MB-OFDM UWB technology, information are sent over different sub-bands using OFDM modulators (Fig. 1.3), band dropping and spectrum shaping are two practical interference mitigation techniques that can be used to tackle the problem of interference to other devices.

In band dropping technique, if the MB-OFDM UWB system detect the presence of a primary user, it jumps to another empty sub-band based on its hopping pattern. In contrast in spectrum shaping methods, the spectrum of the MB-OFDM UWB system is shaped in order to release a part of radio spectrum used by the primary user. Since, band dropping is

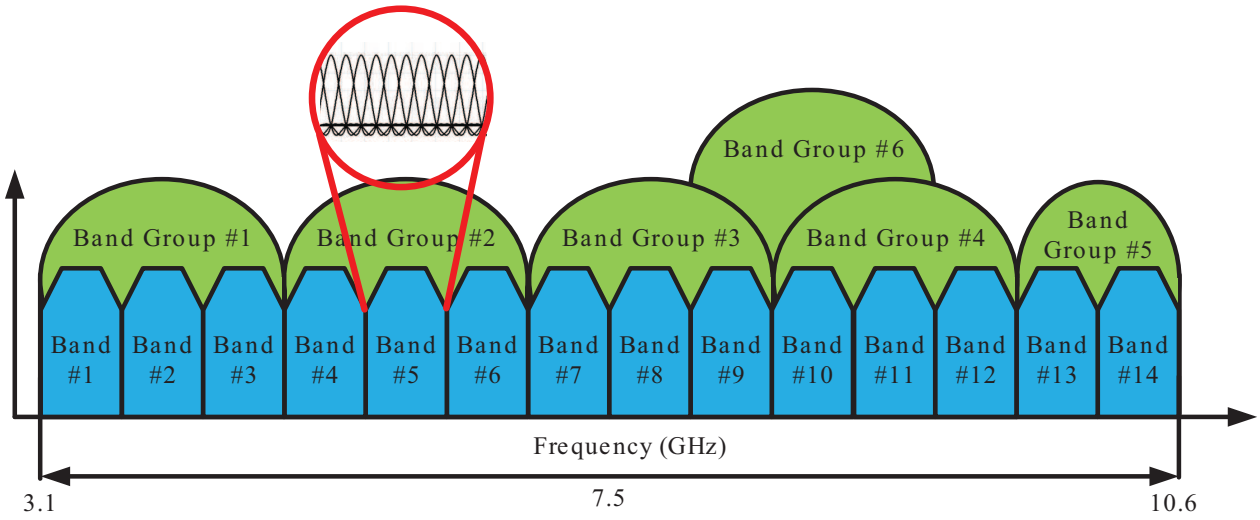

Figure 1.3 Frequency band plan of MB-OFDM UWB systems [7].

not efficient when a large number of UWB systems share radio spectrum with a primary user, in this thesis we considered spectrum shaping approach. The following is a list of proposed spectrum shaping techniques for OFDM-based cognitive radio systems which may be used in UWB systems.

- **Tone nulling technique**: One of the most common techniques for shaping the spectrum of an OFDM signal is to turn off tones which are within the frequency band of the primary user. Although this technique is the easiest way of spectrum shaping, it can generate shallow notch because of the spectral leakage emanating from adjacent non-zero tones. It is obvious that to create a deep notch a large number of tones have to be turned off.
- **Time-domain windowing technique**: Smoothing of the time domain waveform can improve the out-of-band interference of the OFDM signal by controlling the sidelobes effects of subcarriers [17]. However, time-domain windowing technique has an adverse effect on the system throughput due to symbol extension in time.
- **Subcarrier weighting (SW)**: In SW technique, sidelobes of OFDM subcarriers within the null-band are suppressed by weighting all the tones with optimal coefficients to create deeper notch [18].
- **Multiple-choice sequences (MCS)**: In this method, after nulling OFDM subcarriers within the frequency band of primary user, non-zero modulated data symbols are mapped into an optimal sequence with lower sidelobes which leads to a deeper notch [19]. MCS also suffers from system throughput reduction due to the required side information to be transmitted.

- **Adaptive symbol transition (AST)**: In AST method, in order to cancel out the sidelobes in null-band, the duration of an OFDM symbol is extended with the amount of extension calculated by some optimization [20].
- **Active interference cancellation (AIC)**: In AIC, specific tuned subcarriers, called protection tones, are placed in two sides of the null-band in order to suppress the spectral leakage of the active subcarriers [21, 22, 23].

Since AIC algorithm presents the best performance between all these techniques, it is a good candidate for spectrum sharing in OFDM-based cognitive radios as well as MB-OFDM UWB systems. The basic AIC technique which has been proposed by Yamaguchi [21], has some limitations including high complexity, spectrum overshoot, loss of throughput and ignoring the effect of the wireless fading channel. Recently, very few extended versions of the AIC method have been proposed in literature to address these problems, however, none of them has addressed all these problems simultaneously. Therefore, the request for an efficient spectrum shaping technique with low complexity, less throughput reduction and respecting the regulatory spectrum masks motivates the first part of our research.

1.4 Non-Gaussian Interference Analysis

Generally, in ubiquitous communication systems, the behaviour of the environment noise such as thermal noise is modeled with Gaussian distribution. However, in many realistic communication systems, due to the outliers in noise sample (such as high amplitude interferences) the distribution of the noise deviates from Gaussian distribution which is referred to as non-Gaussian interference. Hence, the performance of the conventional systems, which are designed based on the Gaussianity assumption of the environment noise, degrades in presence of the non-Gaussian interference. Impulsive noise has been observed in wired and wireless communication systems. For instance in wireless systems, man-made electromagnetic noise [24], co-channel interference[25], time-hopping ultra-wideband interference [26] and radar clutter are of this kind. As well in wired communication systems such as digital subscriber line and power-line communication systems, noises and interference signals generated from electric motors, silicon-controlled rectifiers, electrostatic dischargers and switching devices have impulsive nature.

Sine in this thesis the UWB networks are considered as practical scenario to investigate the coexistence issues, we next provide an overview of various source of interference in UWB networks. Then we provide a brief description of some common distributions which are used to approximating the behaviour of the non-Gaussian interference for several communication environments.

1.4.1 Interference in UWB networks

As described in Section 1.2, regulatory bodies has ordered power limitations for indoor and outdoor applications of UWB systems. Due to this power limitations, UWB communication systems require sensitive receivers which are highly susceptible to interference from existing systems such as narrowband systems or other UWB devices. In general, interference in UWB networks may be divided into three main types including interference from narrowband wireless systems, multiple user interference (MUI) and inter-network interference (INI). So far, modeling and mitigation of the first two categories of interferences have been conducted in many studies. Several analytical studies have been done concerned with the effects of narrowband interference signals on the performance of UWB systems [27, 28] where it has been shown that this type of interference has Gaussian distribution. The MUI has been also widely investigated in a number of studies using simulations and analytical methods [29, 30, 31, 32]. It has been presented that according to the UWB technologies, the MUI signals can be modeled with Gaussian distribution in DS-UWB networks or non-Gaussian distribution in IR-UWB networks.

However, to the best of our knowledge, very few studies have been reported addressing the issue of inter-network interference between UWB systems employing different transmission techniques [33, 26]. The reasons for this may be traced to the facts that standard bodies have been supposed to take account of coexistence of several UWB devices. In [26], an analytical framework to calculate the asymptotic BER of a bit-interleaved coded-modulation OFDM system impaired by UWB interferences has been proposed. It has been shown that although the interference from DS-UWB systems to the MB-OFDM and IR-UWB systems can be approximated with the Gaussian distribution, the interference from IR-UWB systems to the MB-OFDM systems has impulsive behavior and cannot be modeled with Gaussian distributions.

Therefore, an accurate approximation model of the INI is essential for performance analysis and robust receiver design of a MB-OFDM UWB system impaired by an IR-UWB signal. Since, none of these studies have addressed statistic analysis and modeling of the INI signals, the request for deriving and validating such an approximation model as well as presenting a robust receiver to non-Gaussian noise have motivated the rest of our research.

1.4.2 Mathematical Descriptions of Non-Gaussian Noise

The statistic of various impulsive noises have been analytically or empirically modeled in the literature in order to perform system performance analysis or optimum receiver design. The common distribution for modeling impulsive noises in the wired communication systems

are gated Bernoulli-Gaussian (BG) [34], Gaussian mixture [35] and the Middleton's class A [36]. On the hand, impulsive noises in the wireless communication systems are modeled with the generalized Gaussian (GG) [37], the symmetric α-stable (SαS) [32], the Gaussian-Laplacian mixture [38] and the Gaussian mixture. Throughout this thesis we focus only on two main distributions including the symmetric α-stable and generalized Gaussian distributions.

Symmetric α-Stable Distribution (SαS)

The α-stable distribution is well-suited distribution for modeling impulsive interference signals with heavy-tailed distributions as well as Gaussian noise as a special case. Since SαS distribution can describe the heavy tails and asymmetric behavior of impulsive noises, it has the capability of approximating empirical noises. The SαS distribution is described by its characteristic function (cf) [39]:

$$\phi(w) = \begin{cases} \exp\Big(j\mu w - \sigma^{\alpha}\ |w|^{\alpha}\big[1 - j\text{sign}(w)\beta\tan(\pi\alpha/2)\big]\Big), & \alpha \neq 1 \\ \exp\Big(j\mu w - \sigma^{\alpha}\ |w|^{\alpha}\big[1 + j\text{sign}(w)\beta\log(|w|)\big]\Big), & \alpha = 1 \end{cases} \tag{1.1}$$

where $\alpha \in (0, 2]$, $\beta \in [-1, 1]$, $\mu \in \mathbb{R}$ and $\sigma > 0$ are a characteristic exponent, a skewness, a location and a scale parameters, respectively. The characteristic exponent measures the thickness of the distribution's tails and enables α-stable distribution to model a wide range of impulsive signals. The scale parameter is similar to the variance of the Gaussian distribution and measures the distribution's spread around the location parameter. As illustrated in Fig. 1.4 α-stable distribution can be used to model different noises from high impulsive $\alpha = 0.5$ to low impulsive $\alpha = 1.5$ as well as zero and non-zero skewness parameter, β.

Generalized Gaussian Distribution (GGD)

The generalized Gaussian distribution is a flexible family of distributions which can be use to accurately approximate noise in practical communication systems. The flexibility of GGD in comparison with Gaussian distribution is as a result of an extra parameter (i.e. shaping parameter) that determines the shape of the distribution. The probability density function of the GGD is obtained by generalizing the Gaussian density as following:

$$P_z(z) = \frac{p}{2\Gamma(1/p)A(p,\sigma)} e^{-\left(\frac{|z-\mu|}{A(p,\sigma)}\right)^p} \tag{1.2}$$

where $A(p,\sigma) = \left(\frac{\sigma^2\Gamma(1/p)}{\Gamma(3/p)}\right)^{1/2}$, p, σ^2 and μ are the scale parameter, the shape parameter, the variance and the mean of the GGD, respectively. $\Gamma(x)$ is the Gamma function. The value of p

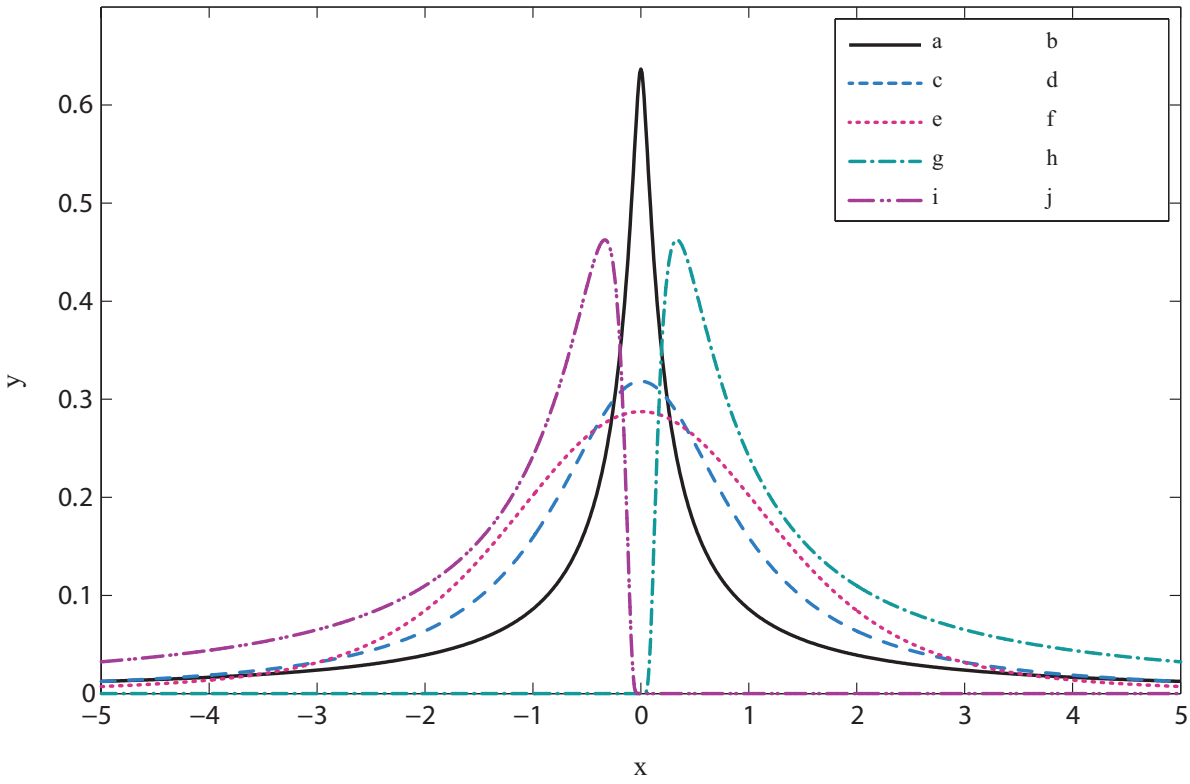

Figure 1.4 Symmetric α-stable probability density functions which can be used to model different empirical data samples, from high impulsive $\alpha = 0.5$ to low impulsive $\alpha = 1.5$ as well as zero and non-zero skewness parameter, β.

determines the degree of impulsiveness of the GGD relative to the Gaussian distribution. The GGD includes standard Gaussian distribution ($p = 2$) and Laplacian distribution ($p = 1$) as two special cases. It is obvious from Fig. 1.5 that as shaping parameter of the generalized Gaussian distribution changes, wide range of non-Gaussian distributions can be covered.

1.5 Non-Gaussian Interference Cancellation

The destructive effect of the impulsive noise on the performance of wired and wireless communication systems is widely investigated in the literature. As mentioned in the previous section, there are several source of impulsive noises including man-made noise [24], co-channel interference[25], time-hopping ultra-wideband interference [26] and radar clutter which have severe impact on the performance of communication systems. Since conventional communication systems are designed to operate in the additive white Gaussian noise, practical wired and wireless communication systems have to employ interference cancellation techniques in order to deliver promised level of quality of service in presence of the non-Gaussian impulsive noises.

There are several interference cancellation techniques reported in the literature according to transceiver technologies. Several adaptive receivers have been proposed for single carrier systems such as IR-UWB systems that obtained superior performance of multiuser interferences (MUI) [29]. Optimum adaptive rake structures have been proposed based on an accurate estimation of the probability density function of the MUI and the MUI-plus-noise [38, 40, 41, 42]. In contrast, it is shown that for moderate impulsive noise power and high numbers of subcarriers, multi-carrier systems are more resilient to the impulsive interference compared to single-carrier systems as it spreads out the impulsive noise signal over all subcarriers. However, in highly impulsive environments or for small value of subcarriers, the OFDM receivers cannot cope with impulsive interference and experience severe performance degradation. Therefore, various parametric and non-parametric interference mitigation techniques have been reported in the literature to improve the performance of OFDM-based systems impaired by non-Gaussian impulsive noises.

In parametric methods, the receiver is designed considering an accurate statistical model of the impulsive noise through estimating the parameters of the noise distribution. As mentioned before, a number of approximation models such as the generalized Gaussian (GG) [37], the symmetric α-stable (SαS) [32], the Gaussian-Laplacian mixture (GLM) [38], the Gaussian mixture [35], the Bernoulli-Gaussian [34] and the Middleton's class A [36] distributions are used to model the statistical characteristics of the impulsive noise in wireless and wired communication systems. In [43] a robust L_p-norm decoding metric has been proposed for

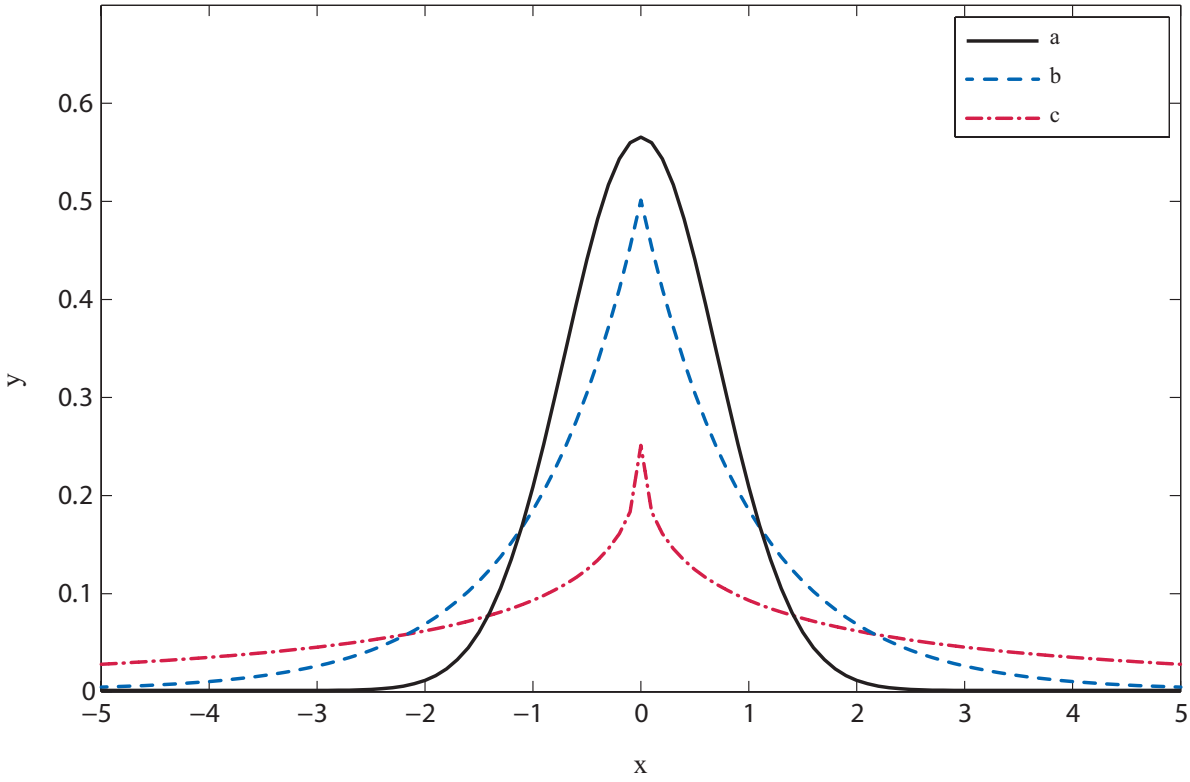

Figure 1.5 Generalized Gaussian distribution probability density functions where $\sigma^2 = 1$ and $\mu = 0$.

the bit-interleaved coded modulation based OFDM system where p is the shaping parameter of the generalized Gaussian distribution used to model the impulsive noise. Pre-filtering methods are other mitigation techniques based on the Alpha-Stable-Symmetric distribution which have been proposed in [44]. Although parametric methods improve the performance of the system by utilizing the interference model, the estimation process requires training overheads and inaccurate parameter estimation results in severe performance degradation.

The other approach is non-parametric methods which do not rely on the knowledge about statistical parameters of the interference signal. Therefore, these types of impulsive interference mitigation techniques are not sensitive to the parameter estimation error. Caire et al. [45] proposed the application of the compressed sensing to mitigate the impulsive noise in OFDM systems by estimating the noise from the null tones of the received signal which was subject to a sufficient recovery condition [46]. Another impulsive noise mitigation technique adopting the block-based compressed sensing was proposed in [47] which has tow different modes including suppression mode (recovery of the support of the non-zero impulsive noise samples) and cancellation (the actual reconstruction of impulsive noise samples). In [46], sparse Bayesian learning (SBL) methods were proposed to mitigate asynchronous sparse impulsive noise in power line communication systems. In this method, SBL techniques have been used to estimate the impulsive noise and subtract it from the received signal. In [48], a frequency domain interference cancellation technique was employed where the impulsive noise is estimated and subtracted from the received signal after the FFT operation process.

The other non-parametric methods which do not require prior knowledge on the statistical noise model are blanking/clipping non-linearity techniques [49, 50]. These are of the efficient impulsive noise mitigation techniques, in which the received signal is compared with a predefined threshold, T, and noise samples with values higher than T are set to zero (blanking) or replaced with a predefined value (clipping). In contrast with abovementioned non-parametric interference mitigation techniques which have high implementation complexity, blanking /clipping non-linearity methods are very simple to implement. However, due to the nonlinear behaviour of the blanking/clipping technique, the orthogonality between the OFDM subcarriers (even for optimum threshold) is destroyed which may cause inter-carrier interference after FFT process. Therefore, in our research, we aim at improving the performance of the blanking non-linearity technique by proposing signal processing algorithms to cancel the inter-carrier interference after FFT process.

1.6 Motivations, Objectives, Contributions and Organization of the Thesis

1.6.1 Motivations and Objectives

As explained in Section 1.2, the coexistence issues between MB-OFDM UWB systems and legacy wireless communication systems as well as UWB systems with different technologies which may be extended to other spectrum sharing approaches and applications, motivated this project. Therefore, the main goal of this thesis is threefold:

- Propose spectrum shaping techniques in order to mitigate the possible interference from MB-OFDM UWB system to the legacy communication systems (Chapter 2).

- Provide an analytical framework that allows us to accurately study and analyze the effect of non-Gaussian noises such as the TH-UWB interference signal on the performance of a MB-OFDM UWB system (Chapter 3).

- Propose a robust MB-OFDM UWB receiver with optimal performance in the presence of non-Gaussian noises (Chapter 4).

To do so, this thesis aims at proposing a MB-OFDM UWB transceiver which incorporates coexistence mechanisms including spectrum shaping and potential interference mitigation techniques. These objectives lead to copping with significant design challenges in achieving the desired spectral efficiency, link reliability, and coverage range of UWB systems.

1.6.2 Contributions and Organization of the Thesis

Based on the aforementioned objectives and methodology, in this thesis, three main problems in spectrum sharing paradigm are chosen to be studied. Notice that we consider a MB-OFDM UWB system as a practical scenario to investigate the coexistence issues, however obtained results and our contributions are applicable to other OFDM-based cognitive radio spectrum sharing techniques.

In **Chapter 2**, we address the issue of mitigating potential interferences from MB-OFDM UWB systems to other wireless communication systems. For this purpose, as mentioned in Section 1.3, the AIC method is considered due to its performance compared to other spectrum shaping techniques. In order to tackle well-known drawbacks of the conventional AIC (C-AIC) method, enhanced versions of the AIC technique with low complexity, less throughput reduction and respecting the regulatory spectrum masks for single and multiple transmit antennas applications are proposed.

Since the non-constrained C-AIC technique suffers from the spectrum overshoot problem, in order to satisfy regulatory issues power constraints are applied to the C-AIC technique. There are two ways of applying power constraints on the protection tones including single constraint on the total power of the protection tones and an individual power constraint for each protection tone. Since the former method results in a notch depth reduction [22], we conduct a study on the later one which leads to a multi-constrained minimization problem (MCMP). Since a solution to the MCMP has high computational complexity, an iterative solution which turns the MCMP into a set of simple least squares problems with single quadratic inequality constraint is proposed. Therefore, the complexity of the constrained AIC technique is reduced without affecting the depth of the created notch. The other downside of the C-AIC are ignoring wireless fading channels and creating inflexible notches. Therefore, the C-AIC algorithm is modified in order to add the capability of controlling the depth and the width of the created notch. To do so, a specific equation which can control the characteristics of the created notch is derived to calculate the spectral leakage of the active subcarriers corresponding to the victim band. Moreover, the optimum value of the protection tones is found considering the effect of the interference fading channel. Since multiple input multiple output (MIMO) are known as a promising technique to enhance the performance, improve the throughput and increase the coverage range of wireless communication systems, in the final part of this chapter two novel spectrum shaping methods for OFDM-based cognitive radio systems with multiple transmit antennas are proposed. For this purpose, the main idea behind the aforementioned AIC-based technique is combined with bulk and per-tone transmit antenna selection (TAS) techniques, in order to increase the throughput of the CR system.

Our simulation results show that the proposed enhanced-AIC technique for single antenna applications provides higher performance in terms of interference mitigation as well as 0dB spectrum overshoot, less computational complexity and less throughput-loss compared to previous constrained-AIC methods. Furthermore, it is illustrated that although both MIMO TAS-AIC techniques provide identical interference reduction, the per-tone TAS-AIC technique has higher spectral efficiency.

In **Chapter 3**, considering an interferer IR-UWB system, we conduct a study of the effect of non-Gaussian interference on the performance of a MB-OFDM UWB system. Although in [26], it was proved that the Gaussian distribution is unable to accurately approximate the TH-UWB interference, they did not propose an accurate approximation method to model the interference signal. Therefore, we present an analytical framework to analyze the statistical characteristics of a TH-UWB interference on a MB-OFDM UWB system. In order to approximate the TH-UWB interference signal, we employ generalized Gaussian and Symmetric-α-Stable distributions which are two of the well-known distributions used for mo-

deling impulsive and heavy-tailed signals. We estimate parameters of the GG and the SαS distributions using the maximum likelihood and a regression-type methods, respectively. We validate the accuracy and tractability of the approximation methods by means of comparison with the probability and cumulative distribution functions of the empirical signal. Our results show that both distributions are accurate for low (interference-to-noise ratio) INR, while SαS provides a more accurate approximation for high INR.

Moreover, using provided analytical framework, the impact of TH-UWB's parameters on the BER of a MB-OFDM UWB system is widely analyzed, where such an analysis is not presently available in the literature. We demonstrate that the BER of a MB-OFDM UWB system depends highly on time-hopping parameters of the interference signal. Furthermore, we investigate the effect of the time-dispersive interference channel on the impulsive behaviour of the TH-UWB. Our simulation results show that while the mild time-dispersive channel does not affect the impulsive behavior of the interference signal, a highly time-dispersive channel may turn an impulsive interference signal into a Gaussian distributed signal.

Besides the interference modeling we provide an analytical BER analysis of a MB-OFDM UWB system impaired by an empirical TH-UWB interference. For this purpose, we first derive the exact moment generating function (MGF) of the IR-UWB interference. Then, we perform an exact analysis of the BER performance of a MB-OFDM UWB, based on the Laplace transform of the MGF of interference signal, AWGN noise and fading channel . Our simulation results show that the empirical simulation, approximation result and analytic analysis are in good agreement.

In **Chapter 4**, we address the issue of performance improvement for a MB-OFDM UWB system impaired by non-Gaussian noises. For this purpose, blanking non-linearity methods is adopted to mitigate the impulsive noise in time domain. As mentioned, the blanking technique suffers from performance loss due to the inter-carrier interference impairment. Therefore, in order to cancel out ICI, we adopt the algorithms of [51] to propose two different impulsive interference cancellation methods.

The basic idea behind these interference cancellation methods is that the possible ICI after FFT processor in frequency domain is reconstructed and subtracted from all the other subcarriers in each OFDM symbols. Therefore, in the first method called parallel inter-carrier interference cancellation (PIC) method, ICI within each OFDM symbol is cancelled out simultaneously. However, a proper initialization is required before ICI reconstruction, and any erroneous ICI reconstruction may cause performance loss. The second proposed method is iterative successive inter-carrier interference cancellation (SIC) method in which the ICI reconstruction and subtraction is done sequentially one subcarrier after another in each OFDM symbol. In order to increase the performance of the ICI cancellation, subcarriers are sorted

according to the measured signal to interference ratio. Therefore, the first subcarrier to be detected has the least ICI compared to the last one. Due to this fact, in contrast to PIC, the ICI reconstruction in SIC is started without any initialization.

Our simulation results show that PIC and SIC inter-carrier interference cancellation methods substantially improve the performance of the non-linearity blanking. However, any error in the initializing step of PIC and the sorting process of SIC can result in severe performance degradation. Furthermore, it is illustrated that SIC perform more effectively compared to PIC due to the fact that in SIC the ICI reconstruction is carried out based on the most reliable subcarrier to the least one which decreases the possibility of error propagation.

Chapter 5 provides a general discussion on the assessment of different aspects of our research, including its motivations, objectives and contributions. Finally, in **Chapter 6** we conclude this thesis with a summary of the results obtained in this dissertation and provide some possible future extensions of this thesis.

CHAPTER 2

ARTICLE 1: ENHANCED ACTIVE INTERFERENCE CANCELLATION TECHNIQUE FOR OFDM-BASED COGNITIVE RADIO: SINGLE & MULTIPLE TRANSMIT ANTENNAS APPLICATIONS

Farshad Sarabchi, and Chahé Nerguizian
Poly-Grames Research Center, Department of Electrical Engineering,
École Polytechnique de Montréal
Montréal, QC, Canada
Submitted to the IEEE Transaction on Wireless Communication on Dec. 2013

2.1 Abstract

Spectrum shaping is of great interest in efficient utilization of the radio spectrum in cognitive radio (CR) systems. One of the most popular spectrum shaping methods used along with the orthogonal frequency division multiplexing (OFDM) is active interference cancellation (AIC). In this paper, enhanced versions of the AIC are proposed for single and multiple transmit antennas applications. For single antenna, our contribution is twofold. First, a throughput-efficient E-AIC is presented which is indeed capable of creating notches with flexible characteristics. Second, a multi-constraint approach is used to address the spectrum overshoot problem of conventional-AIC techniques, which leads to a multi-constraint minimization problem (MCMP). In order to reduce the complexity of the MCMP's solution, a novel iterative SVD-based algorithm is proposed. Simulation results show that the proposed enhanced-AIC (E-AIC) technique provides higher performance in terms of sidelobes suppression with 0dB overshoot, less computational complexity and less throughput-loss compared to previous constrained-AIC methods. For multiple transmit antennas, two novel AIC techniques are proposed based on main ideas behind bulk and per-tone transmit antenna selection (TAS) approaches. Simulation results depict that although both techniques provide identical interference reduction, the per-tone TAS-AIC technique has higher spectral efficiency.

2.2 Introduction

The explosive growth of wireless communication systems has made the radio spectrum a precious resource. Efficient utilization and sharing the highest possible of the available spectrum is one of the major issues to be solved due to the presence of different types of

wireless devices. Consequently, both academia and industry have been motivated to improve the employment method of this spectrum with a particular interest in unlicensed reuse of already licensed spectrum. Cognitive radio (CR) technology is recognized as a solution to opportunistically use the radio spectrum without interfering to licensed users [4]. Hence, in CR networks, secondary (unlicensed) users are equipped with spectrum sensing and spectrum sharing capabilities to employ licensed frequency bands without generating any interference to the primary (licensed) users. To this end, after detecting the presence of the primary user (PU), CR systems have to clear the corresponding frequency band. Therefore, the modulation technique which is used in CR systems needs to have a flexible scheme such that it could be able to shape the spectrum of the transmitted signal.

According to the spectral flexibility of the orthogonal frequency division multiplexing (OFDM), it is an attractive candidate to be used in CR systems. The easiest way of spectrum shaping in OFDM based-CR systems is to turn off the OFDM subcarriers corresponding to the bandwidth of the primary user (i.e. victim band). However, due to the spectral leakage of active subcarriers (originates from sidelobes of active subcarriers), the created notch may not be acceptable to avoid the interference to the primary user. Therefore, in order to solve the out-of-band radiation problem of the OFDM modulation, mitigation techniques may have to be used to fulfill licensing regulations. Several interference mitigation and sidelobes suppression methods have been proposed in the literature including: subcarrier weighting (SW) [18], multiple choice sequences (MCS) [19], adaptive symbol transition (AST) [20] and active interference cancellation (AIC) [21]. Among all proposed mitigation techniques, AIC seems to be of the great interest, due to its high efficiency. In AIC method, some specific subcarriers, called protection tones, are designed and considered in both sides of the victim band such that the abovementioned spectral leakage is cancelled out. However, the AIC technique which has been proposed by Yamaguchi [21], has a few downsides such as high complexity, spectrum overshoot, loss of throughput and ignoring the effect of the wireless fading channel. In order to reduce the complexity and enhance the performance of AIC, an improved AIC technique has been proposed in [22]. In [52] another improved version of AIC has been used to address the spectrum overshoot problem of the protection tones. A new joint time/frequency scheme considering knowledge of the channel is proposed in [53] to study the time/frequency trade-off in AIC and AST methods. In [54], a modified AIC technique considering the effect of ultra wideband channel with the capability of controlling the characteristics of the created notch has been presented. Moreover, some extended versions of the AIC method have been proposed to address the problem of the interference avoidance for OFDM-based cognitive radios with multiple transmit antennas. In [55], an improved AIC algorithm is presented based on jointly optimization of the protection tones over all transmit

antennas. Another extended version of AIC for MIMO application is presented in [56], in which the optimum AIC subcarriers are designed in order to be sent only in one transmit antenna such that the spectral leakage from all active subcarriers of the same antenna and other transmit antennas is cancelled out. In [53] the main idea of the joint time/frequency scheme has been also extended to MIMO applications.

To the best of our knowledge, very few investigations have been reported in the literature addressing the issue of high complexity, spectrum overshoot and data throughput reduction, where none of them has tackled all these problems simultaneously. For instance, in order to solve the problem of the spectrum overshoot two different techniques have been proposed. However, these techniques addresses the spectrum overshoot at the cost of increasing the computational complexity [22] or decreasing the data throughput [52] of the CR system. Therefore, the request for an efficient spectrum shaping technique with low complexity, less throughput reduction and respecting the regulatory spectrum masks for single and multiple transmit antennas applications has motivated our research.

The contribution of this paper is threefold:

- The non-constrained conventional AIC (C-AIC) technique suffers from the spectrum overshoot problem. Since applying single constraint on the total power of the protection tones may result in a notch depth reduction, in [22], individual power constraints are applied to each protection subcarrier. This technique leads to a multi-constrained minimization problem (MCMP), which has a solution with high computational complexity. Therefore, in this paper a new enhanced AIC algorithm is proposed to reduce the complexity of the constrained AIC technique without decreasing the depth of the created notch. In the proposed technique using an iterative method the MCMP is turned into a set of simple least squares problems with single quadratic inequality constraint.

- The conventional AIC algorithm is modified in order to add the capability of controlling the depth and the width of the created notch. To do so, the spectral leakage of the active subcarriers corresponding to the victim band is calculated employing a specific equation which can control the characteristics of the created notch. Moreover, the optimum value of the protection tones is found considering the effect of the interference fading channel.

- Two novel spectrum shaping methods for OFDM-based cognitive radio systems with multiple transmit antennas are proposed. The aforementioned AIC-based technique for single antenna application is combined with the main idea behind the bulk and the per-tone transmit antenna selection (TAS) techniques, in order to increase the throughput of the CR system. In the proposed techniques, a transmit antenna or a subset of subcarriers over all transmit antennas (in bulk and per-tone TAS techniques,

respectively) with the worst interference channel is selected such that the throughput loss of the AIC technique is improved.

The rest of this paper is organized as follows. Section II describes briefly the OFDM-based CR system and the main concept of the conventional AIC method. In section III, the enhanced AIC algorithm for single antenna application is explained. Two new AIC algorithms for a CR system with multiple transmit antennas are proposed in Section IV. Section V presents the simulation results and finally the conclusions are drawn in Section VI.

2.3 System Model

An OFDM-based cognitive radio system (secondary user, SU) and a legacy communication system (primary user, PU) are considered as an interferer and a victim systems, respectively. Except in Section 2.5 where the secondary user's transceiver is considered as multi-input multi-output (MIMO), the PU and SU have single-antenna transceivers. In the CR system, the input bits are mapped to symbols, $\mathbf{X} = [X_l; l \in Z_N]$, using generic modulators such as M-PSK or M-QAM. After serial to parallel conversion, the OFDM subcarriers are modulated using inverse fast Fourier transform (IFFT) module. It is assumed that the cognitive radio system employs an OFDM modulation with N subcarriers. The baseband OFDM signal in the discrete domain, $\mathbf{x} = [x_n; n \in Z_N]$, can be defined as $x_n = \sum_{l=0}^{N-1} X(l) e^{j2\pi \frac{nl}{N}}$, where x_n and X_l denote n^{th} sample of the transmitted OFDM symbol and the data symbol which modulates the l^{th} subcarrier, respectively.

It is assumed that the cognitive radio system is equipped with an spectrum sensing module which detect the presence of the primary user. In presence of a PU system, the secondary user should lower the spectrum of the transmitted signal at the frequency band of the PU (i.e. the victim band) in order to enable a peaceful coexistence. Note that the victim band consists of the overlapping tones from f_l to f_u as the lower and the upper tones of the victim band, respectively. The simplest and the most common way of shaping the spectrum of an OFDM signal is to turn off tones within the victim band. However, because of spectral leakages (Fig. 2.1(a)) originating from adjacent non-zero tones the generated notch is not sufficiently deep. In 2004, Yamaguchi proposed an interference cancellation technique which creates a deeper notch by adding two specific tuned tones (the edge tones) in both sides of the victim band in order to cancel out the aforementioned spectral leakage (Fig. 2.1(b)) [5]. The spectral leakage

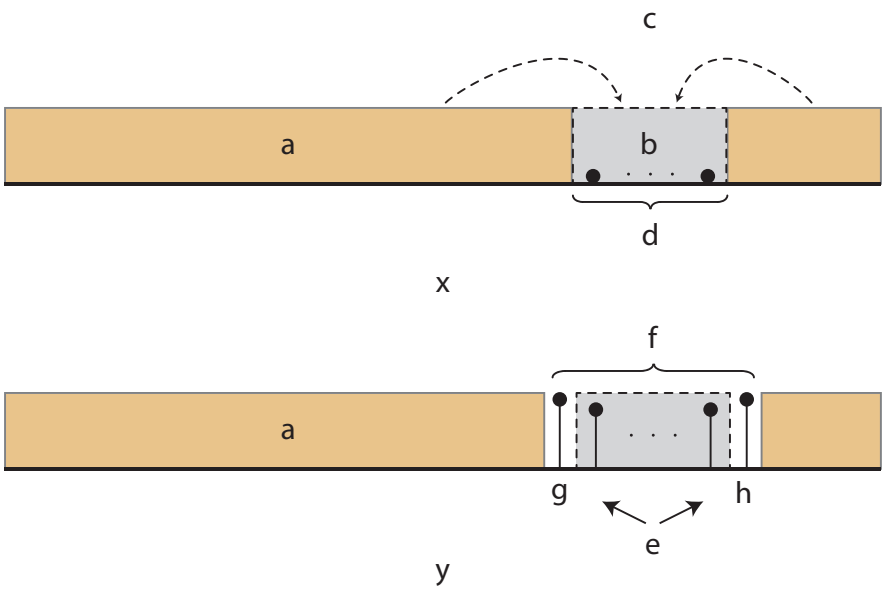

Figure 2.1 The main concept behind the AIC method (a) spectral leakage results in from active subcarriers within the null band and (b) the frame structure of the conventional AIC.

of OFDM tones in the victim band of the PU can be measured by:

$$\begin{aligned} Y(k) &= \frac{1}{N}\sum_{n=0}^{N-1} x(n)e^{-j2\pi\frac{nk}{Nr}} \\ &= \frac{1}{N}\sum_{l=0}^{N-1} X(l)\underbrace{\sum_{n=0}^{N-1} e^{j2\pi\frac{n}{N}(k-\frac{l}{r})}}_{P(l,k)} \end{aligned} \tag{2.1}$$

where $Y(k)$ is the k^{th} up-sampled spectrum of the transmitted signal. It is assumed that the subcarrier spacing in the PU is smaller than the one in the secondary system. Therefore, in order to investigate the spectrum of OFDM symbols in-between each two subcarriers, the interference signal's spectrum is evaluated by up-sampling the transmitted signal with a sampling rate of r. The equation (2.1) can be written in matrix form as follows:

$$\mathbf{Y} = \mathbf{PX} \tag{2.2}$$

where $\mathbf{Y} = [Y_k; k \in Z_{rN}]$ and $\mathbf{P} = [p_{l,k}; l \in Z_{rN}, k \in Z_N]$. The conventional AIC algorithm has two main steps. First, the tones within the victim band and the edge tones are turned off ($\hat{\mathbf{X}} = [X_0,\cdots, X_{f_l-2}, 0,\cdots, 0, X_{f_u+2},\cdots, X_{N-1}]$) and the spectral leakage of the active tones (the interference vector, $\mathbf{I} = \mathbf{P}\hat{\mathbf{X}}$) is calculated. Then the optimum values for the AIC edge

tones are computed in a way that the interference vector corresponding to the victim band is cancelled out. The solution for finding the optimum AIC vector ($\mathbf{\Gamma}_{opt}$), considering constraint on the AIC tones's power, leads to the linear least squared problem with quadratic inequality (LSQI) constraint [22].

$$\Gamma_{opt} = \arg\min_{\Gamma} \|P_{sub}\Gamma + I_1\|^2 \quad \text{s.t.} \quad \|\Gamma\|^2 < \epsilon \tag{2.3}$$

where $\mathbf{I}_1$ is part of the interference vector corresponding to the victim band; $\mathbf{P}_{sub}$ is the submatrix of $\mathbf{P}$ corresponding to the length of $\mathbf{\Gamma}_{opt}$ and $\mathbf{I}_1$; ϵ is the power constraint on the total power of the optimum AIC tones. The length of $\mathbf{\Gamma}_{opt}$ is given by $q = f_u - f_l + 3$.

2.4 Enhanced AIC for SISO System

In this section, the conventional AIC technique is generalized considering the effects of the fading wireless channel, the spectrum overshoot problem and the throughput issue. The main idea behind the presented technique is to propose a new constrained AIC algorithm with a capability of controlling the width and the depth of the created notch in presence of the wireless channel with less computational complexity and less throughput reduction. Before describing the algorithm that exploits this fact, the structure of the enhanced AIC (E-AIC) vector is explained. The E-AIC vector is composed of the null tones (NT) and the protection tones (PT) located in the victim band and at both sides of the victim band, respectively (Fig. 2.2). The number of AIC tones, null tones and protection tones are represented by N_{AIC}, N_{null}, N_{PT}, respectively. It is shown in the sequel that N_{PT} depends on the level of the interference that the PU can tolerate and PU's bandwidth. It is assumed that the number of the protection tones in both sides of the victim band may be different (i.e. α and β tones in the right and the left side of the victim band $N_{PT} = \alpha + \beta$).

As explained in the previous section, the main objective of AIC method is to design an optimal vector, $\mathbf{\Gamma}_{opt}$, which cancels the interference vector, $\mathbf{I}_1$, generated from the sidelobes of active tones. Through simulations, it is found that the width and the length of the created notch highly depend on the method exploited to calculate the vector $\mathbf{I}_1$. The vector $\mathbf{I}_1$ is obtained by extracting a^{th} to b^{th} elements of the vector $\mathbf{I}$ corresponding to the victim band's length and position. From simulation results the optimum way for extracting the vector $\mathbf{I}_1$ is given by [54]:

$$\mathbf{I}_1 = \mathbf{I}(rf'_l + m : r(f'_u - 1) - (m + 2)) \tag{2.4}$$

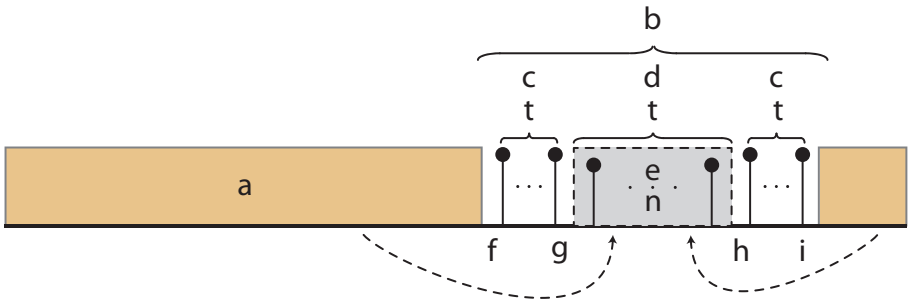

Figure 2.2 The frame structure of the proposed enhanced AIC technique for single antenna applications.

where m is a variable which controls the length of the vector $\mathbf{I}_1$; $f_l' = f_l + \alpha$ and $f_u' = f_u + \beta$. Given (2.4), the capability of controlling the characteristics of the created notch is added to the C-AIC. In the sequel, it is shown that increasing the value of m results in deeper and narrower notch and vice versa.

The other issue which should be considered is the wireless fading channel. Since, the OFDM-based CR signal propagates through a wireless channel, each subcarrier may experience different fading characteristics. Therefore, considering C-AIC technique, received protection tones at the primary user's antenna cannot completely cancel the spectral leakage of the active subcarriers. Consequently, the effect of the fading channel on the efficiency of the AIC algorithm should be compensated. The received signal at the PU may be represented by:

$$r_{PU} = x_{PU}(t) \otimes h_{PU}(t) + \underbrace{x_{SU}(t) \otimes h_{SU}(t)}_{I_{SU}(t)} + n(t) \tag{2.5}$$

where $x_{PU}(t)$ and $x_{SU}(t)$ are the PU and the cognitive radio signals ; $h_{PU}(t)$ and $h_{PU}(t)$ are the impulse response of the PU channel (between the PU's transmitter and receiver) and the interference channel (between the SU's transmitter and the PU's receiver), respectively. $n(t)$ is Additive White Gaussian Noise. The k^{th} up-sampled spectrum of the interferer signal at the PU's receiver, $I_{SU}(k)$, is given by:

$$\begin{aligned} I_{SU}(k) &= \frac{1}{N}\sum_{n=0}^{N-1}\left(\sum_{\tau=0}^{L-1} x_{SU}(n-\tau)h_{SU}(\tau)\right)e^{-j2\pi\frac{nk}{Nr}} \\ &= \frac{1}{N}\sum_{l=0}^{N-1} X_{SU}(l)\underbrace{\left(H_{SU}(l)\sum_{n=0}^{N-1} e^{j2\pi\frac{n}{N}(l-\frac{k}{r})}\right)}_{\bar{P}(l,k)} \end{aligned} \tag{2.6}$$

where $H_{SU}(l)$ and L are the frequency response of the interference channel at l^{th} subcarrier and the number of channel taps, respectively. It is assumed that the channel state information of interference channel is known at the transmitter of the CR system. Therefore, in order to consider the effect of the fading channel, the FFT kernel matrix of the CR system, $\mathbf{P}$, is multiplied by the frequency response of the interference channel. By substituting $\mathbf{P}$ with $\bar{\mathbf{P}}$ in (2.2) and using (2.4), the interference vector, $\mathbf{I}_1$, is obtained.

Spectrum overshoot problem is another fact that should be considered in calculating the optimum AIC tones. Therefore as shown in (2.3), finding the optimum AIC tones leads to a LSQI optimization problem. In order to address the spectrum overshoot problem, two different approaches has been proposed in the literatures. In the first method a single constraint is applied on the total power of the protection tones (as in (2.3)). Since, different protection tones have different contributions in generating the spectrum notch, using the single constraint method may not solve the spectrum overshoot. However, in [53], a new Singular value decomposition-improved (SVD-improved) constrained AIC technique is proposed in order to obtain a trade-off between the amounts of spectrum overshoot and sidelobes suppression. The other method is to impose different power constraints on different protection tones. In this case the LSQI problem turns into multi-constraints minimization problem (MCMP) [57], which has highly complex nonlinear optimization solution.

$$\Gamma_{opt} = \arg\min_{\Gamma} \|P_{sub}\Gamma + I_1\|^2 \quad \text{s.t.} \quad \|\Gamma_i\|^2 < \epsilon_i \tag{2.7}$$

In [57], an iterative single-constraint technique is proposed to approximate MCMP, which still has high computational complexity specially when N_{PT} is large. Despite of the high computational complexity of MCMP, the multi-constraints least square minimization method provides more optimal and efficient AIC vector. Therefore, in this paper, a novel technique is proposed to tackle the spectrum overshoot problem with less complexity by imposing the power constraint on each pair of protection tones on both sides of the null band. Although, the sequel problem still is kind of a nonlinear optimization problem, its complexity is lower than the one proposed in [57].

In the proposed method, in order to reduce the complexity of the MCMP, the protection tones are found pair by pair ($\{\Gamma_1,\ \Gamma_{N_{PT}}\}, \{\Gamma_2,\ \Gamma_{N_{PT}-1}\}, ..., \{\Gamma_{N_{PT}/2},\ \Gamma_{N_{PT}/2+1}\}$), iteratively. Therefore, for each pair of protection tones the MCMP is simplified to a single constraint least square optimization problem. Note that since the protection tones have the most contributions in generating the spectrum notch, the power of the null tones is usually much smaller than the power constraints. Therefore, predefined thresholds are applied only to the protection tones.

Hence, in order to find the optimum AIC vector, $N_{PT}/2$ number of iterations is needed. In each iteration (for instance at i^{th} iteration), first the interference vector (the spectral leakage) corresponding to the active tones and the protection tones which are computed in the previous iterations ($\{\Gamma_1, \cdots, \Gamma_{i-1}\}$ and $\{\Gamma_{N_{PT}-(i-1)+1}, \cdots, \Gamma_{N_{PT}}\}$) is calculated. Then, the optimum value of the i^{th} pair of the protection tones $\Gamma^{(i)} = \{\Gamma_i, \Gamma_{N_{PT}-(i-1)}\}$ is found by solving a least square problem with single constraint such that the interference vector is suppressed, i.e:

$$\begin{aligned} \mathbf{\Gamma}_{opt}^{(i)} = \arg\min_{\Gamma^{(i)}} \|\bar{\mathbf{P}}_1^{(i)}\mathbf{\Gamma}^{(i)} + \mathbf{d}_1^{(i)}\|^2 \\ \text{s.t.} \quad \|\mathbf{\Gamma}^{(i)}\| < \epsilon_i \end{aligned} \tag{2.8}$$

where $\mathbf{d}_1^{(i)} = \bar{\mathbf{P}}_0\hat{\mathbf{X}} + \sum_{j=1}^{i-1}\left(\bar{\mathbf{p}}_{f_l-(N_{PT}/2-i+j+1)}\,\mathbf{\Gamma}^{(i-j)} + \bar{\mathbf{p}}_{f_u+(N_{PT}/2-i+j+1)}\,\mathbf{\Gamma}^{(N_{PT}-i+j+1)}\right)$ is the spectral leakage from $\hat{\mathbf{X}}$ and $\mathbf{\Gamma}^{(i-1)}$, in which, $\hat{\mathbf{X}}$ is a sub-vector of $\mathbf{X}$ whose subcarriers corresponding to the AIC tones are set to zero, $\bar{\mathbf{p}}_j$ is the j^{th} column of $\bar{\mathbf{P}}$ and $\bar{\mathbf{P}}_0$ is submatrix of $\bar{\mathbf{P}}$ defined as $\bar{\mathbf{P}}_0 = \left[\bar{p}_{l,k};\ l \in Z_{(1\cdots f_l-N_{PT}, f_u+N_{PT}\cdots N)}, k \in Z_{(a\cdots b)}\right]$; $\bar{\mathbf{P}}_1^{(i)}$ is a submatrixes of $\bar{\mathbf{P}}$ defined as $\bar{\mathbf{P}}_1^{(i)} = \left[\bar{p}_{l,k};\ l \in Z_{\left(f_l-(N_{PT}/2-i),\, f_u+(N_{PT}/2-i)\right)}, k \in Z_{(a\cdots b)}\right]$. Note that a and b are the lower and the upper indices of the up-sampled interference vector given by $a = r(f_l - N_{PT}/2) + m$ and $b = r(f_u + N_{PT}/2 - 1) + (m+2)$, respectively.

The solution to the LSQI problem with spherical constraint is well-investigated problem in nonlinear optimization applications. Given $\bar{\mathbf{P}}_1^{(i)}$ has rank 2 and using the singular value decomposition (SVD) the unconstraint minimum norm solution is obtained by [58]:

$$\mathbf{\Gamma}_{opt}^{(i)} = \sum_{k=1}^{2} \frac{\xi_k}{\sigma_k}\mathbf{v}_k \tag{2.9}$$

where

$$\begin{aligned} \bar{\mathbf{P}}_1^{(i)} &= \mathbf{U}\mathbf{\Sigma}\mathbf{V} = \sum_{k=1}^{2}\sigma_k\mathbf{u}_k\mathbf{v}_k^T \\ \xi_k &= u_k^T\mathbf{d}_1^{(i)} \end{aligned}$$

in which $\mathbf{\Sigma} = \text{diag}(\sigma_1, \sigma_2)$ is an $m\times 2$ diagonal matrix; $\mathbf{U} = \left[\mathbf{u}_1 \mid \mathbf{u}_2 \mid \cdots \mid \mathbf{u}_m\right]$ and $\mathbf{V} = \left[\mathbf{v}_1 \mid \mathbf{v}_2\right]$ are $m\times m$ and 2×2 unitary matrix where $\mathbf{u}_l$ and $\mathbf{v}_l$ are left-singular and right-singular vectors, respectively. For simplicity of notation the superscript (i), $1 \le i \le N_{PT}/2$, in σ_k, ξ_k, $\mathbf{u}_k$ and $\mathbf{v}_k$ is dropped, respectively. If (2.9) does not satisfy the predefined power constraint (ϵ_i), solution of the LSQI problem with spherical constraint (2.8) is obtained by

using the method of Lagrange multipliers [58] which is given by:

$$\mathbf{\Gamma}_{opt}^{(i)} = -\Big((\bar{\mathbf{P}}_1^{(i)})^H \bar{\mathbf{P}}_1^{(i)} + \lambda_i \mathbf{I}\Big)^{-1} \bar{\mathbf{P}}_1^{(i)} \mathbf{d}_1^{(i)} \tag{2.10}$$

where λ_i is the optimum Lagrange multipliers which may be obtained by solving the secular equation:

$$f(\lambda_i) \;=\; \sum_{k=1}^{2} \Big(\frac{\sigma_k \xi_k}{\sigma_k^2 + \lambda_i}\Big)^2 - \epsilon_i^2 \tag{2.11}$$

Therefore, the algorithm of the Enhanced-AIC technique based on the aforementioned discussion is given in Algorithm 1. Since, σ_k, ξ_k and $\mathbf{v}_k$ depend only on the specifications of the required spectrum notch, it can be pre-calculated at the beginning of the algorithm for various number of protection and null tones.

Algorithm 1 Enhanced-AIC

$\mathbf{d}_1^{(1)} \leftarrow \bar{\mathbf{P}}_0 \hat{\mathbf{X}}$
for $i = 1, \cdots, N_{PT}$ **do**
  if $\sum_{k=1}^{2} \Big(\frac{\xi_k^{(i)}}{\sigma_k^{(i)}}\Big)^2 > \epsilon_i^2$ **then**
    Find λ_i such that $\sum_{k=1}^{2} \Big(\frac{\sigma_k^{(i)} \xi_k^{(i)}}{{\sigma_k^{(i)}}^2 + \lambda_i}\Big)^2 = \epsilon_i^2$
    $\mathbf{\Gamma}_{opt}^{(i)} = -\Big((\bar{\mathbf{P}}_1^{(i)})^H \bar{\mathbf{P}}_1^{(i)} + \lambda_i \mathbf{I}\Big)^{-1} \bar{\mathbf{P}}_1^{(i)} \mathbf{d}_1^{(i)}$
  else
    $\mathbf{\Gamma}_{opt}^{(i)} = \sum_{k=1}^{2} \frac{\xi_k^{(i)}}{\sigma_k^{(i)}} \mathbf{v}_k^{(i)}$
  end if
  $\mathbf{d}_1^{(i+1)} \leftarrow \bar{\mathbf{P}}_0 \hat{\mathbf{X}} + \sum_{j=1}^{i} \bar{\mathbf{p}}_{f_l - (N_{PT}/2 - i + j + 1)} \mathbf{\Gamma}^{(i-j)} + \bar{\mathbf{p}}_{f_u + (N_{PT}/2 - i + j + 1)} \mathbf{\Gamma}^{(N_{PT} - i + j + 1)}$
  $\mathbf{\Gamma}_{opt} \leftarrow \mathbf{\Gamma}_{opt}^{(i)}$
end for
return Γ_{opt}

2.5 Enhanced AIC for MIMO System

In this section, two new interference mitigation techniques for OFDM-based CR with multiple transmit antennas are proposed based on the idea explained in Section 2.4. A MIMO OFDM-based CR system with N_t transmit and N_r receive antennas is considered in presence of a victim narrowband system with one receive antenna. It is assume that the primary user's bandwidth is spread over N_{null} subcarriers of the CR system from f_l to f_u. Considering $N_t \times N_r$

CR system and a single antenna primary user, a MIMO channel between transmitter and receiver of the CR system, called the desired channel, and a multi-input single-output (MISO) channel between CR and PU systems, called the interference channel, are formed, respectively. The primary system receives N_t interfering signals which propagate through a MISO fading channel. It is supposed that the interference channel state information is available at the transmitter of the CR system. In such a system, one possible interference mitigation technique is to send optimum AIC tones through all transmit antennas. In this case the AIC tones are jointly optimized such that the generated interference at the location of the primary user is minimized [53, 59]. Although such a technique can provide an efficient interference reduction, the overall spectral efficiency of the CR system may reduce and the total transmitted power on the protection tones may exceed relative to the maximum allowable transmit power. Moreover, the jointly AIC tones optimization has high computational complexity.

In the sequel, in order to reduce the negative impact of the jointly optimization of the AIC tones, two new AIC-based interference cancellation techniques are proposed. The main idea behind these methods is to design one optimum AIC vector (transmitted through one antenna) such that the aggregate interference from non-zero tones (the ones from the other antennas and from the tones outside of the victim band of the antenna which carries the AIC tones) is minimized. In the first technique, all components of the designed AIC vector is sent from one of the transmit antennas which is selected based on the bulk transmit antenna selection (TAS) approach [60]. However, in order to improve the throughput of the CR system, in the second proposed technique the per-subcarrier transmit antenna selection approach [60] is adopted to distribute the designed optimum AIC tones over different transmit antennas.

2.5.1 Bulk TAS-AIC Technique

The frame structure of the proposed algorithm is the same as the one of the previous section (Fig. 2.2). It consists of N_{PT} protection tones and N_{Null} null tones which are placed in two sides and within the victim band, respectively. As mentioned earlier, an optimum AIC vector is designed and sent from one of the transmit antennas such a way that the interference from N_t cognitive radio transmit antennas is canceled out in the location of the primary user's receiver (Fig. 2.3).

The bulk TAS algorithm is adopted to select one of the transmit antennas to convey the AIC vector. However, common TAS algorithms are based on minimizing the instantaneous bit error probability or maximizing capacity (throughput). Our objective is to select a transmit antenna which maximize the BER of the CR system. Therefore, in this case, by sending the AIC vector through an antenna which has the worst desired channel, the BER of the CR system is improved. In order to choose an antenna with the weakest channel over the frequency

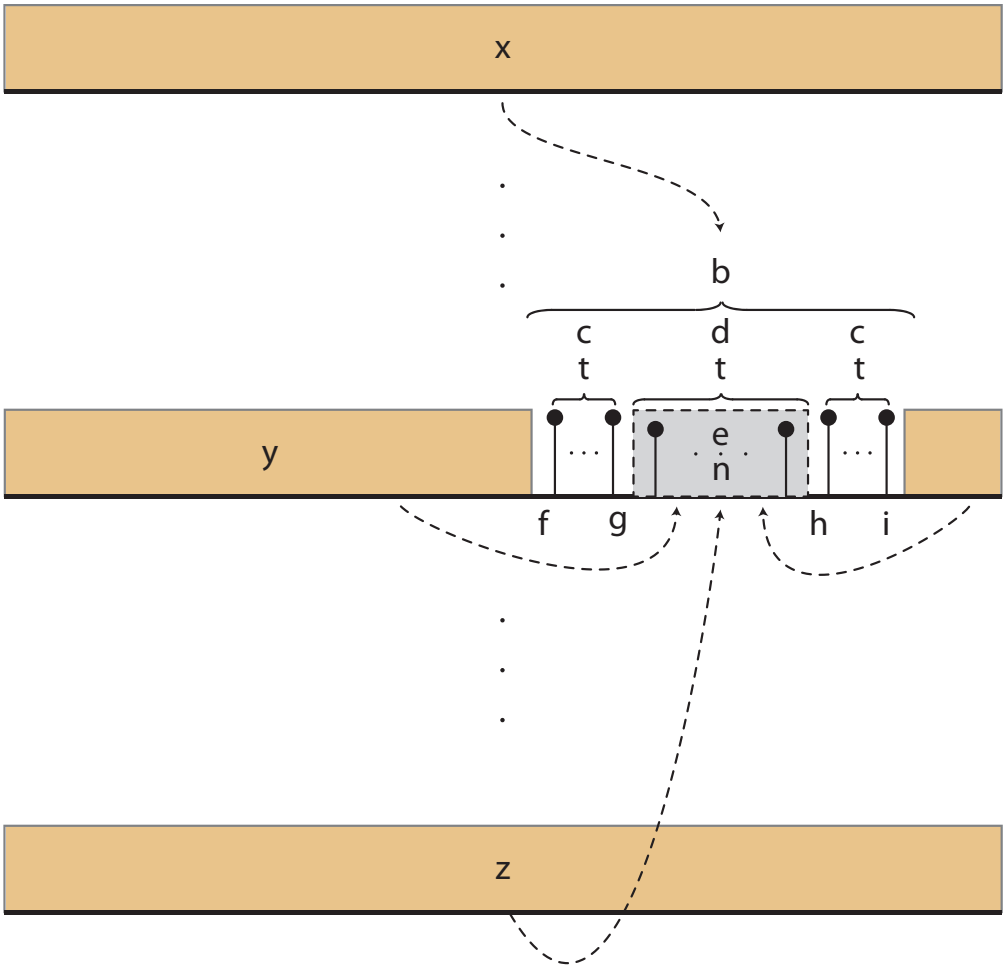

Figure 2.3 The frame structure of the proposed bulk TAS-AIC technique, the AIC tones are sent from i^{th} transmit antenna.

band of the victim system, our selection criterion is to choose an antenna which minimizes the SNR over the AIC tones at the receiver of the CR system. The SNR minimization process is performed by minimizing the column Frobenius-based norm of the desired channel matrix. Hence, the antenna which maximizes the number of tones with the minimum channel Frobenius-based norm over the AIC tones is selected, i.e.:

$$\mathcal{I} = \arg \max_{k \in \Omega_i} \min_{1 \leqslant i \leqslant N_t} \sum_{j=1}^{N_r} |h_{j,i}(k)|^2 \tag{2.12}$$

where $\mathcal{I}$ and Ω_i are the selected antenna and a subset of OFDM subcarriers corresponding to the AIC tones of i^{th} transmit antenna, respectively; $h_{j,i}(k)$ denotes the channel frequency coefficient between i^{th} transmit antenna and j^{th} receive antenna on the k^{th} subcarrier. The antenna selection may be performed at the receiver of the CR system and the number of the

selected antenna may be sent to the CR transmitter. Therefore, at the receiver, in the first step, the column Frobenius-based norm of the desired channel is calculated for all subcarriers of AIC vector. Then, for each subcarrier, an antenna which minimizes the computed norms is found. Finally, an antenna which consists of the maximum number of tones with the minimum norm is selected.

Let the optimum AIC vector be sent from i^{th} transmit antenna. Similar to the previous section, for the l^{th} iteration, the first step in AIC-based techniques is to calculate the spectral leakage of the non-zero tones, $\mathbf{d_i}^{(l)}$. Next, using (2.4), the interference vector corresponding to the victim band $\mathbf{d}_{1,i}^{(l)}$ is found. Therefore, similar to the Section 2.4, the optimum pair of the protection tones transmitting through i^{th} antenna at the l^{th} iteration, $\Gamma_i^{(l)}$, which minimize $\mathbf{d}_{1,i}^{(l)}$ is given by:

$$\begin{aligned} \mathbf{\Gamma}_{opt}^{(l)} = \quad & \underset{\Gamma_i^{(l)}}{\arg\min} \quad \|\bar{\mathbf{P}}_{1,i}^{(l)}\mathbf{\Gamma}_i^{(l)} + \mathbf{d}_{1,i}^{(l)}\|^2 \\ & \text{s.t.} \qquad \|\mathbf{\Gamma}_i^{(l)}\| < \epsilon_l \end{aligned} \tag{2.13}$$

where $\bar{\mathbf{P}}_{1,i}^{(l)}$ is a submatrixes of $\bar{\mathbf{P}}_\mathbf{i}$ corresponding to l^{th} pair of the protection tones (as defined in (2.8)); $\bar{\mathbf{P}}_i$ is the FFT kernel matrix of CR system which is multiplied by the up-sampled frequency impulse response of the interference channel between i^{th} CR transmit antenna and the PU receive antenna. $\mathbf{d}_{1,i}^{(l)}$ is defined as $\mathbf{d}_i^{(l)}(rf_l' + m : r(f_u' - 1) - (m + 2))$ which is given by:

$$\begin{aligned} \mathbf{d}_i^{(l)} = \bar{\mathbf{P}}_{0,i}\hat{X}_i \quad + \quad & \sum_{\substack{j=1 \\ j\neq i}}^{N_t} \bar{\mathbf{P}}_j X_j \\ + \quad & \sum_{j=1}^{i-1} \bar{\mathbf{p}}_{f_l-(N_{PT}/2-i+j+1)}\mathbf{\Gamma}^{(i-j)} \; + \; \bar{\mathbf{p}}_{f_u+(N_{PT}/2-i+j+1)}\mathbf{\Gamma}^{(N_{PT}-i+j+1)} \end{aligned}$$

where $\hat{X}_i$ denotes a sub-vector of data stream of i^{th} antenna whose subcarriers corresponding to the AIC tones are set to zero; X_j denotes data streams corresponding to the antennas which convey regular modulated data stream; $\bar{\mathbf{P}}_{0,i}$ is the submatrix of $\bar{\mathbf{P}}_i$ corresponding to non-zero subcarriers of the i^{th} antenna; and $\bar{\mathbf{p}}_j$ is the j^{th} column of $\bar{\mathbf{P}}_i$. Finally, the same procedure as in Section 2.4 is used to find an optimum AIC vector which minimize the interference vector $\mathbf{d}_{1,i}^{(l)}$.

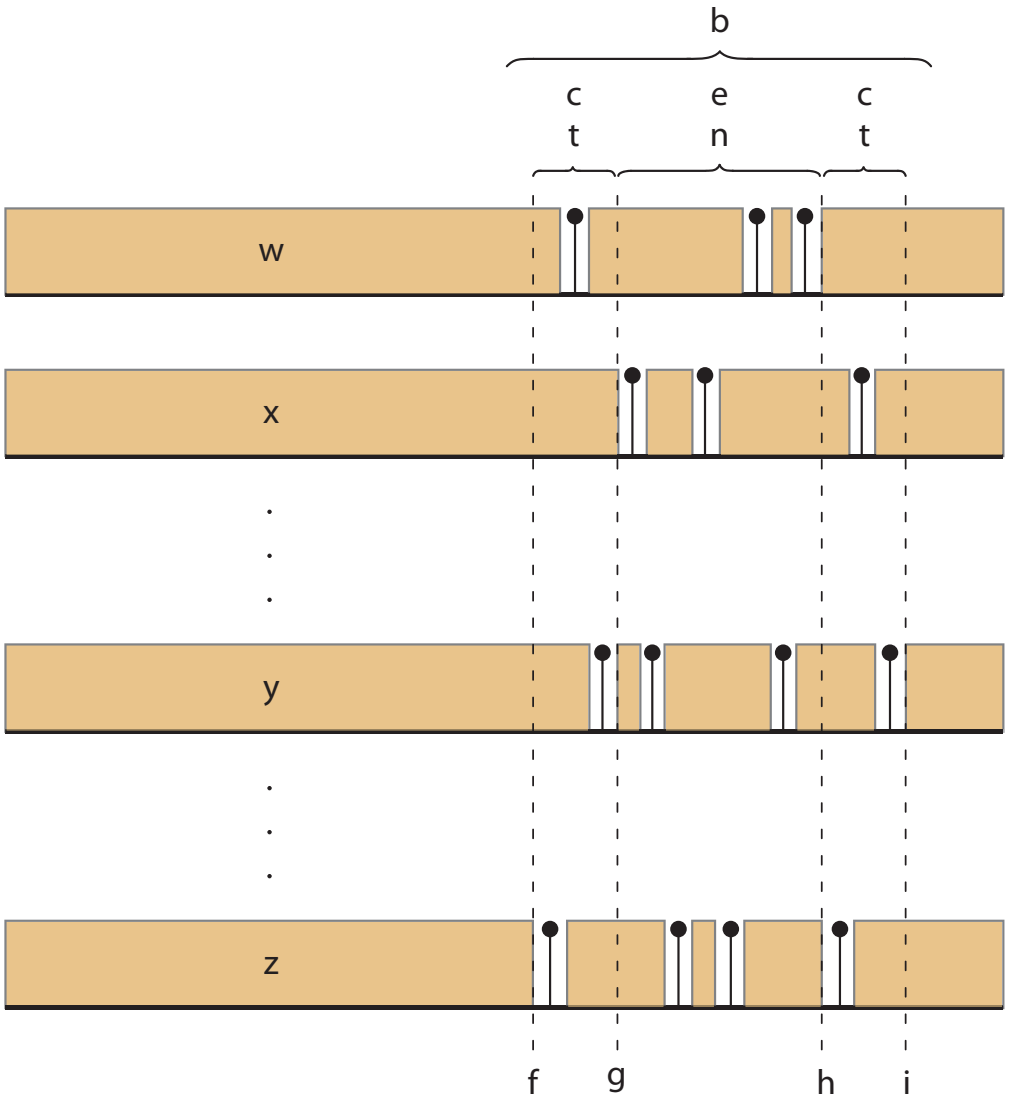

Figure 2.4 The frame structure of the proposed per-one TAS-AIC technique, the AIC tones are distributed over subcarriers with the weakest desired channel among all transmit antennas.

2.5.2 Pre-tone TAS-AIC Technique

In the pre-tone TAS-AIC technique, the main idea behind the per-tone transmit antenna selection is combined with the proposed E-AIC technique in order to improve the spectral efficiency of the CR system using interference mitigation algorithm. To do so, the optimum AIC tones are distributed over different transmit antennas such that the throughput loss of the proposed E-AIC method is minimized (Fig. 2.4). As shown, the AIC tones consisting of protection tones and the tones within the victim band are distributed over that subcarriers which have the weakest desired channel among all transmit antennas. Therefore, the selection criterion is to find a subset of subcarriers in order to minimize the SNR over the AIC tones

at the receiver of the CR system. Hence, each subcarrier corresponding to the AIC vector is sent through an antenna which has the smallest frequency channel gain, i.e.:

$$\mathcal{S} = \arg \min_{\substack{k \in \Omega_i \\ 1 \leqslant i \leqslant N_t}} |h_{j,i}(k)|^2 \tag{2.14}$$

where $\mathcal{S}$ denote a subset of subcarriers over different antennas. The pre-tone TAS algorithm may be performed at the receiver of the CR system. Then, the subset of the subcarriers and corresponding transmit antennas may be sent to the CR transmitter.

Let the optimum AIC vector be sent over the subset of the subcarriers $\mathcal{S}$ which is selected in advance. Similar to the bulk TAS-AIC algorithm, the optimum l^{th} pair of the protection tones which minimize the interference vector is obtained by:

$$\begin{aligned} \mathbf{\Gamma}_{opt}^{(l)} = \quad & \arg\min_{\Gamma^{(l)}} \quad \|\hat{\mathbf{P}}_1^{(l)} \mathbf{\Gamma}^{(l)} + \mathbf{d}_1^{(l)}\|^2 \\ & \text{s.t.} \qquad \|\mathbf{\Gamma}^{(l)}\| < \epsilon_l \end{aligned} \tag{2.15}$$

where $\hat{\mathbf{P}}_1^{(l)}$ is a submatrixes of $\bar{\mathbf{P}}_i$ defined as $\hat{\mathbf{P}}_1^{(l)} = \Big[\bar{p}_i^{l,k};\ l \in Z_{\left(f_l-(N_{PT}/2-i),\, f_u+(N_{PT}/2-i)\right)}, k \in Z_{(a \cdots b)}, i \in \Omega\Big]$; similar to Section **??**, $\mathbf{d}_1^{(l)}$ is extracted from $\mathbf{d}^{(l)}$ which is given by:

$$\mathbf{d}^{(l)} = \sum_{n=1}^{N_t} \bar{\mathbf{P}}_n \hat{X}_n \ + \ \sum_{j=1}^{i-1} \bar{\mathbf{p}}_{f_l-(N_{PT}/2-i+j+1)} \mathbf{\Gamma}^{(i-j)} \ + \ \bar{\mathbf{p}}_{f_u+(N_{PT}/2-i+j+1)} \mathbf{\Gamma}^{(N_{PT}-i+j+1)}$$

where $\hat{X}_n$ denotes a data corresponding to the n^{th} transmit antenna defined as $\hat{X}_n = \big[x_k^n;\ k \notin \Omega, n \in Z_{(1,\cdots,N_t)}\big]$; and $\bar{\mathbf{p}}_j$ is the j^{th} column of $\bar{\mathbf{P}}_i$. Finally, the same procedure as in Section 2.4 is used to find an optimum AIC vector which minimizes the interference vector $\mathbf{d}_{1,i}$.

2.6 Simulation Results

To evaluate the performance of the proposed algorithms, an OFDM-based cognitive radio system with the FFT size of 128, an up-sampling rate of 4 is considered. OFDM subcarriers are modulated using the QPSK modulation. A frequency-selective Rayleigh fading multipath channel with 10 taps is assumed as an interference channel. In MIMO CR system with N_t transmit antennas, the efficiency of the proposed AIC algorithms are investigated underN_t independent interference channels between secondary user transmitters and primary user receiver. The power spectrum seen in the simulation results have been obtained from 100,000 simulation runs.

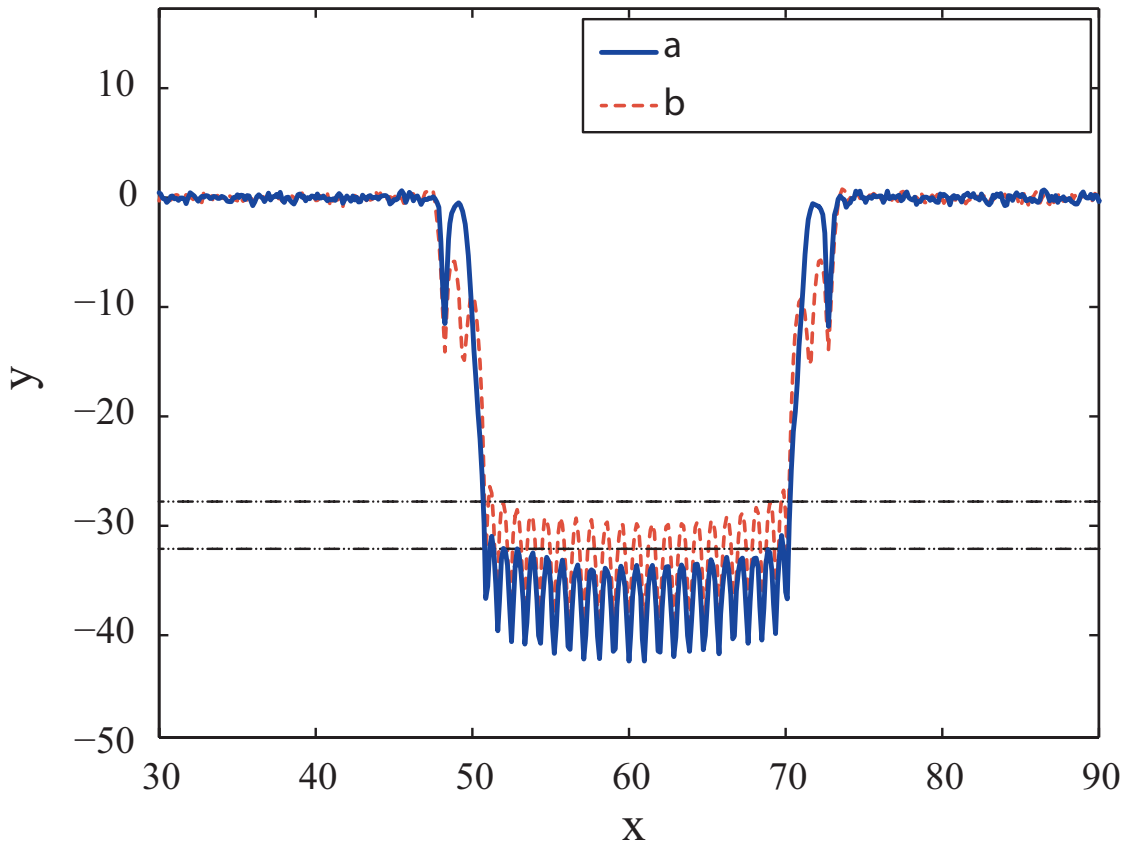

Figure 2.5 Comparison of the multi- and single-constraint approaches given $N_{Null} = 20$ and $N_{PT} = 6$.

2.6.1 Enhancement in terms of Overshoot Reduction and Channel Consideration

In this section, the performance of the proposed technique for tackling the overshoot problem and considering the interference wireless channel is shown.

In Fig. 2.5, the performance of the constrained E-AIC technique with single-constraint and the multi-constraint minimization approach is compared. Given $N_{null} = 20$, $N_{PT} = 6$ and in order to obtain 0dB overshoot, for the single-constraint approach only one power constraint is applied to the norm of the calculated optimum AIC vector, however for multi-constraint approach different power constraints $(\epsilon_i, i = 1, \ldots, 3)$ are applied to pairs of the protection tones $\Big(\Gamma_i = \big[\Gamma_i, \Gamma_{N_{PT}+1-i}\big]\Big)$. As shown, the multi-constrained E-AIC technique results in a deeper notch compares to the single-constrained AIC method. This fact is due to the inherent feature of the optimum AIC vector and the proposed optimization algorithm. As mentioned before, the contribution of the protection tones in cancelling out the spectral leakage decreases when we move from two sides of the AIC vector to its center. Therefore,

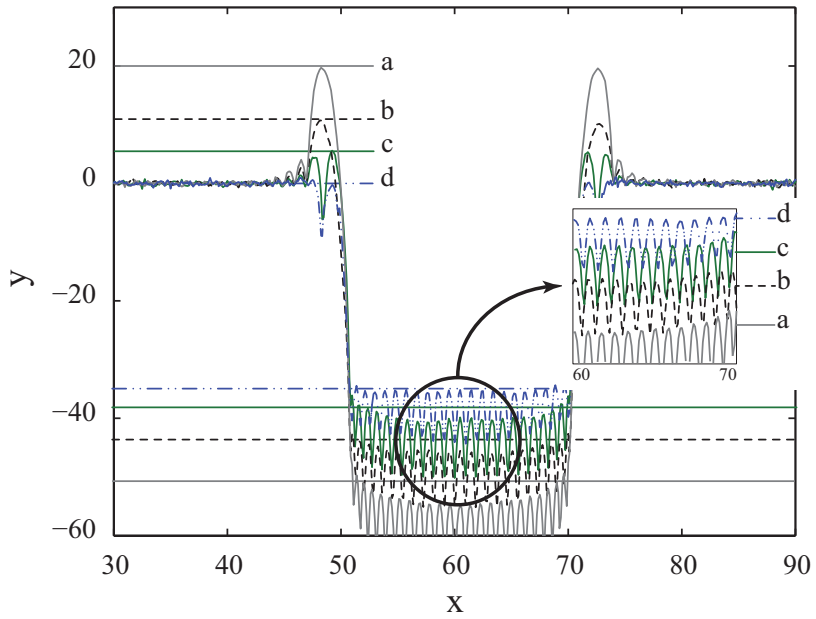

Figure 2.6 Effect of power spectrum thresholds on the depth of the created notch, given $N_{Null} = 20$ and $N_{PT} = 6$

constraints on the protection tones have to become looser as well. To this end, targeting 0dB overshoot, a tighter constraint have to be applied to the total power of the protection tones which results in a shallower notch compares to multi-constrained AIC. Hence, in order to create a deeper notch (same as that created with multi-constrained E-AIC method), the single constrained E-AIC technique have to use more protection tones which leads to the spectral efficiency reduction. For instance, the proposed multi-constrained AIC method has a higher spectral efficiency compared to the approaches that have been proposed in [52] and [57]. In [52], it has been shown that in order to create 30dB interference reduction over 20 subcarriers, 8 cancellation subcarriers are needed. Also, in [57], it has been demonstrated that the -30dB spectrum overshooting probability of the proposed methods is very high for a total protection tones of less than 8.

In Fig. 2.6 the performance of the proposed iterative multi-constraint E-AIC method is depicted for different overshoot thresholds. Given $N_{null} = 20$ and $N_{PT} = 6$, three different constraints $(\epsilon_i, i = 1, \ldots, 3)$ are used for pairs of protection tones such that the predefined thresholds are obtained. As it is obvious, the deepest notch is acquired for unconstrained E-AIC method and by decreasing the threshold, a shallower notch is obtained. This is due to the fact that by reducing the threshold of the power spectrum overshoot, the total power of the AIC tones which are used to cancel out the spectral leakage is reduced. Hence, there is an obvious trade-off between the acceptable overshoot and the depth of the created notch.

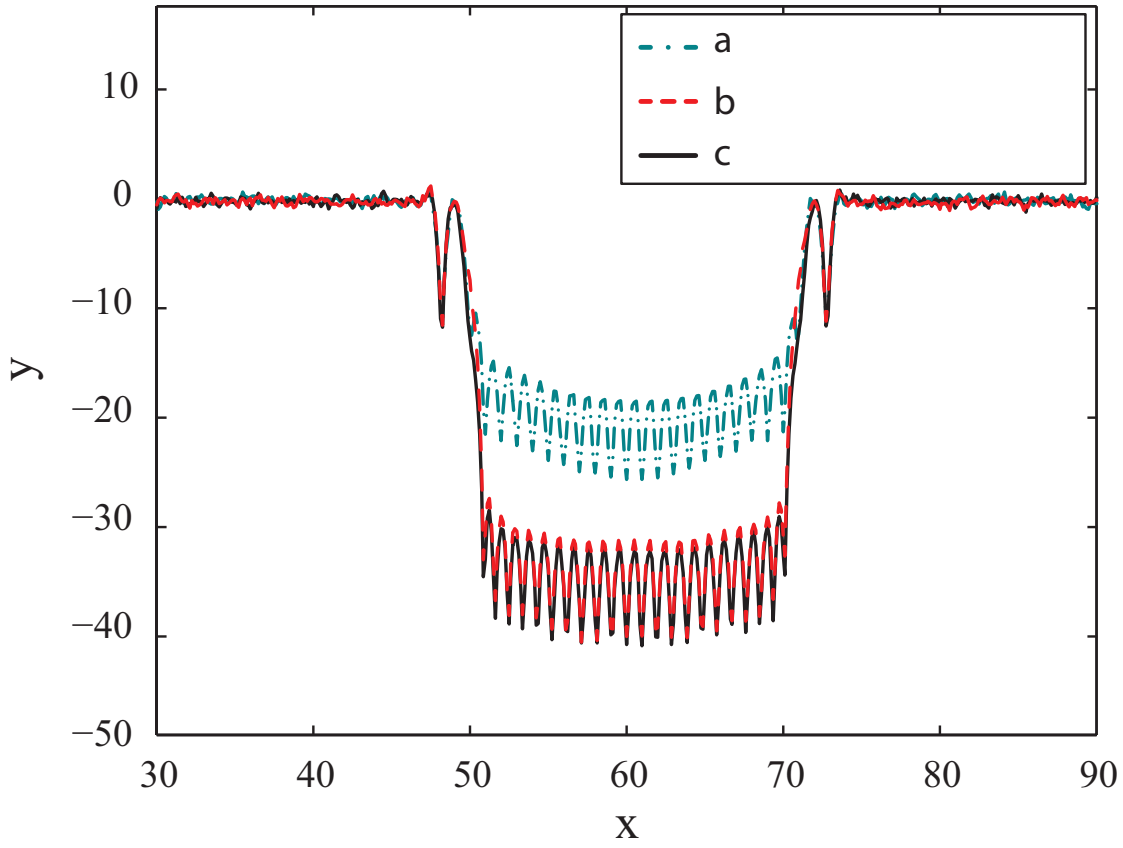

Figure 2.7 Performance of the conventional and the enhanced AIC techniques in presence of the fading channel.

In Fig. 2.7 the performance of the C-AIC and the E-AIC methods in the presence of the frequency selective fading channel is compared given $N_{null} = 20$ and $N_{PT} = 6$. It is seen that the efficiency of the C-AIC is deteriorated in presence of the interference channel; and it may not achieve extra performance gain over tone nulling technique. Despite the effect of the multipath fading channel, the E-AIC algorithm achieves approximately 15 dB performance gain over the C-AIC algorithm. Therefore, the E-AIC technique presents a better solution for the coexistence problem of CR and PU systems with/without considering the multipath fading channel.

2.6.2 Enhancement in terms of Notch Characteristics

In order to verify the capability of the proposed E-AIC algorithm in controlling the depth and the width of the created notch, the spectrum of the OFDM signal is investigated for different scenarios. Fig. 2.8 depicts the ability of E-AIC algorithm to create notches with variable depths. It is assumed that the primary user is spanned over 20 subcarriers of a CR

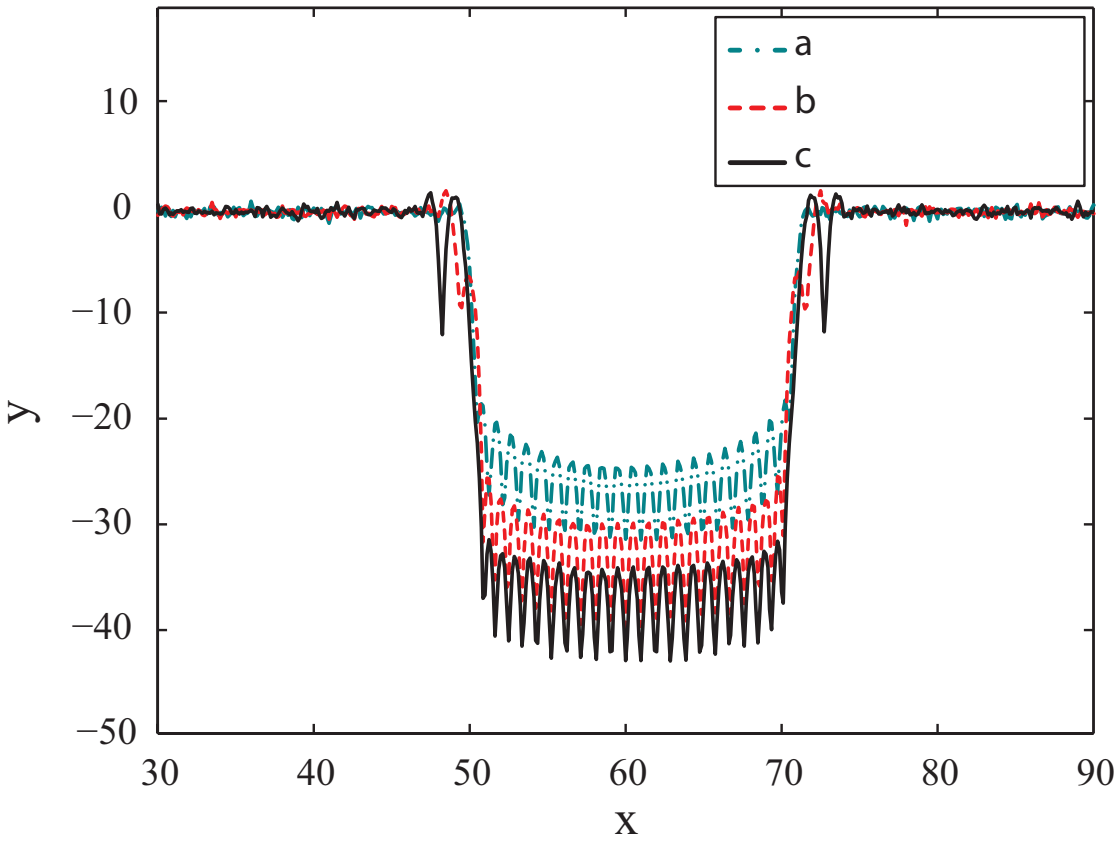

Figure 2.8 Power spectrum of the output OFDM signal using the E-AIC methods for different value of m, given $N_{Null} = 20$.

system from tones #51 to #70 (i.e. $N_{null} = 20$). According to the distance between the PU and CR systems, the maximum allowable power of the interference signal may change. Therefore as shown, by increasing the value of m, a deeper notch is obtained. However, for a fix number of the null tones, more numbers of the protection tones should be used. For instance, if m is set to zero, only two protection tones are needed to achieve 25dB interference reduction ; however for $m = 8$, six protection tones are used to create a 35dB notch. Hence, in order to create a deeper notch, more number of protection tones are needed which causes a significant throughput loss of the CR system.

In Fig. 2.9, the constrained E-AIC algorithm's flexibility in creating notches with different width and depth is investigated. In the sequel simulations, the notch width is computed based on a known power spectrum threshold which is set to 90% of the maximum achievable notch depth. In Fig. 2.9-(a) given a fixed $N_{AIC} = 22$, the depth and the width of the created notch are compared as a function of the variation of m. It shows that the depth of the generated notch is inversely proportional to its width. Hence, given a fixed N_{AIC}, a deeper

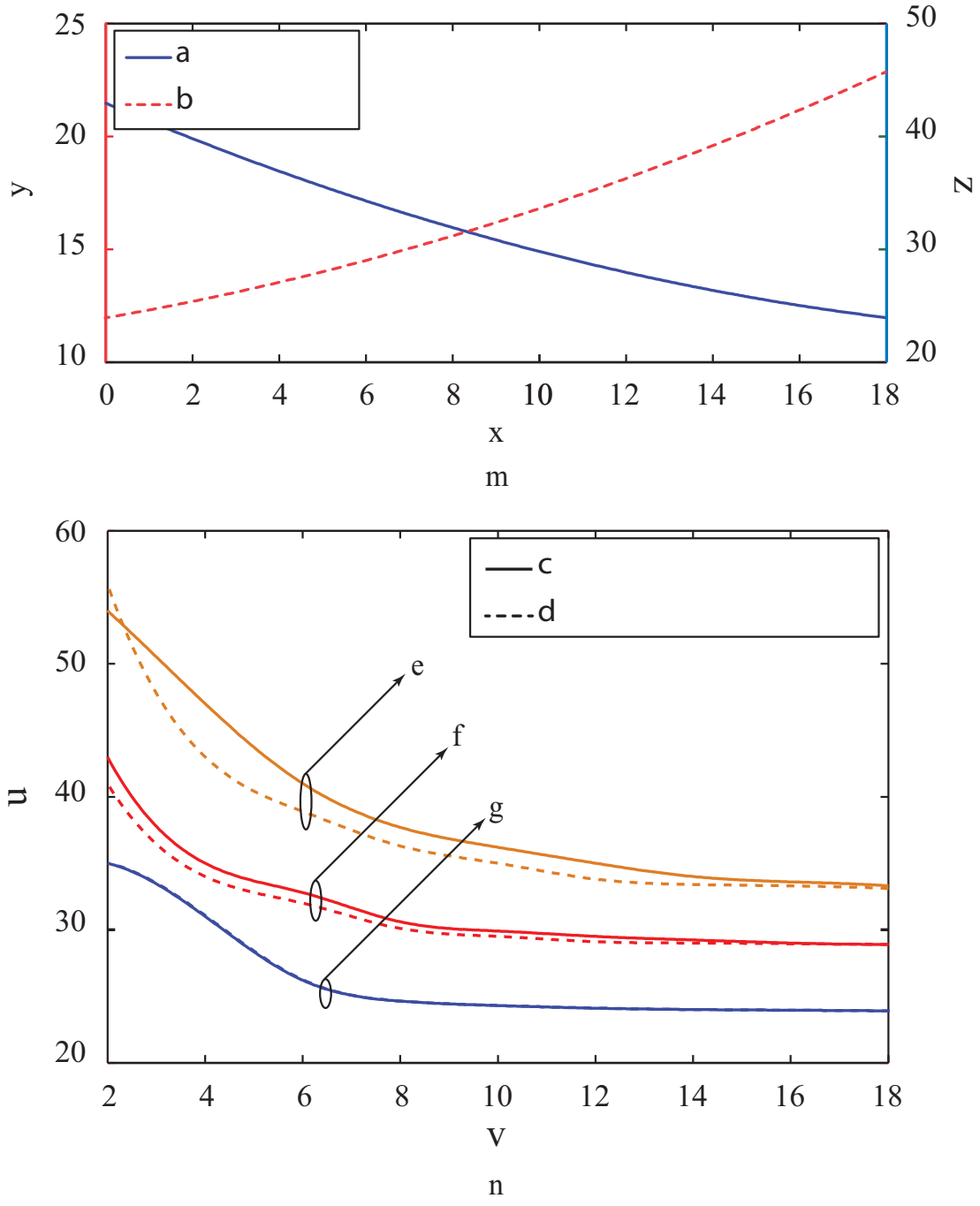

Figure 2.9 Capability of creating flexible notches (a) The trade-off between the notch depth and the notch width and (b) variation of the depth of the created notch as a function of number of null tones.

notch is achievable in a cost of narrower notch. In Fig. 2.9-(b), the maximum achievable interference reduction for different victim bandwidths (i.e. different N_{null}) is studied given various numbers of the protection tones. Furthermore, in order to investigate the bandwidth efficiency of different constrained E-AIC methods, the results of Single-Constrained Minimization Problem (SCMP) and MCMP approaches are compared. With a given threshold on the value of maximum allowable interference, the minimum number of the protection tones may determined for different victim bandwidths. The simulation results confirm the previous finding that first the constrained E-AIC technique requires more protection tones to generate a notch which is the same as that created with unconstrained one. Second, it is shown that the constrained E-AIC technique which employs the proposed iterative MCMP method is more bandwidth efficient compared to single constrained LSQI approach. Consequently, the OFDM-based CR system which is equipped with the proposed E-AIC algorithm may flexibly adapt itself to the technical requirements addressed by different regulations with less throughput reduction compared to the other AIC-based methods.

2.6.3 E-AIC for CR System with Multiple Transmit Antennas

In this section, the performance of the proposed sidelobes suppression technique for cognitive radio systems with multiple transmit antennas is studied. In Fig. 2.10, the power spectrum density of the received signal at the location of the primary user is presented in order to compare the performance of the bulk and per-tone TAS based E-AIC methods. It is assumed that the CR system has $N_t = 4$ transmitter antennas and the primary user spreads over $N_{null} = 20$ subcarriers. It is seen that the proposed techniques have identical performance, and distributing the components of the optimum AIC vector over different subcarriers and transmit antennas does not affect the depth of the created notch.

In Fig. 2.11, the effect of the number of the transmit antennas on the performance of the proposed techniques is depicted. It is assumed that the primary user is spanned over $N_{null} = 20$ subcarriers of the CR system. Since, both bulk and per-tone TAS E-AIC techniques have the same performance, only bulk TAS E-AIC method is studied in this figure. It is shown that increasing the number of the transmit antennas for $N_t > 2$ does not affect the depth of the created notch. Therefore, the performance of the proposed interference mitigation techniques is not sensitive to the number of the transmit antennas. However, the interference suppression in a system with multiple antennas is less than the one with single antenna, which is due to the extra spectral leakage from different transmit antennas compared to the SISO CR system.

In Fig. 2.12, the throughput loss of different AIC techniques used in a CR system with multiple transmit antennas is depicted. A MIMO V-BLAST OFDM-based CR system with N_t

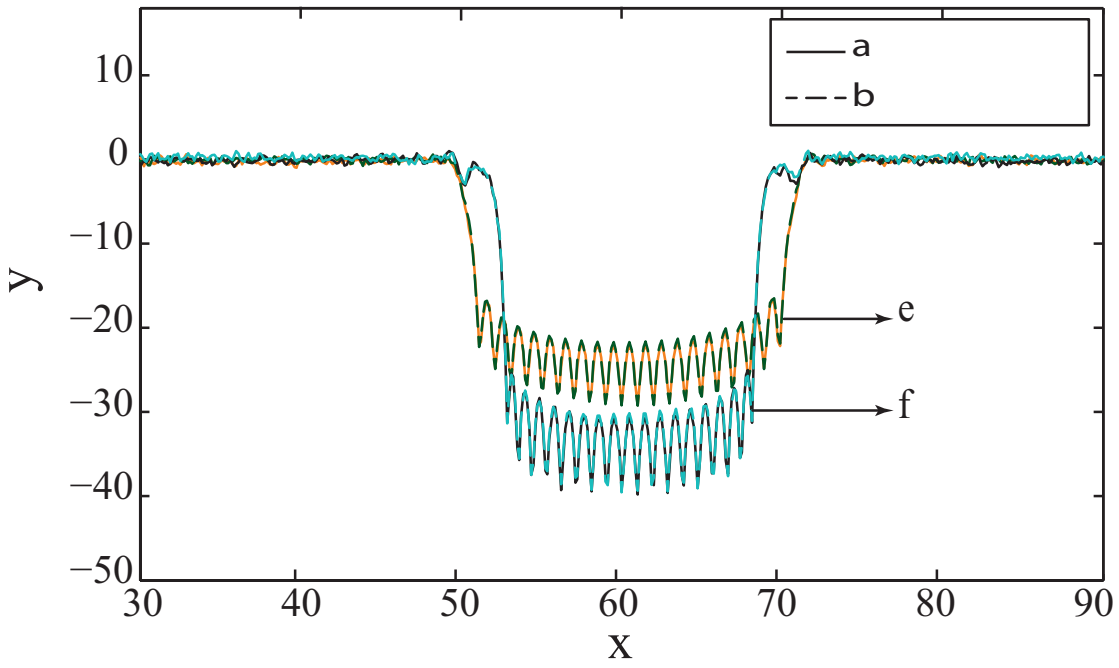

Figure 2.10 Power spectrum of a OFDM-based CR system using the bulk and the per-tone TAS-AIC techniques for different N_{PT}.

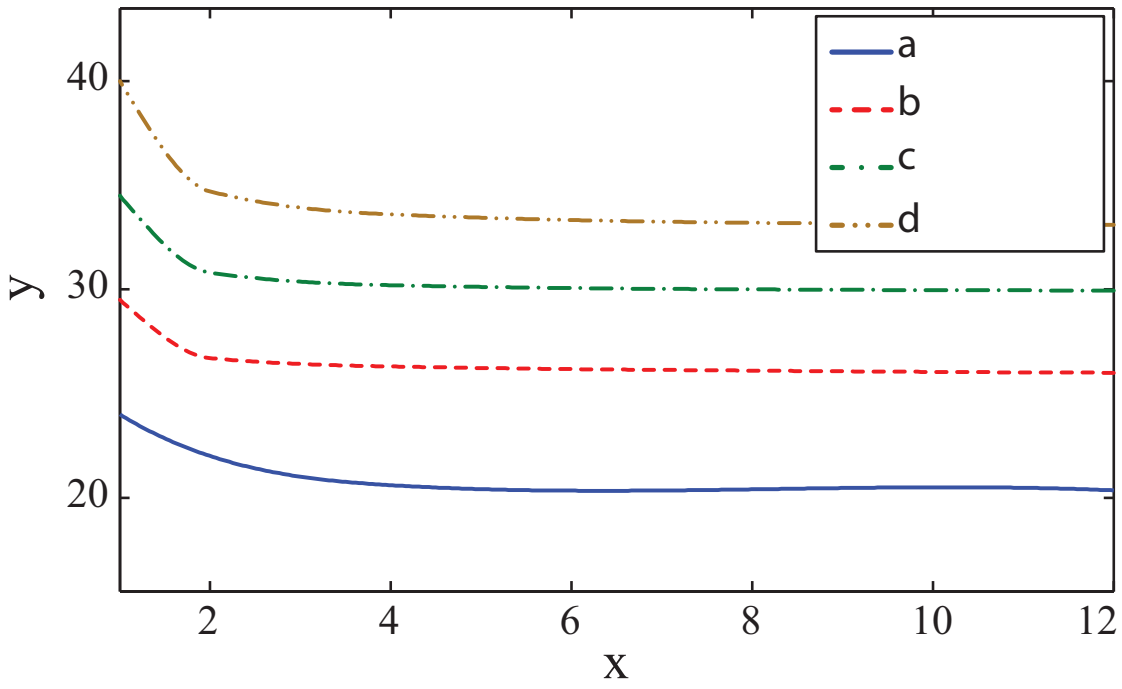

Figure 2.11 The depth of the created notch versus the number of transmit antennas for different N_{PT}.

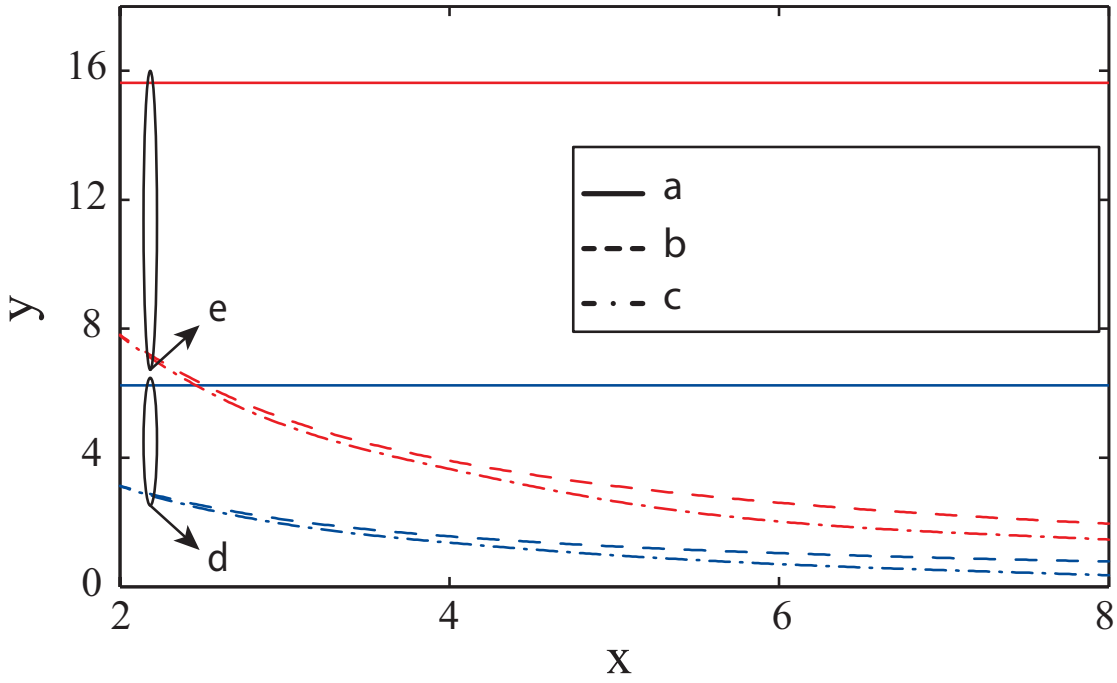

Figure 2.12 Throughput loss of the proposed methods versus number of transmit antennas, SNR = 20.

transmit and N_r receive antennas is considered. Since successive cancellation is able to achieve the channel capacity, the transmitted data are detected using the minimum mean squared error detector with ordered successive interference cancellation (OSIC) technique [61]. In this figure the throughput loss of the proposed bulk and per-tone TAS-AIC methods are compared with the one proposed in [59]. It can be seen in Fig. 2.12 that when AIC tones are transmitted over all antennas, the throughput loss of the CR system does not change as a function of the number of transmit antennas (N_t). However, considering the proposed algorithms, the CR system experiences lower throughput reduction for any number of transmit antennas and the throughput loss decreases by increasing N_t. This is due to the fact that in the proposed methods, since only one set of AIC tones are sent over one transmit antenna or a subset of transmit antennas (in bulk or per-tone TAS-AIC, respectively), the throughput loss is inversely proportional to N_t. Therefore, by increasing the number of transmit antennas, the throughput loss decreases. Moreover, it is shown that the per-tone TAS-AIC method provides a more spectral efficient solution than the bulk TAS-AIC technique. This can be justified in the following way. In the bulk TAS-AIC technique, AIC tones are transmitted over an antenna which maximizes the number of subcarriers with the minimum channel Frobenius-based norm. Hence, still some of the AIC tones are transmitted over subcarriers which do not have the minimum channel Frobenius-based norm. However, in the per-tone TAS-AIC

method, all of the AIC tones are sent over subcarriers which have the weakest channels (among all transmit antennas). Thus, the bulk TAS-AIC technique has higher throughput loss compared to the per-tone TAS-AIC method. Furthermore, the gap between the throughput loss of these methods increases with the number of antennas. This is because of the fact that in the per-tone TAS-AIC method, by increasing N_t, the probability of finding subcarriers with the least SNRs increases. Therefore, the probability of sending AIC tones over useless subcarriers increases which leads to a throughput improvement.

2.7 Conclusion

In this paper, the problem of the interference mitigation in OFDM-based Cognitive Radio systems for single antenna and multiple antennas applications has been studied. An enhanced version of the AIC technique considering the spectrum overshoot problem and the complexity issues has been proposed. In order to improve the performance of the conventional constrained AIC technique in terms of the achievable interference reduction, multi-constraint approach has been adopted.To do so, different power constraints have been applied to the protection tones which transforms the single-constraint least square optimization problem into a multi-constraint minimization problem. To reduce the complexity of the solution to MCMP, a novel iterative SVD-based algorithm has been presented. Moreover, the proposed E-AIC technique has been equipped with the ability of controlling the characteristics of the created notch. The simulation results have shown that the proposed E-AIC technique provides higher performance in terms of sidelobes suppression with 0dB spectrum overshoot and less computational complexity compared to the previous constrained AIC methods. It has been observed that for a fixed number of subcarriers corresponding to the victim band and a fixed notch depth, the proposed technique requires less number of protection tones which leads to more spectral efficient CR system. Furthermore, it has been shown that applying distinct power constraints to the protection tones results in more efficient interference reduction technique (in terms of notch depth) than applying single constraint to the total power of the protection tones.

Two novel E-AIC techniques have been proposed for OFDM-based CR systems with multiple transmit antennas. In order to improve the spectral efficiency and the performance of the interference mitigation technique, the main ideas behind the bulk and the per-tone transmit antenna selection approaches have been combined with the proposed E-AIC technique for SISO applications. Our simulation results have shown that both presented techniques provide acceptable interference reduction performance and less throughput loss compared to the previous methods. It has been observed that the number of the transmit antennas does

affect the depth of the created notch. However by increasing the number of the transmit antennas, the per-tone TAS-AIC method provides higher throughput compared to the bulk TAS-AIC technique.

CHAPTER 3

Article 2: IMPACT OF TH-UWB INTERFERENCE SIGNALS ON MB-OFDM UWB SYSTEMS: INTERFERENCE MODELING AND PERFORMANCE ANALYSIS

Farshad Sarabchi, and Chahé Nerguizian
Poly-Grames Research Center, Department of Electrical Engineering,
École Polytechnique de Montréal
Montréal, QC, Canada
Submitted to the Journal of Wireless Communication and Mobile Computing on August 2013 and revised on May 2014

3.1 abstract

In this paper, the coexistence issue between multiband-orthogonal frequency-division multiplexing (MB-OFDM) and time-hopping ultra-wideband (TH-UWB) networks is widely analyzed. For this purpose, to study and model the TH-UWB interference, an analytical framework which describes key features of the interference distribution is provided. The interference distribution is studied in the context of TH-UWB's signaling parameters. Our results reveal that the interference distribution highly depends on its time-hopping parameters. Therefore, choosing proper time-hopping parameters leads to less destructive interferences. The Generalized Gaussian (GG) and the Symmetric-α-Stable (SαS) distributions are used to model the interference-plus-noise signal. The maximum likelihood and a characteristic function-based regression-type methods are adopted to estimate parameters of GG and SαS distributions, respectively. Moreover, the interference channel effects on the impulsive behavior of the TH-UWB signal is studied. It is shown that impulsive behavior of the faded interference signals highly depends on the channel time-dispersiveness. Furthermore, an exact performance of a MB-OFDM system impaired by a TH-UWB system is derived. The comparison of the analytical performance, the empirical simulation and the approximation results show that both approximation methods are valid for low interference-to-noise-ratio (INR), while SαS provides a more accurate approximation for high INR.

3.2 Introduction

Efficient utilization and sharing the available radio spectrum is one of the major issues to be solved due to the rapid growth of wireless communication systems. Consequently, improving the employment method of the radio spectrum with a particular interest in unlicensed reuse of already licensed spectrum has been of significant interest. Ultra wideband (UWB) systems are known as the primary candidate for short-range wireless systems to operate as underlay systems. UWB systems can be divided into two main categories, those based on orthogonal frequency division multiplexing (OFDM), and those based on impulse radio (IR). IR-UWB systems mainly can be implement using direct-sequence codes (DS-UWB) and time-hopping codes (TH-UWB).

Due to the huge bandwidth of UWB systems, interference is one of the most important issues, which may be divided into three categories: narrowband interference from legacy wireless systems (i.e WLAN and WiMAX), multiuser interference (between UWB systems using same transmission techniques) and internet-work interference (between UWB systems using different transmission techniques). The most important part in interference analysis is interference modeling which plays a critical role in system analysis. So far, modeling and mitigation of the first two categories of interferences have been analyzed in many studies. The narrowband interference has been presented in several research works [27, 28]. The authors of [27] provide the BER of a MB-OFDM system in the presence of WiMAX systems showing that WiMAX interference can be modeled as Gaussian approximation (GA). Multiuser interference (MUI) in TH-UWB systems has been analyzed in [29, 30, 31, 32]. It has been shown that the MUI in TH-UWB networks has an impulsive behaviors and the Gaussian approximation of the MUI may underestimate the BER performance of the victim system [29]. Therefore, this has motivated an accurate modeling and optimal receiver design for TH-UWB systems in presence of the MUI signals. In [30, 31, 32], it was shown that the Laplacian, the generalized Gaussian and the α-Stable distributions can be employed in order to describe the MUI distribution in the TH-UWB networks.

To the best of our knowledge, very few investigations have been reported in the literature addressing the issue of internet-work interference (INI) between UWB systems [33, 26]. Outage probability and average BER expressions of a MB-OFDM UWB system in presence of TH-, DS- and MB-OFDM UWB interference signals are provided in [33]. It has been assumed that interference signals from all three different UWB technologies on a MB-OFDM UWB system may be model using Gaussian approximation. The authors of [26] presented an analytical framework to calculate the asymptomatic BER of a bit-interleaved coded-modulation OFDM system impaired by UWB interferences. They showed that, while the GA may be used

to accurately model DS- and MB-OFDM UWB interference signals, the GA of TH-UWB interference signals may underestimate the BER of an OFDM system. However, none of these studies have addressed statistic analysis and modeling of INI from a TH-UWB system into a MB-OFDM UWB system. Moreover, the impact of the TH-UWB's signaling parameters on the distribution of the interference signal is not investigated. Therefore, since an accurate model of the interference signal would be helpful for performance analysis of a MB-OFDM UWB system, the request for deriving and validating such an approximation model has motivated our research.

The contribution of this paper is threefold:

- In [26], although authors proved that the TH-UWB interference has a non-Gaussian distribution, they did not propose an approximation method to model the interference signal. In this paper, an analytical framework to analyze the statistical characteristics of a TH-UWB interference on a MB-OFDM UWB system is presented. Due to the flexibility of the generalized Gaussian (GG) and the Symmetric-α-Stable (SαS) distributions, they are used to model the TH-UWB interference signal. Parameters of the GG and the SαS distributions are estimated using the maximum likelihood method and a characteristic function-based regression-type method, respectively. The accuracy and tractability of the approximation methods are established by means of comparison with the probability and cumulative distribution functions (pdf and cdf, respectively) of the empirical signal.
- The impact of TH-UWB system's parameters on the BER performance of a MB-OFDM UWB system is widely analyzed, where such an analysis does not presently available in the literature. It is shown that the BER of a MB-OFDM UWB system highly depends on time-hopping parameters of the interference signal. Moreover, the effect of the time-dispersive interference channel on the impulsive behaviour of the TH-UWB signal is shown.
- An analytical BER analysis of a MB-OFDM UWB system impaired by an empirical TH-UWB interference is provided. We note that in related works an exact BER of a MB-OFDM system considering the TH-UWB interference as an additive Gaussian noise is provided in [33] and an asymptomatic BER analysis of a BICM-OFDM system impaired by IR-UWB signals have been presented in [26].

The reminder of this paper is organized as follows. Signal and channel models of the MB-OFDM and the TH-UWB systems are presented in Section II. An analytical framework for interference analysis and modeling of the TH-UWB interference is given in Section III. The analytical performance analysis of a MB-OFDM UWB system impaired by a TH-UWB signal is provided in Section IV. In Section V, a comparison of the performance for the exact

analysis, the empirical simulation and the approximation methods are presented, and the conclusion is given in Section VI.

Notation: In this paper, $\lfloor\cdot\rfloor$ and $\lceil\cdot\rceil$ denote the floor and the ceiling functions; $\Re\{\cdot\}$ and $\Im\{\cdot\}$ denote the real part and the imaginary part of a complex number; and $E\{\cdot\}$, $\otimes$ and $(\cdot)^*$ denote statistical expectation, convolution and complex conjugation, respectively.

3.3 System Model

The structural diagram of the investigated scenario is given in Fig. 3.1. Channel and signal models for MB-OFDM UWB and TH-UWB systems are described in [11] and [12], respectively. Subscripts p and s denote desired and interference signals.

3.3.1 MB-OFDM UWB Signal Model

In a MB-OFDM UWB system the UWB spectrum is divided into 14 non-overlapping sub-bands of 528 MHz bandwidth each [11]. In a particular l^{th} time-slot, the binary sequence is divided into blocks of b bits and mapped to M-PSK ($M \triangleq 2^b$) symbols, x_k^l, to form modulated sequences $x \triangleq \{x_1^l \ ... \ x_k^l \ ... \ x_N^l\}$. The modulated symbols are then transmitted over one of the sub-bands using OFDM modulation with N sub-carriers, which is given by:

$$s_p(t) = \sum_{l=-\infty}^{\infty} \sum_{k=0}^{N-1} x_k^l \phi_k(t - lT_s - T_{ZP})) \tag{3.1}$$

where $\phi_k(t) \triangleq \exp(j2\pi\Delta f k t)$, $-T_{ZP} \leq t \leq T_{FFT}$, is the k^{th} basis function of the OFDM modulation, and $T_{FFT} = 1/\Delta f$ is the IFFT duration. Δf, T_s and T_{ZP} are the frequency separation of subcarriers, the OFDM symbol duration and the Zero-Padding duration, respectively.

3.3.2 TH-UWB Signal Model

The TH-UWB system is modeled based on the IEEE 802.15.4a standard [12]. A combination of a Burst Position Modulation (BPM) and a Binary Phase-Shift Keying (BPSK), which determines the position and the polarity of the burst pulses, is used to carry two information bits. In particular, the TH-UWB signal is modeled as:

$$s_s(t) = \sum_{m=-\infty}^{\infty} (1 - 2a^m) \sum_{n=0}^{N_{cpb}} d_n^m p(t - mT_f - b^m T_{BPM} - c^m T_{burst} - nT_c) \tag{3.2}$$

where T_f and T_c are the frame and the chip duration of a TH-UWB signal, respectively. T_{burst} and T_{BPM} are the burst duration and the time shift used by the burst position modulation.

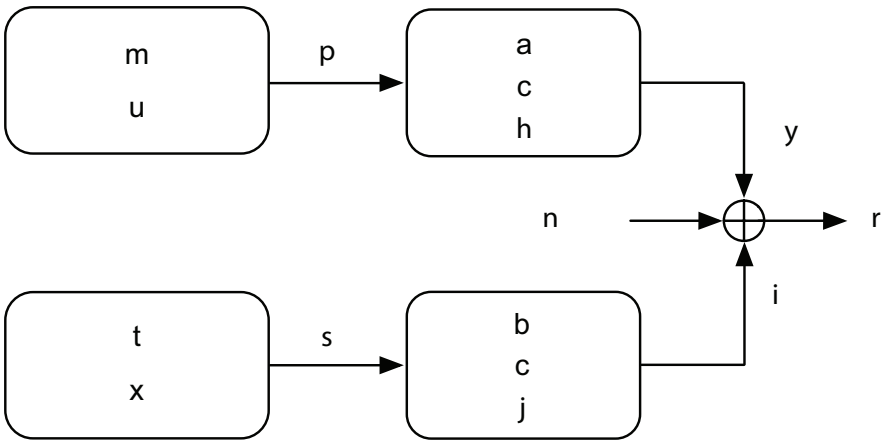

Figure 3.1 System Model.

As shown in Fig. 3.2, the TH-UWB frame is divided into two parts each consisting of a burst position and a guard interval. The guard interval, during which the system is idle, is deployed to reduce inter-symbol-interference effects. The so-called frame duration consists of N_{burst} bursts, whereas, each burst is divided into N_{cbp} consecutive chips ($T_f = N_{burst}\, T_{burst} = N_{burst}\, N_{cbp}\, T_c$). The N_{cpb}, number of chips per burst, varies according to the required data rate. a^m and $b^m \in \{0, 1\}$, are information bits which are encoded into the burst polarity and the burst position, respectively. $d_n^m \in \{-1, +1\}$ and $c^m \in \{0, 1, ..., N_{hop}\}$ denote the scrambling code and the hopping code with N_{hop} burst hoping positions, respectively. $p\,(t)$ is the transmitted UWB pulse with unit energy and T_p width.

3.3.3 Receiver Processing and Channel Models

The received MB-OFDM UWB signal includes three main parts: the desired MB-OFDM UWB signal $y(t)$, the TH-UWB interferer signal $i(t)$, and the additive white Gaussian noise $n(t)$ and is given by:

$$r(t) = \underbrace{s_p(t) \otimes h_p(t)}_{y(t)} + \underbrace{s_s(t - \tau_i) \otimes h_s(t)}_{i(t)} + n(t), \tag{3.3}$$

where $h_p(t)$ and $h_s(t)$ are the channel impulse responses of the desired MB-OFDM UWB system and the interferer channel, respectively. τ_i is the timing offset of the TH-UWB system which is uniformly distributed on $[0, T_s]$. For the MB-OFDM UWB system, a channel model which is proposed by the 802.15.3a task group to provide statistical models for short range, high rate and indoor applications is adopted. As for the TH-UWB system, a channel model which is presented by the 802.15.4a task group to provide models for longer range, low rate,

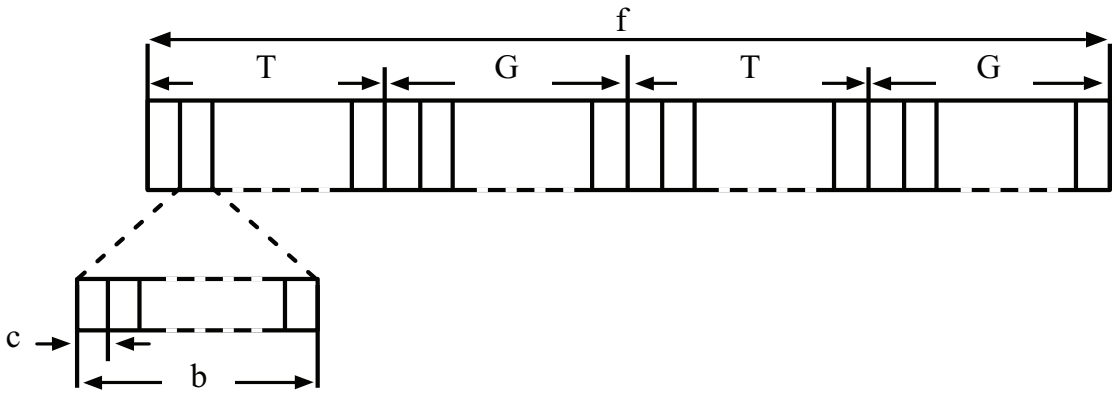

Figure 3.2 The symbol structure of a TH-UWB signal.

indoor and outdoor applications is used. Both models have the same statistical structure which is based on the modified Saleh-Valenzuela model [62]. However, there are some differences in modeling the phase of each ray, the ray arrival rate and the intra-cluster decaying constant [63].

At the MB-OFDM UWB's receiver, $r(t)$ is applied to a filterbank matched to $\phi_k^*(T_s - t)$ to calculate the k^{th} decision metric given by:

$$\begin{aligned} r_k &= r(t) \otimes \phi_k^*(T_s - t)|_{t=T_s} \\ &= x_k \underbrace{\int_0^{T_p} h_p(\varphi) e^{-j2\pi\Delta fk\varphi} d\varphi}_{H_p[k]} + \underbrace{\int_0^{T_{FFT}} s_s(\beta - \tau_i) e^{-j2\pi\Delta fk\beta} d\beta}_{\tilde{i}_k} \underbrace{\int_0^{T_s} h_s(\varphi) e^{-j2\pi\Delta fk\varphi} d\varphi}_{H_s[k]} + n_k, \end{aligned} \tag{3.4}$$

where $H_p[k] = g_k^p e^{j\theta_k}$ and $H_s[k] = g_k^s e^{j\eta_k}$ are the frequency-domain channel gains of the desired and the interference channels for k^{th} subcarrier, respectively. Throughout this paper, it is assumed that g_k^p and g_k^s are independent and identically distributed random variables (RV) which are modeled as independent and identically distributed (i.i.d) Rayleigh distribution [64]. Furthermore, T_{ch_p} and T_{ch_s} are the length of the desired and the interference channel impulse responses, respectively. The contribution of the interference signal at the k^{th} subcarrier then can be obtained by simplifying i_k using (3.2):

$$\begin{aligned} i_k &= g_k^s e^{j\eta_k} \tilde{i}_k \\ &= g_k^s e^{j\eta_k} \int_0^{T_{FFT}} s_s(\beta - \tau_i) e^{-j2\pi\Delta fk\beta} d\beta \\ &= g_k^s e^{j\eta_k} \sum_{m=M_l^{(l)}}^{M_u^{(l)}} (1 - 2a^m) \sum_{n=0}^{N_{cpb}-1} d_n^m \vartheta(k, \tau_i, \tau_{TH}(m, n, b^m, c^m)), \end{aligned} \tag{3.5}$$

where

$$\vartheta(k,\tau_i,\tau_{TH}(m,n,b^m,c^m)) \;=\; \int_{T_l^{(l,n)}}^{T_u^{(l,n)}} p\left(\beta-\tau_{TH}(m,n,b^m,c^m)-\tau_i\right)e^{-j2\pi\Delta f k\beta}\mathrm{d}\beta, \quad (3.6)$$

with $\tau_{TH}(m,n,b^m,c^m) \triangleq mT_f + b^mT_{BPM} + c^mT_{burst} + nT_c$. The lower and the upper bounds of the summation, $\{M_l^{(l)}, M_u^{(l)}\}$, are obtained corresponding to the number of the TH-UWB frames arriving within the l^{th} MB-OFDM symbol which are given by:

$$\begin{cases} M_l &= \lfloor lT_s/T_f \rfloor \\ \\ M_u &= \lfloor (l+1)T_s/T_f \rfloor \end{cases}, \quad (3.7)$$

For instance, Fig. 3.3-(a) depicts that how one OFDM symbol covers multiple TH-UWB frames. Considering $T_s \simeq 3T_f$, it can be calculated from (3.7) that four TH-UWB frames are arrived within the l^{th} MB-OFDM frame. In contrast, 3.3-(b) shows that given $T_f \simeq 3T_s$, l^{th} MB-OFDM frame overlaps with a portion of a TH-UWB frame. The integration interval $[T_l^{(l,n)}, T_u^{(l,n)}]$ are acquired from the position of the pulse bursts within each TH-UWB frame, which is given by:

$$\begin{cases} T_l^{(l,n)} &= min\big\{max\{lT_s, \tau_{TH}(m,n,b^m,c^m)\}, (l+1)T_s\big\} \\ \\ T_u^{(l,n)} &= max\big\{min\{(l+1)T_s, \tau_{TH}(m,n+1,b^m,c^m)\}, lT_s\big\} \end{cases}, \quad (3.8)$$

Considering Fig. 3.3-(b) lower and upper bounds of the integral corresponding to l^{th} MB-OFDM symbol, $T_l^{(l,n)}$ and $T_u^{(l,n)}$, can be calculated from (3.8) for each chip duration (n to $n+1$). However, as $(l+1)^{th}$ MB-OFDM symbol dose not overlap with any TH-UWB burst signal, the lower and upper bounds of the integral are equal to $(l+1)T_s$ which leads to (3.6) equal to zero.

3.4 Interference Analysis and Modeling

Since determining the exact pdf of a TH-UWB interferer signal is a complex and time consuming process, an accurate probability model should be utilized for performance analysis of a MB-OFDM UWB system impaired by a TH-UWB interference. Firstly, in order to model the interference distribution, we need to characterize its statistical nature. Generally, the pdf of an interference-plus-noise (IPN) signal is required to analyze the performance of the

Figure 3.3 Different symbol structures of (a) a MB-OFDM symbol covers multiple TH-UWB frames (b) one TH-UWB frame overlaps with multiple MB-OFDM symbols.

victim system or to design an optimum receiver. However, in order to study the impact of time-hopping parameters of the TH-UWB interference on the performance of a MB-OFDM

system, only the effect of the interference (high interference-to-noise ratio (INR)) is explored in section 3.4.1.

3.4.1 Interference characterization

As mentioned previously, the statistical model of the MUI in TH-UWB networks has been widely investigated in the literature [29, 65]. In TH-UWB networks, considering the transmission of a burst pulse whose duration is much smaller than the frame duration, the distribution of the MUI is no longer Gaussian and it has more impulsive nature [29]. Similarly to the MUI in TH-UWB networks, the inter-network interference from a TH-UWB into a MB-OFDM UWB systems has an impulsive nature [26]. Although previous investigations on the MUI suggested that its impulsiveness only depends on N_{burst} and N_{cbp} of the TH-UWB system and the INR [65], subsequent studies have shown that the impulsiveness of INI not only is a function of these parameters but also depends on the ratio of the MB-OFDM UWB and TH-UWB symbols' durations (i.e. T_s to T_f). For instance, in TH-UWB networks, for a fixed number of chips, increasing N_{burst} results in an increment in the impulsive behavior of the interference [65]. However, our studies on INI show that according to the ratio of T_s to T_f and for the same fixed value of N_{cbp}, increasing N_{burst} may lead to a reduction in the impulsiveness of the interference signal.

This discrepancy is due to the difference between the frame structures of the TH-UWB and the MB-OFDM UWB systems. To make this explicit let us define interference duty cycle which is used to measure the impulsiveness of INI. The interference duty cycle is defined as the ratio of T_i to T_s, where T_i is the TH-UWB bursts' duration corresponding to one OFDM symbol which may be obtained from (3.5) and (3.8). The interference duty cycle is conversely proportional to the amplitude of the INI pdf at zero magnitude. Considering MUI in a TH-UWB network, victim and interferer systems have an identical frame structure. Therefore, changing the time-hoping parameters does not affect the overlapping ratio of the victim and the interferer signals, hence the interference duty cycle remains unchanged. However, in coexistence of the MB-OFDM UWB and the TH-UWB systems, where the frame structures are different (Fig. 3.4), the number of TH-UWB symbols interfering with one MB-OFDM symbol is a function of the signaling parameters (N_{burst} and N_{cbp}) of the TH-UWB system (cf. (3.5) - (3.8)). Consequently, changing the time-hopping parameters of the interferer system affects both the TH-UWB signal distribution and the overlapping ratio of the victim and interfering systems (i.e interference duty cycle).

Let us give an intuitive clarification to this fact. To study the effect of TH-UWB parameters on its statistical characteristics, two different scenarios are examined. In the first scenario, the variation of the $N_{burst} = \{8, 32, 64\}$ for a fixed $N_{cbp} = 4$ is studied. While, in

the second one, the variation of the $N_{cbp} = \{4, 16, 32\}$ for a fixed $N_{burst} = 8$ is investigated. Fig. 3.4 depicts the frame structure of the TH-UWB signal for these scenarios. As shown, by changing N_{burst} or N_{cbp} for each scenario, each OFDM symbol overlaps approximately with four, one and a fraction of one TH-UWB symbol. In order to study the distribution of the INI, the empirical histogram of the interference signal for these scenarios are shown in Fig. 3.5. It can be observed that for all scenarios, the distribution of the TH-UWB signal compared to the pdf of the Gaussian distribution is not only highly impulsive but also it has heavy-tailed distribution.

For the first scenario (Fig. 3.4 (b)), by increasing the number of the bursts while $T_s/T_f > 1$ (for instance from 8 to 32), the total number of the pulses, overlap with each OFDM symbol, is reduced. This fact leads to an interference duty cycle reduction. Hence, the distribution of the interference signal deviates from the Gaussian distribution and becomes more impulsive (Fig. 3.5 (b) compared to Fig. 3.5 (a)). On the other hand, increasing N_{burst} when $T_s/T_f < 1$ (for instance from 32 to 64), it does not affect the interference duty cycle. Therefore, the pdf of the INI does not change. In contrast, considering the second scenario (Fig. 3.4 (c)), while $T_s/T_f > 1$, increasing N_{cpb} (from 4 to 16) does not affect the total number of the pulses overlap with each OFDM symbol, therefore the pdf of the interference signal does not change. However, for $T_s/T_f < 1$, the number of burst pulses is grown as N_{cpb} increases from 16 to 32, which leads to an interference duty cycle growth. Hence, the interference distribution tends to the Gaussian and becomes less impulsive (Fig. 3.5 (c) compared to Fig. 3.5 (a)). Consequently, this implies that there is an obvious relationship between the impulsive behavior of the interference signal and the ratio of T_s to T_f.

3.4.2 Interference Modeling

After investigating the statistical nature of the TH-UWB interference, let us now drive a distribution model to accurately approximate the total noise (INI plus AWGN noise). In order to model the impulsiveness and the heavy-tailedness of the MUI's distribution in TH-UWB networks, a number of approximation models such as the generalized Gaussian (GG) [37], the symmetric α-stable (SαS) [32], the Gaussian-Laplacian mixture (GM) [38] and the Gaussian mixture [35] distributions have been presented in the literature. Since the GG and the SαS distributions have flexible classes of pdfs, in the sequel, they are employed to develop accurate and tractable models for the IPN signal ($z(t) = i(t) + n(t)$).

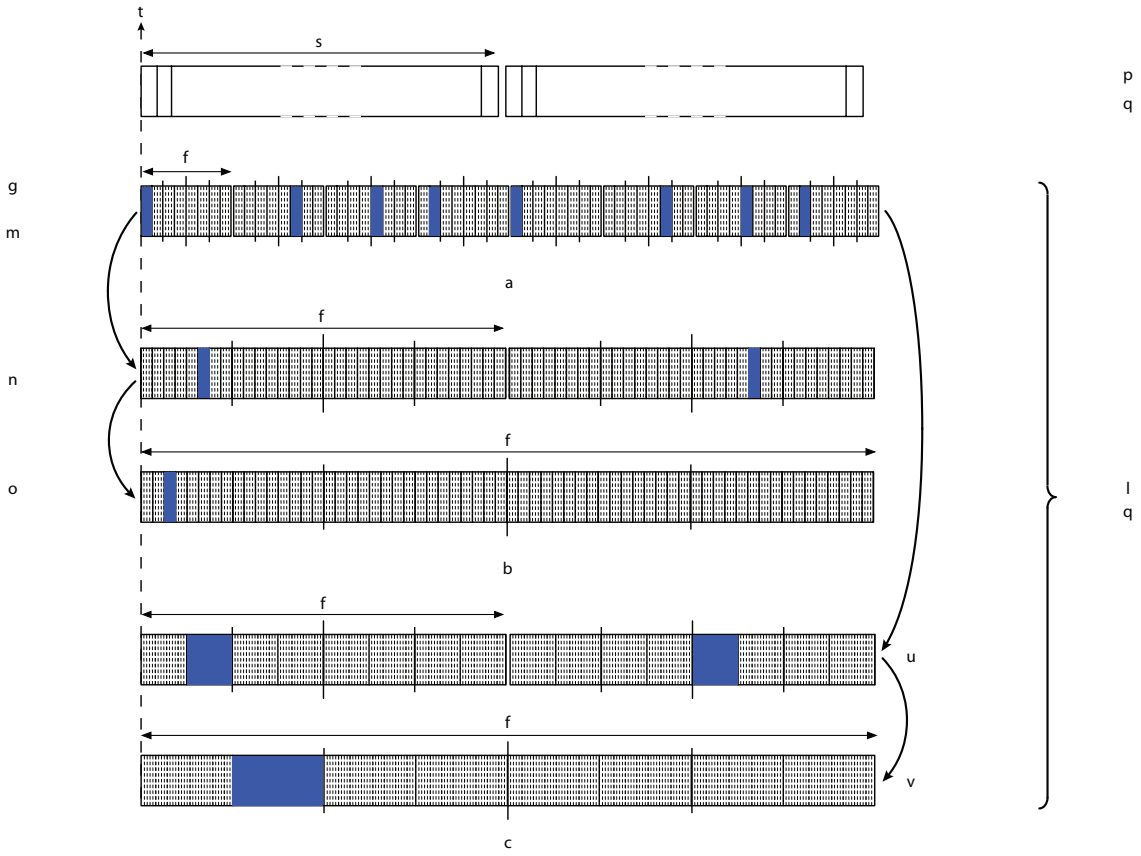

Figure 3.4 The symbol structure of (a) a MB-OFDM signal and a TH-UWB signal with $N_{burst} = 8$ and $N_{cbp} = 4$, (b) TH-UWB signals with $N_{cbp} = 4$ and $N_{burst} = \{32, 64\}$ and (c) TH-UWB signals with $N_{burst} = 8$ and $N_{cbp} = \{16, 32\}$.

Generalized Gaussian Distribution

A random variable z has a generalized Gaussian distribution if its pdf is given by [66]:

$$P_z(z) = \frac{p}{2\Gamma(1/p)A(p,\sigma)} e^{-\left(\frac{|z-\mu|}{A(p,\sigma)}\right)^p} \tag{3.9}$$

where $A(p,\sigma) = \left(\frac{\sigma^2\Gamma(1/p)}{\Gamma(3/p)}\right)^{1/2}$, p, σ^2 and μ are the scale parameter, the shape parameter, the variance and the mean of the GGD, respectively. $\Gamma(x)$ is the Gamma function. The value of p determines the degree of impulsiveness of the GGD relative to the Gaussian distribution. The GGD includes standard Gaussian distribution ($p = 2$) and Laplacian distribution ($p = 1$) as two special cases. Therefore, by properly estimating p from the empirical IPN signal, the GGD is able to model the TH-UWB interference. There are different estimation methods such as Maximum Likelihood (ML), moment and kurtosis for estimating the shape parameter of the GGD. In this paper, the Maximum Likelihood is used to estimate the shape parameter and

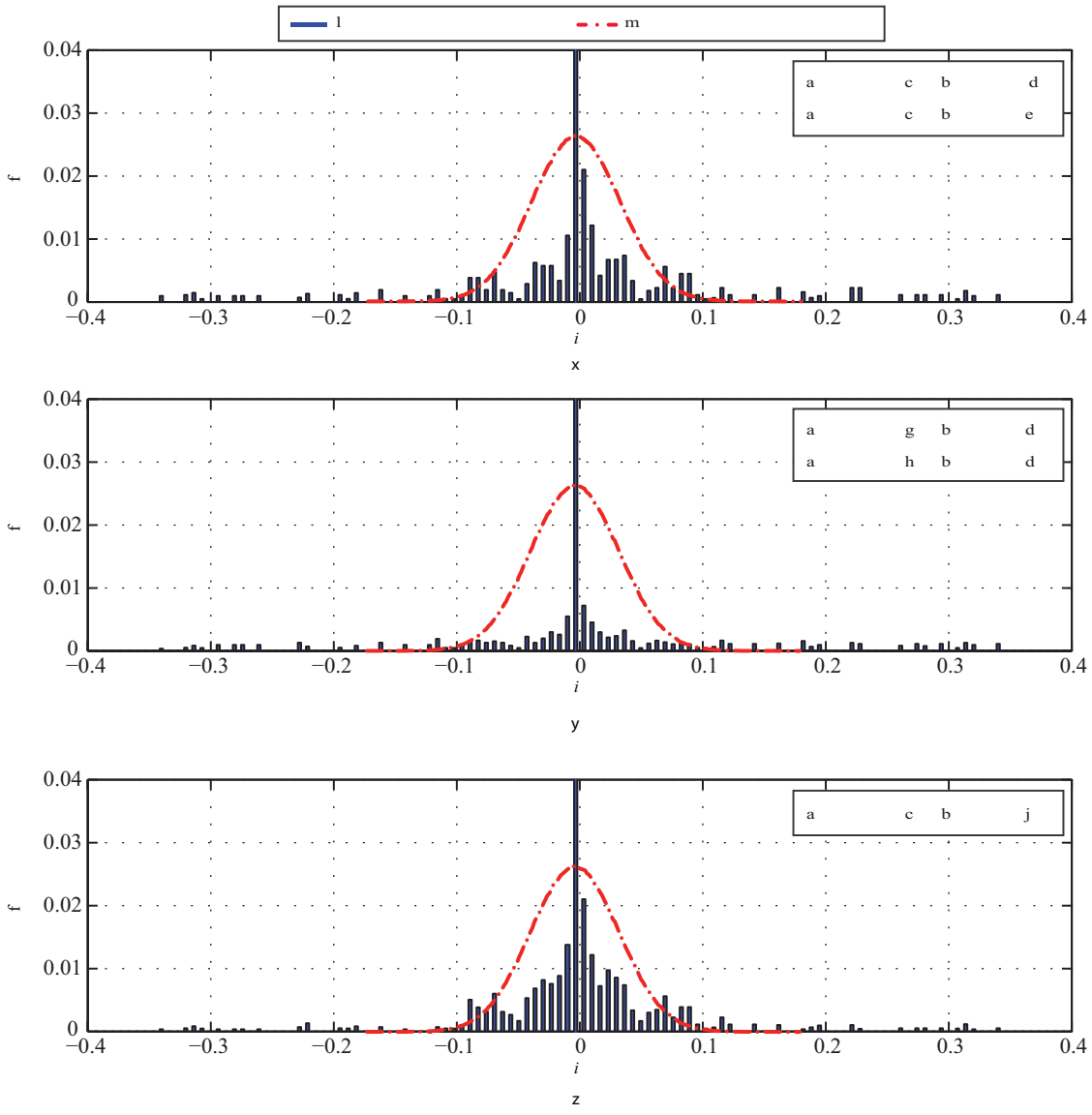

Figure 3.5 Empirical TH-UWB interference signal's pdf plotted with the Gaussian distribution for different time-hoping parameters corresponding to different scenarios.

the variance of the GGD [67]. Given N_s interference plus noise i.i.d samples, the likelihood function is expressed by:

$$\begin{aligned} L(z;\sigma,p) &= \log\prod_{i=1}^{N_s} P_z(z_i;\sigma,p) \\ &= N_s \log\Big(\frac{p}{2\Gamma(1/p)A(p,\sigma)}\Big) - \Big(\frac{1}{A(p,\sigma)}\Big)^p \sum_{i=1}^{N_s} |z_i|^p \end{aligned} \tag{3.10}$$

The optimal estimates of σ and p are obtained by maximizing the likelihood function. In order to determine the estimate of σ, the first derivation of 3.10 with respect to σ is set to zero

$$\frac{\partial L(z;\sigma)}{\partial \sigma} = \frac{N_s}{\sigma} - \frac{p}{(\frac{\Gamma(1/p)}{\Gamma(3/p)})^{p/2}\sigma^{p+1}} \sum_{i=1}^{N_s} |z_i|^p = 0 \tag{3.11}$$

which it has a unique and positive solution and σ_{est} is obtained as

$$\sigma_{est} = \left[\frac{p}{N_s}\Big(\frac{\Gamma(3/p)}{\Gamma(1/p)}\Big)^{1/2} \sum_{i=1}^{N_s} |z_i|^p\right]^{1/p} \tag{3.12}$$

In order to estimate p, the root of the first derivation of the maximum likelihood function, with respect to p, has to be obtained. However, $\frac{\partial L(z;\sigma,p)}{\partial p} = 0$ does not have a closed form solution. Therefore, a root-finding algorithm called the Secant method [68] is adopted to find the estimate of p which maximizes the likelihood function. The secant method is an iterative root-finding algorithm which uses a secant line passing through two points of the function $f(p) = \frac{\partial L(z;\sigma,p)}{\partial p}$ to approximate its root. Hence, considering two approximated points $(p_{k-1}, f(p_{k-1}))$ and $(p_k, f(p_k))$, the Secant algorithm returns an estimate of the function's root as p_{k+1} [68]:

$$p_{k+1} = p_k - \frac{p_k - p_{k-1}}{f(p_k) - f(p_{k-1})} f(p_k) \tag{3.13}$$

where $f(p)$ is the partial derivation of (10) which is given by:

$$\frac{\partial L(z;\sigma,p)}{\partial p} = N_s\left[\frac{1}{p}+\frac{3\psi(1/p)}{2p^2}-\frac{3\psi(3/p)}{2p^2}\right] + \left[\log\Big(\frac{|z_i|}{A(p,\sigma)}\Big)+\frac{3\psi(1/p)}{2p}-\frac{3\psi(3/p)}{2p}\right]\sum_{i=1}^{N_s}\Big(\frac{|z_i|}{A(p,\sigma)}\Big)^p \quad (3.14)$$

where $\psi(.)$ is digamma function. It has been shown that the convergence rate of the Secant method is superlinear with 1.62 [68]. Moreover, it is noted that the Secant algorithm requires two initial points (p_0 and p_1), which have to be determined cautiously. Hence, in order to avoid convergence failure due to the faulty estimation of initial points, the excess kurtosis method which is defined as $\mathfrak{E} = [E\{z^4\}/(E\{z^2\})^2]-3$, is adopted to compute the initial guess for p_0. Using the definition of m^{th} moments of the GGD [69], p_0 is calculated by solving the following equation:

$$\mathfrak{E} = \frac{\Gamma(5/p)\Gamma(1/p)}{(\Gamma(3/p))^2}-3 \quad (3.15)$$

Since, in order to accelerate the convergence to the optimum solution, the signs of $f(p_0)$ and $f(p_1)$ should be different, p_1 is obtained satisfying this condition [68]. However, if we could not find a proper guess for the second point, we can easily choose it a value close to p_0 (e.g. $p_1 = 0.99p_0$).

Symmetric α-Stable

SαS is another well-suited distribution for modeling impulsive interference signals with heavy-tailed distributions. The SαS distribution has been used to model the impulsive behaviour of a wide range of noises in different networks such as UWB [70] and cognitive radios [71]. The SαS distribution is described by its characteristic function (CF) [39]:

$$\begin{cases}\exp\Big(j\mu w-\sigma^\alpha|w|^\alpha\big[1-j\beta\text{sign}(w)\tan(\pi\alpha/2)\big]\Big), & \alpha\neq 1\\ \exp\Big(j\mu w-\sigma|w|\big[1+j\beta\frac{\pi}{2}\text{sign}(w)\log(|w|)\big]\Big), & \alpha=1\end{cases}, \quad (3.16)$$

where $\alpha \in (0,2]$, $\sigma \in R_0^+$, $\beta \in [-1,1]$ and $\mu \in R$ are a characteristic exponent, a scale parameter, a skewness parameter and a location parameter, respectively. The characteristic exponent measures the thickness of the distribution's tails and enables α-stable distribution to model a wide range of impulsive signals. The scale parameter is similar to the variance

of the Gaussian distribution and measures the distribution's spread around the location parameter. Similar to GGD, in order to model the impulsive interference signal using SαS, these parameters have to be estimated. Koutrouvelis [72] proposed an iterative regression-type method using the CF in order to estimate these parameters. Based on an initial estimate of the parameters, the regression-type method proceeds iteratively until a predefined convergence criterion is satisfied. Since, the sample characteristic function, $\hat{\phi}(t)$, of noise samples is a consistent estimator of the characteristic function $\phi(t)$, two linear expression are obtained between the CF and the distribution's parameters. In order to estimate α and σ a linear regression model is given by:

$$y_k = m + \alpha w_k + e_k, \qquad k = 1, 2, \ldots, K \tag{3.17}$$

where $t_k = \frac{\pi k}{25}$, $k = 1, 2, ..., K$ is a set of real number which depends on the sample size N_s, e_k denotes error term, and $m = \log(2\sigma^\alpha)$. Hence, α and σ are estimated by regressing $y_k = \log\big(-\log|\hat{\phi(t_k)}|^2\big)$ on $w_k = \log|t_k|$. where $\hat{\phi(t)} = \frac{1}{N_s}\sum_{i=1}^{N_s}\exp(jtz_i)$ is the sample characteristic function of the noise sample, z_i. The second regression model for estimating β and μ is given by:

$$z_l = \mu u_l - \beta\sigma^\alpha \tan\Big(\frac{\pi\alpha}{2}\Big) sign(u_l)|u_l|^\alpha + \varepsilon_l, \qquad l = 1, 2, \ldots, L \tag{3.18}$$

where $u_l = \frac{\pi l}{50}, l = 1, 2, ..., L$ and e_k are an appropriate real number and error term, respectively. Once α and σ are obtained, for a suitable value of L, $z_l = \arctan\big(\frac{\Im\{\phi(u_l)\}}{\Re\{\phi(u_l)\}}\big) + \pi k_n(u_l)$ is calculated for u_l and used to fit the regression model (3.18). In order to satisfy a pre-specified convergence criterion, the aforementioned steps are repeated with the estimated parameters as initial guesses.

3.4.3 Simulation Results for Interference Modeling

In this section in order to inquire into the accuracy of the aforementioned approximation methods, their pdf and cdf are compared with the ones of the empirical interference signal. For this purpose, parameters of the GG and SαS distributions are estimated from the empirical IPN signal. Once this parameters are estimated, interference samples are generated using these random processes. Generally, a set of realizations of random variables can be directly obtained from its inverse cumulative distribution function. However, the closed form expression of cdf and inverse cdf of GG and SαS distributions are not available. Therefore, an alternative method is to express GG and SαS distributed random variables as functions of other random variables whose cdf or inverse cdf can be evaluated numerically. Consequently,

the approaches presented in [73, 74] are adopted to generate GG and SαS distributed random variables, respectively. Moreover, the signaling parameters' (N_{burst} and N_{cpb}) effects on the impulsive behaviour of the interference signal is studied. Furthermore, the effect of the interference channel on the distribution of the received interference is investigated.

Comparing the approximation methods

Fig. 3.6 depicts the stochastic properties of the empirical signal and the approximation methods when the INR equals to 0dB and 20dB. In order to study the impulsive behaviour of the interference signal, the interference channel is ignored. As shown in Fig. 3.6 (a) and (b), for a weak TH-UWB signal (low INR), where the empirical IPN signal tends to Gaussian distribution, both distributions precisely approximate the IPN signal. However, by increasing INR, the IPN becomes more impulsive and its distribution deviates from the Gaussian distribution (Fig. 3.6(c) and (d)). It is seen that the SαS distribution tends to perfectly follow the distribution of the empirical interference-plus-noise signal around the origin as well as the tail. However, the GG distribution which contradicts the Winsor's principal (all distributions are Gaussian in the middle) has more peaky shape around the origin and it does not perfectly follow the tails of the empirical IPN signal.

Studying the effects of time-hopping parameters

As mentioned in section 3.4.1, the impulsive behaviour of the interference signal is a function of the signaling parameters (i.e. N_{burst} and N_{cpb}) of the TH-UWB system and T_s/T_f. In the sequel, it is shown how changing N_{burst} and N_{cpb} adversely affects the impulsive behaviour of the interference signal. Since the SαS distribution is defined with four different parameters, we choose the shape parameter of the GG distribution (which measures the impulsiveness of interference signal) to investigate the effect of the signaling parameters. To do so, the variation of the shape parameter as a function of the TH-UWB system's signaling parameters is illustrated in Fig. 3.7. It is assumed that SNR = 30 and SIR = 10. It can be observed from 3.7-(a) that for the case where $T_s < T_f$, (e.g. $\{N_{cpb} = 4,\ N_{burst} < 16\}$), increasing the number of bursts leads to more impulsive interference with a relatively smaller estimated value of the shape parameter. However, as mentioned before, for $T_s/T_f < 1$, the interference duty cycle remains constant with increasing N_{burst} and consequently p floors out to a constant value. In contrast, given $T_s/T_f > 1$ (e.g. $\{N_{burst} = 4,\ N_{cpb} < 32\}$) as shown in 3.7-(b), increasing N_{cpb} does not affect the shape parameter of the interference signal. The reason is that, the total number of the TH-UWB chips per each OFDM symbol remains unchanged. However, for the case where the TH-UWB's symbol duration is bigger than the OFDM's one, the

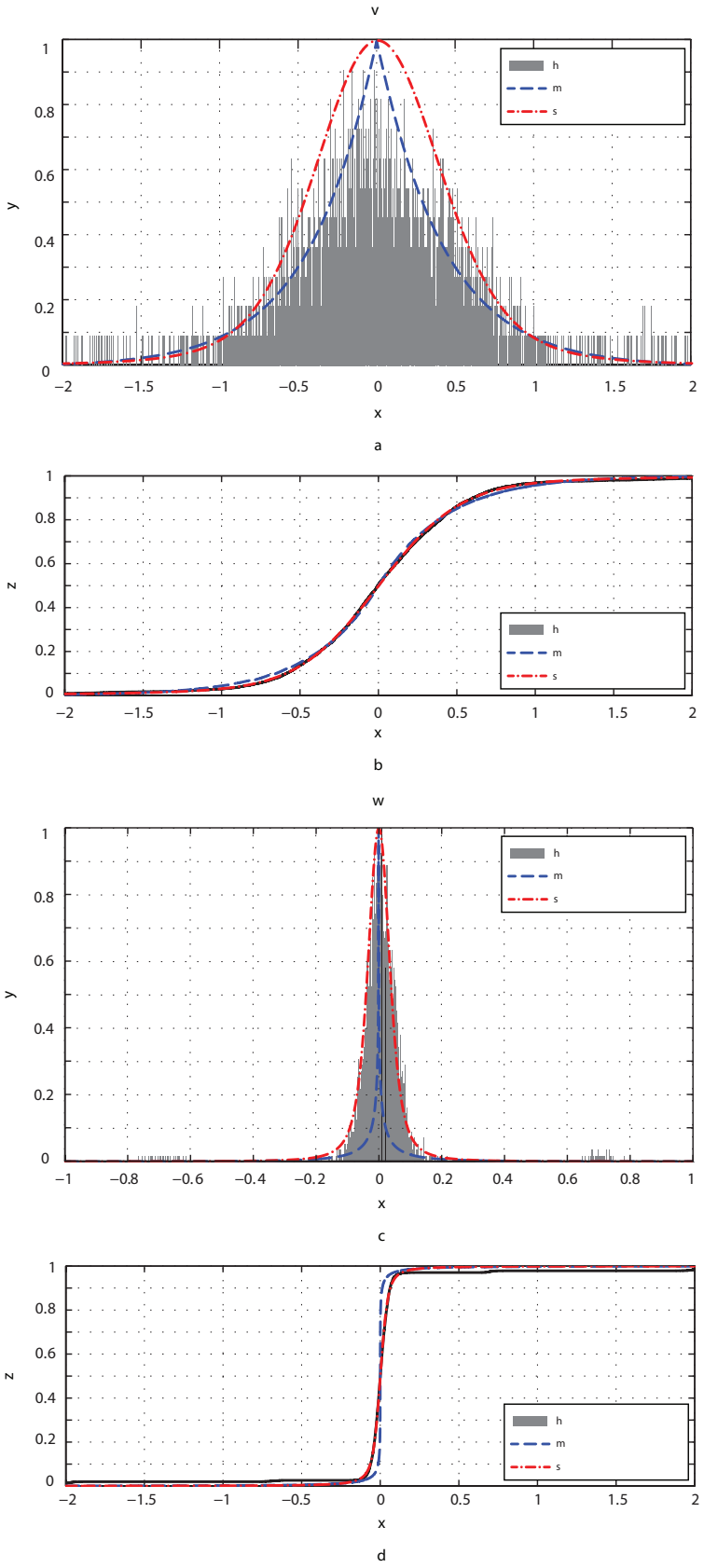

Figure 3.6 A comparison of the pdf and cdf of the interference plus noise signal with GGD and SαS distributions (a) and (b) for INR = 0dB, (c) and (d) for INR = 20dB, respectively.

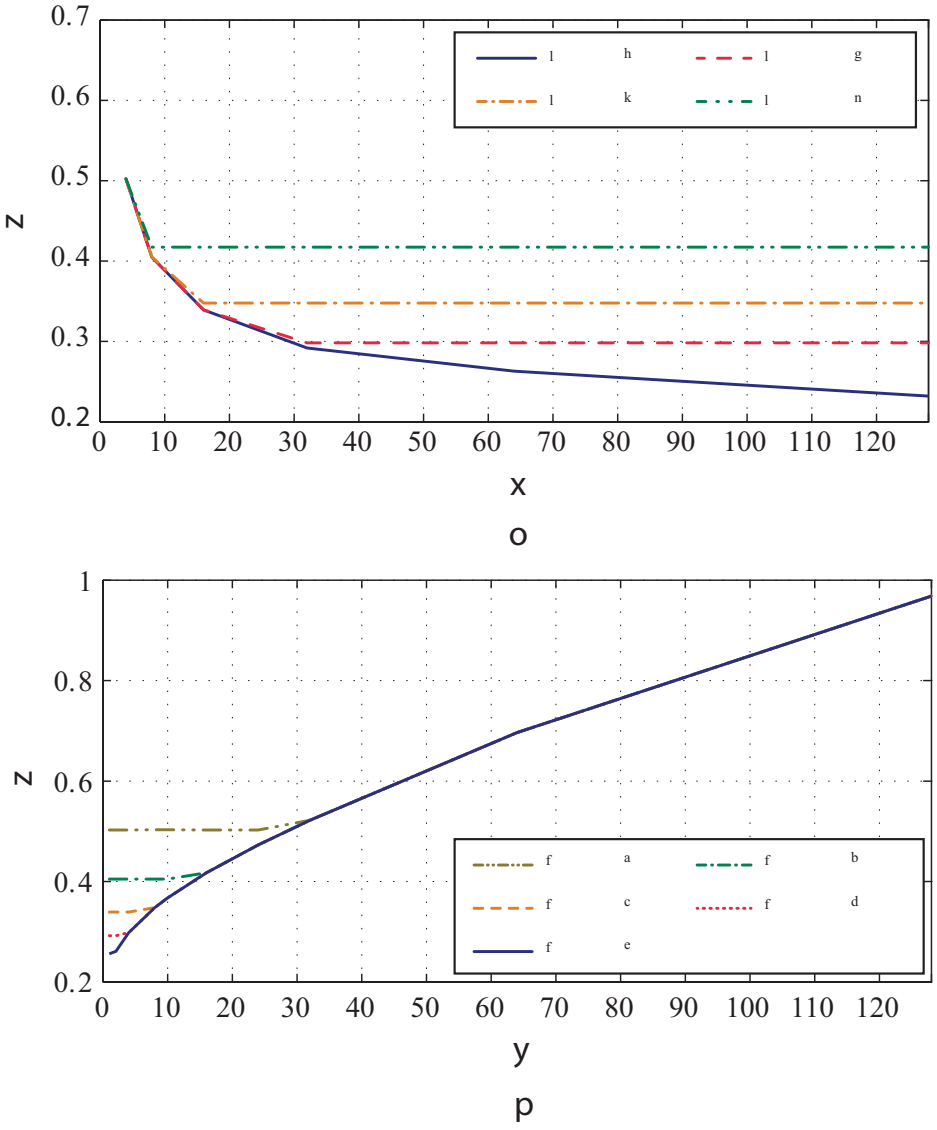

Figure 3.7 Shaping parameter versus interference signal's time-hopping parameters in order to study the effect of the TH-UWB's signaling parameters on the impulsive behaviour of the interference signal (a) p, vs. N_{burst} and (b) p, vs. N_{cpb} for SIR = 10 dB and SNR = 30 dB.

shape parameter of the interference signal monotonically grows as N_{cpb} increases, due to the fact that the interference duty cycle tends to one, hence, the interference process approaches to a less impulsive distribution by the Central Limit Theorem. Since, realizing date rates is performed by different signaling parameters [12], one can reduce the impulsiveness of the generated interference for that date rate. For instance, considering a TH-UWB signal of 27.24 Mb/s the INI signal is more impulsive ($p = 0.5$) for $\{N_{burst} = 128, N_{cpb} = 32\}$ compared to $\{N_{burst} = 32, N_{cpb} = 128\}$ where $p = 0.98$. Consequently, our results show that choosing the proper TH-UWB system's properties may reduce the destructive effect of the INI on the MB-OFDM UWB system's performance. Also, Fig. 3.7 supports the interference characterization of 3.4.1.

Examining the effects of the fading interference channel

Fig. 3.8 illustrates the effect of the fading channel on the distribution of the interference signal. Since, the interference channel's characteristics (802.15.4.a channel [75]) are different in various environments (such as office, residential, industrial and etc.), they adversely affect the distribution of the interference signal. Note that among all available scenarios [75], non line-off-sight (NLOS) residential environment has the shortest RMS delay spread and the highest number of paths capturing 85% of the channel energy (NP85%). In contrast, the line-off-sight (LOS) outdoor channel has the longest RMS delay spread and lowest NP85%. Fig. 3.8 (a-c) show the histogram of the empirical IPN signal in AWGN, residential with NLOS and open outdoor with LOS environments, respectively. The NLOS-residential environment is more time-dispersive compared to the LOS-outdoor channel. It can be seen from Fig. 3.8-(b) that since the LOS-outdoor environment does not have severe time-dispersion parameters, it does not significantly affect the pdf of the interference signal. However, in the NLOS-residential environment (Fig. 3.8-(c)), the impulsiveness of the IPN signal is decreased due to the time-dispersiveness characteristics of the channel.

3.5 Performance Analysis

In this section, we adopt the framework presented in [27] to provide an analytical analysis of the exact BER performance of a MB-OFDM system in the presence of a TH-UWB signal. From (3.5) and considering coherent reception, the decision metric, d_{x_k}, for subcarrier k is given by:

$$\begin{aligned} Re\{e^{-j\theta_k} r_k\} &= \Re\{e^{-j\theta_k} x_k H_p[k]\} + \Re\{e^{-j\theta_k} \tilde{i}_k H_s[k]\} + \Re\{e^{-j\theta_k} n_k\} \\ &= y_k + i_k + \nu_k = d_{x_k} \end{aligned} \tag{3.19}$$

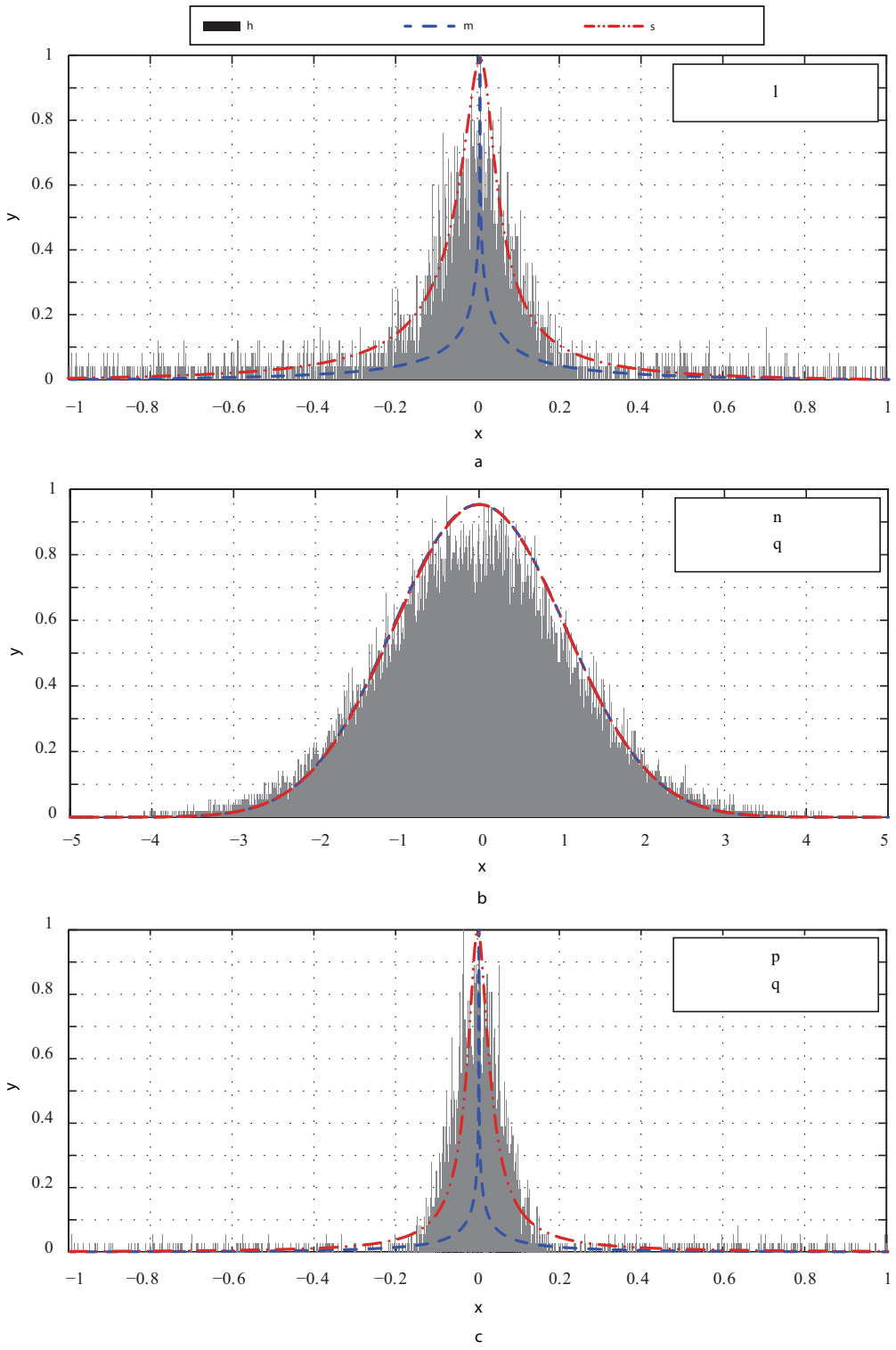

Figure 3.8 A comparison of the empirical interference plus noise signal's pdf with GG and SαS distributions considering different interference channel (a) the AWGN, (b) the residential environment with NLOS link and (c) the open outdoor environment with LOS scenario. $N_{cpb} = 32$, $N_{burst} = 32$.

It is noted that since the BER of the QPSK modulation and BPSK modulation are the same, without loss of generality, QPSK modulation at the MB-OFDM system can be replaced with two independent BPSK modulations, without affecting the BER performance of the system [27]. Thus, we consider x_k^l as a real BPSK symbol which yields $y_k = x_k^l g_k^p$. The noise component ν_k is the filtered Gaussian noise, and the interference component i_k substituting (3.5) into (3.19) can be expressed by:

$$i_k = g_k^s \cdot \Re\left\{ e^{-j(\theta_k - \phi_k)} \sum_{m=M_l}^{M_u} (1-2a^m) \sum_{n=0}^{N_{cpb}-1} d_n^m \vartheta(k, \tau_i, \tau_{TH}(m,n,b^m,c^m)) \right\} \tag{3.20}$$

The BER of a MB-OFDM system for subcarrier k using the moment generating function of the decision metric is given by [76]:

$$P_e(k) = Pr\{d_{x_k} < 0\} = \frac{1}{2\pi j} \int_{c-j\infty}^{c+j\infty} \Phi_{d_{x_k}(s)} \frac{\mathrm{d}s}{s} \tag{3.21}$$

where c is a real-valued parameter which assures the convergence of the above mentioned integral [76]. $\Phi_{d_{x_k}(s)}$ is the MGF of d_{x_k} which is given by:

$$\begin{aligned} \Phi_{d_{x_k}}(s) &\triangleq \mathbb{E}\{e^{-sd_{x_k}}\} \\ &= \mathbb{E}\left\{ e^{-s(y_k+i_k+v_k)} \right\} \end{aligned} \tag{3.22}$$

Given y_k, i_k and v_k are independent variables and $x_k \in \{\pm 1\}$, we can simplify (3.22) to:

$$\Phi_{d_{x_k}}(s) = \Phi_{g_k^p}(s) \Phi_{i_k}(s) \Phi_{v_k}(s) \tag{3.23}$$

in which $\Phi_{g_k^p}(s) = 1 - \sqrt{2\pi} s e^{s^2/2} Q(s)$ and $\Phi_{v_k}(s) = e^{\sigma_v^2 s^2/2}$ are the MGF of the desired channel's gain and the Gaussian noise, respectively. $\Phi_{i_k}(s)$ is the MGF of the interference signal which is represented by:

$$\Phi_{i_k}(s) = \mathbb{E}_{\tau_i}\left\{ \mathbb{E}_{g_k^s}\left\{ \Phi_{i_k}(s|\tau_i, g_k^s) \right\} \right\} \tag{3.24}$$

Exploiting (3.20), the MGF of i_k conditioned on the τ_i and g_k^s $\left(\Phi_{i_k}(s|\tau_i, g_k^s) = \mathbb{E}\{e^{-si_k}|\tau_i, g_k^s\} \right)$

becomes:

$$\Phi_{i_k}(s|\tau_i, g_k^s) \;=\; \mathbb{E}\Bigg\{\exp\Bigg[-s\Re\Big\{g_k^s \sum_{m=M_l}^{M_u}(1-2a^m)\sum_{n=0}^{N_{cpb}-1} d_n^m \vartheta(k,\tau_i,\tau_{TH}(m,n,b^m,c^m))\Big\}\Bigg]\Bigg\} \tag{3.25}$$

in which $a^m \in \{0,1\}$ and $d_n^m \in \{\pm 1\}$. Since $\tau_{TH}(m,n,b^m,c^m) \triangleq mT_f + nT_c + b^m T_{BPM} + c^m T_{burst}$ consists of two independent discrete random variables, $\upsilon_1 = b^m T_{BPM}$ and $\upsilon_2 = c^m T_{burst}$, its probability density function can be obtained through convolution of pdf of these variables, $p_{\tau_{TH}}(\tau_{TH}) = p_{\upsilon_1}(\upsilon_1) * p_{\upsilon_2}(\upsilon_2)$, which yields to:

$$p_{\tau_{TH}}(\tau_{TH}) = \frac{1}{2N_{hop}} \sum_{C=0}^{N_{hop}-1}\sum_{b=0}^{1} \delta(\tau_{TH} - mT_f - nT_c - CT_{burst} - bT_{BPM}) \tag{3.26}$$

Thus, $\Phi_{i_k}(s|\tau_i, g_k^s)$ can be accurately derived by averaging e^{-si_k} with respect to a^m, d_n^m and $\tau_{TH}(m,n,b^m,c^m)$, which can be obtained as (the inner expectation is over a^m and d_n^m):

$$\begin{aligned}
\Phi_{i_k}(s|\tau_i, g_k^s) &= \mathbb{E}_{\tau_{TH}}\Bigg\{\mathbb{E}\Bigg\{\exp\Big[-s\Re\Big\{g_k^s\sum_{m=M_l}^{M_u}(1-2a^m)\sum_{n=0}^{N_{cpb}-1} d_n^m\vartheta(k,\tau_i,\tau_{TH}(m,n,b^m,c^m))\Big\}\Big]\Bigg\}\Bigg\} \\
&= \mathbb{E}_{\tau_{TH}}\Bigg\{\prod_{m=M_l}^{M_u}\prod_{n=0}^{N_{cpb}-1}\mathbb{E}\Big\{\exp\Big[-s\Re\big\{g_k^s(1-2a^m)d_n^m\vartheta(k,\tau_i,\tau_{TH}(m,n,b^m,c^m))\big\}\Big]\Big\}\Bigg\} \\
&= \mathbb{E}_{\tau_{TH}}\Bigg\{\prod_{m=M_l}^{M_u}\prod_{n=0}^{N_{cpb}-1}\Big[\cosh\Big(-s\Re\big\{g_k^s\vartheta(k,\tau_i,\tau_{TH}(m,n,b^m,c^m))\big\}\Big)\Big]\Bigg\} \\
&= \frac{1}{2N_{hop}}\sum_{C=0}^{N_{hop}-1}\sum_{b=0}^{1}\prod_{m=M_l}^{M_u}\prod_{n=0}^{N_{cpb}-1}\cosh\Big(-s\Re\Big\{g_k^s\vartheta(k,\tau_i,\tau_{TH}(m,n,b,C))\Big\}\Big)
\end{aligned} \tag{3.27}$$

The overall MGF can be obtained by averaging (3.27) over τ_i and g_k^s:

$$\Phi_{i_k}(s) \;=\; \frac{1}{T_s}\int_0^{T_s}\int_0^{\infty}\Phi_{i_k}(s|\tau_i, g_k^s) f_g(g)\,\mathrm{d}g\,\mathrm{d}\tau_i \tag{3.28}$$

where $f_g(g)$ is the pdf of g_k^s. Given $\Phi_{i_k}(s)$, $\Phi_{g_k^p}(s)$ and $\Phi_{\nu_k}(s)$ the MGF of the decision metric, $\Phi_{d_{x_k}}(s)$, can be derived from (3.23). Then, the BER performance of the MB-OFDM system can be obtained using (3.21). Since, this integral does not have a closed-form solution, a numerical method has to be used. One of the highly accurate exact calculation methods for this type of integrals is a numerical integration which is based on the Gauss-Chebyshev quadrature (GCQ) rule [76]. The main advantage of this approach is that it can be used even

when there is not a closed form expression for $\Phi_{d_{x_k}}(s_i)$ and only a moderate numerical values taken from $\Phi_{d_{x_k}}(s_i)$ are available. Therefore, we adopt the Gauss-Chebyshev quadrature rule [76, 77, 78] in order to numerically solve the integral in (3.21), which is given by:

$$P_e(k) = \frac{1}{N}\sum_{i=1}^{N/2}\left\{\Re\big\{\Phi_{d_{x_k}}(s_i)\big\} + \xi_i \Im\big\{\Phi_{d_{x_k}}(s_i)\big\}\right\} + \varepsilon \tag{3.29}$$

where $s_i \triangleq c + cj\xi_i$ is a limited number of complex points in which (3.23) is evaluated and $\xi_i \triangleq \tan\big([2i-1]\pi/2N\big)$. ε is the error term of GCQ which is negligible for sufficient large value of N. In order to obtain the desired degree of accuracy, one can evaluate aforementioned equation for increasing value of N till the result satisfies the desired degree of accuracy. In our case, 84 points were sufficient to obtain an accurate result. Furthermore, the convergence speed of the GCQ is determined by c whose value minimizes $\Phi_{d_{x_k}}(s)$. Interested readers are referred to [76, 77, 78] for more details on how to use the Gauss-Chebyshev quadrature rule to solve integrals such as (3.29).

3.6 Numerical and Simulation Results

In this section, BER analysis of a MB-OFDM UWB system in presence of a faded TH-UWB interference signal is presented. The accuracy and applicability of the GGD and the SαS approximation methods are studied by comparing the empirical and analytical results. Moreover, the effect of the time-hoping parameters (i.e. N_{burst} and N_{cpb}) of the TH-UWB system and the interference channel on the performance of the MB-OFDM system are analyzed. The MB-OFDM UWB system and the TH-UWB signal parameters are considered according to the ECMA-386 [11] and IEEE 802.15.4a (with $T_c = 2$ns) [12] standards , respectively. The second derivation of the Gaussian pulse with a time constant of 0.25ns has been employed for TH-UWB transmissions. The IEEE 802.15.4a [75] and IEEE 802.15.3a [79] are considered as the interference and the desired channel models. SNR and SIR are defined as signal-to-noise and signal-to-interference ratio, respectively.

Fig. 3.9 depicts the BER versus SNR of a MB-OFDM UWB system impaired by a TH-UWB interference signal. The approximation models and the analytical BER expression for a MB-OFDM system (3.29), obtained in section 3.4.2 and 3.5 respectively, are validated by means of numerical and simulation results. The CM1 and LOS-outdoor channels are considered as the desired and the interference channels, respectively. It can be seen that the numerical result is in a perfect match with the empirical simulation for all range of SNR. However, the approximation methods may perform differently due to the fact that capturing the interference signal's tail is crucial in the accuracy of the victim system's BER estimation.

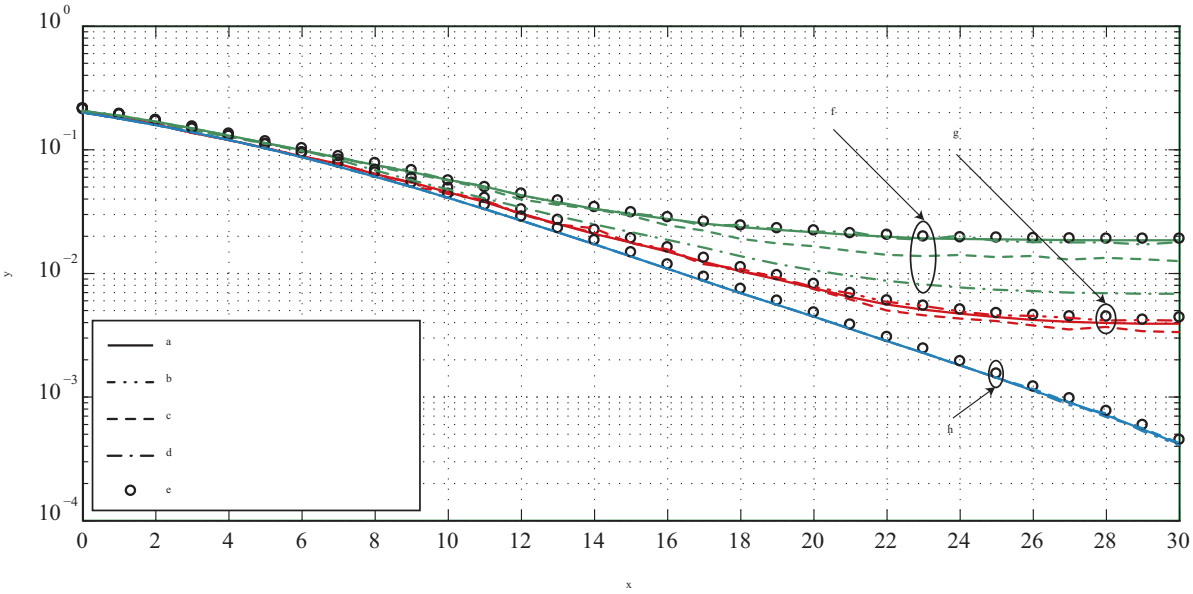

Figure 3.9 BER versus SNR for MB-OFDM UWB system impaired by a TH-UWB signal. Lines, markers and solid lines represent empirical, exact and approximation simulation results, respectively. $N_{cpb} = 32$, $N_{burst} = 32$.

Therefore, the Gaussian distribution, which can not model heavy-tailed interference signals, is not a proper approximation for the TH-UWB interference (since it significantly underestimates the BER). The presented BER results show that the SαS method accurately estimates the BER performance of the MB-OFDM UWB system. However, the GG method slightly underestimates the BER of the victim system. The difference between the accuracy of these approximation methods is due to their abilities in modeling the interference signal's tail (SαS distribution provides a better match to the tail of the TH-UWB interference signal (Fig. 3.6) compare to the GG method) when the interference signal is stronger than the noise signal (high INR). Thus, for SIR = 40 (low INR), both approximation methods perform well for all range of SNR.

Fig. 3.10 depicts the effect of the desired and the interference channels on the performance of the victim system and on the impulsive behaviour of the TH-UWB interference signal, respectively. The CM1 model is considered as the desired channel. The open outdoor (farm), the NLOS-residential and the NLOS-industry environments from the least to the most time-dispersive channels, respectively, are considered as interference channels. As it can be seen, due to the time-dispersive characteristic of the interference channel, the impulsive behavior of the TH-UWB signal is slightly decreased. For instance, in a farm environment, the distribution of the interference signal is not affected by the interference channel (results in an error floor at 1.3×10^{-2}). While, for the NLOS-industrial environment, the BER of the

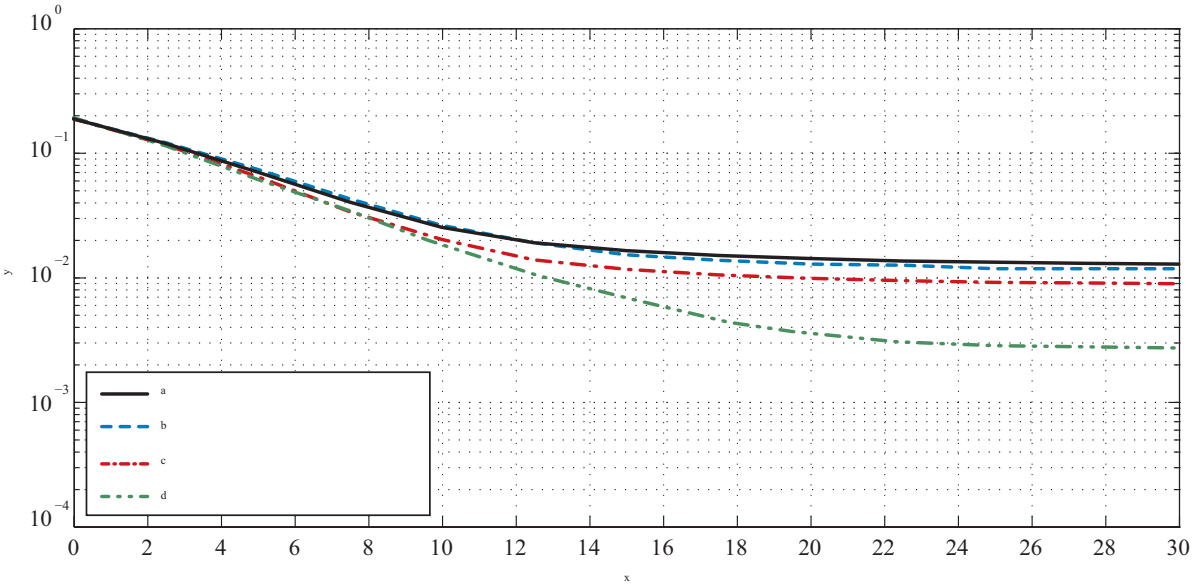

Figure 3.10 BER versus SNR for different interference channel, $N_{cpb} = 16$, $N_{burst} = 16$ and SIR $= 10\,\text{dB}$.

MB-OFDM system experiences an error floor of 3×10^{-3}.

As previously mentioned in section 3.4.1, the signaling parameters (N_{burst} and N_{cpb}) of the TH-UWB is another factor which affects the impulsive behavior of the interference signal. Note that the signaling parameters is a function of the data rates of the TH-UWB system which is taken from the standard [12]. In order to analyze the effect of time-hopping parameters, BER curves of a MB-OFDM UWB system impaired by a TH-UWB system with different data rates are compared in Fig. 3.11. First, it depicts that the TH-UWB interference becomes more impulsive as the data rate increases from 0.11 Mb/s to 27.24 Mb/s. Therefore, a TH-UWB system which operates with data rate of 27.24 Mb/s creates significantly severe interference than the one working with data rate of 0.11 Mb/s. Moreover, it shows that even for a fixed data rate (such as the mandatory data rate of 0.85 Mb/s) changing the time-hopping parameters of the TH-UWB system (from $\{N_{burst} = 32, N_{cpb} = 16\}$ to $\{N_{burst} = 8, N_{cpb} = 64\}$) affects the impulsiveness of the interference. Hence, for a given data rate, one can choose signaling parameters of the TH-UWB system in a way that decrease the impulsiveness of the INI. Second, it is shown that the BER curves obtained from SαS method are in a perfect match with the empirical simulation results for all considered values of time-hopping parameters.

To get a better understanding of the time-hopping parameters' effect on the BER of a MB-OFDM system, BER versus N_{burst} and N_{cpb} is depicted in Fig. 3.12. In order to evaluate the impact of the interference, non-faded desired and interference channels are considered

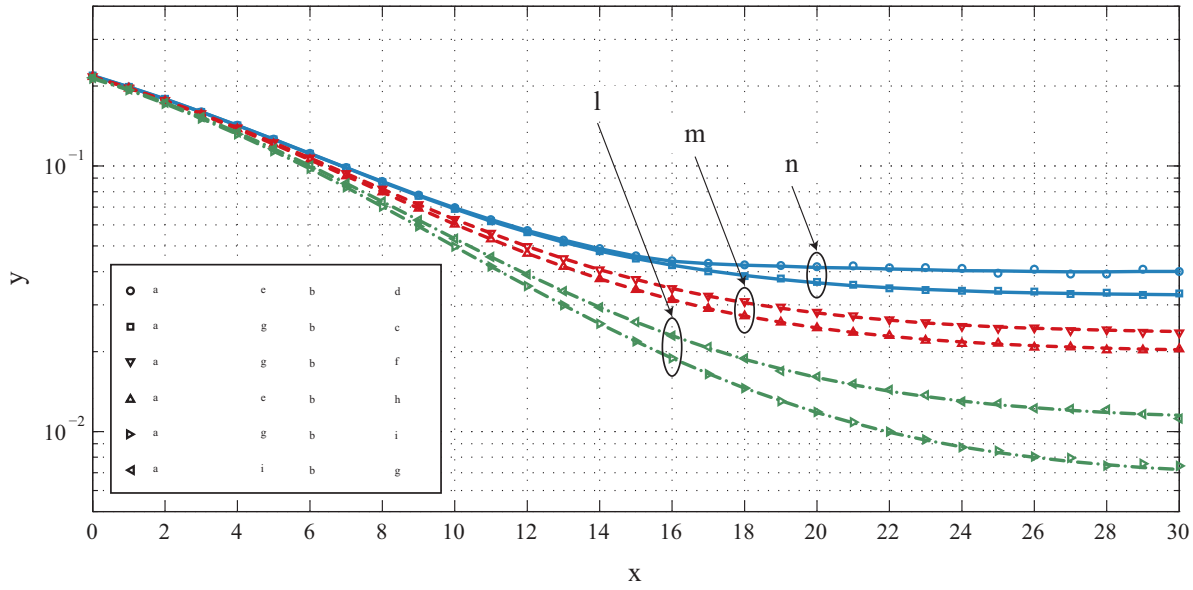

Figure 3.11 BER versus SNR for MB-OFDM UWB system impaired by a TH-UWB signal. Lines and markers represent empirical and SαS approximation simulation results, respectively.

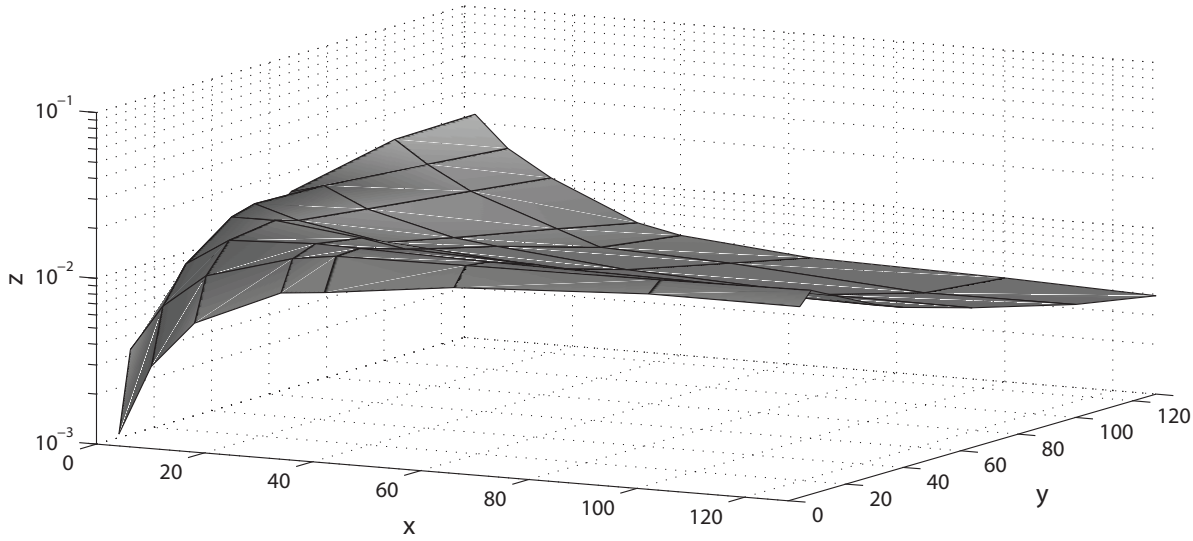

Figure 3.12 BER versus $\{N_{cpb}, N_{burst}\}$ for MB-OFDM UWB system impaired by a TH-UWB signal. SNR = 25 dB and SIR = 10 dB.

and the simulation result is analyzed for high SNR and SIR=10 dB. As we expect from the previous discussion, the influence of the TH-UWB interference on the BER of the MB-OFDM UWB system extremely depends on the time-hopping parameter of the interfering system and on the value of T_s/T_f. Given $N_{cpb} = 2$ and $N_{burst} < 64$, the BER of the MB-OFDM UWB system is significantly deteriorated with increasing N_{burst}, due to the growth

of the interference signal's impulsive behavior. In contrast, for $N_{burst} > 64$ (i.e $T_s/T_f < 1$), the BER does not degrade by increasing N_{burst}. However for higher N_{cpb}, the maximum BER is taken place in smaller N_{burst} and the growth of N_{burst} results in a BER improvement. This is due to the fact that the interference signal's impulsive behavior remains constant (Fig. 3.7-(a)), and moreover, some of the OFDM symbol are not affected by the interference signal (the second OFDM symbol in Fig. 3.4-(b)). Furthermore, it can also be observed that for low N_{burst} ($N_{burst} = 4$), the BER degrades as N_{cpb} increases, which is due to the averaging effect of the interference symbol duration. Since the TH-UWB symbol duration becomes longer with increasing N_{cpb}, the averaging effect of the TH-UWB symbols during one MB-OFDM symbol decreases, which leads to a severe degradation of the BER. As a result, the performance of a MB-OFDM UWB system which is impaired by a TH-UWB system extremely depends on the signaling parameters of the interferer system. Hence, for a fixed date rate of a TH-UWB system, by selecting an appropriate time-hoping parameters one can improve the BER performance of the MB-OFDM UWB system.

3.7 Conclusion

In this paper, inter-network interference between the MB-OFDM UWB and the TH-UWB technologies has been studies intensively. Statistical characteristics and key features of the TH-UWB interference signal's distribution has been analyzed analytically. It has been shown that the impulsive behavior of the TH-UWB interference signal on a MB-OFDM UWB system highly depends not only on the time-hopping parameters of the interferer system but also on the ratio of T_s to T_f. For example, given a small value of N_{cpb}, the impact of increasing N_{burst} on the impulsive behavior of the interference signal is much more severe than the one obtained for large values of N_{cpb}. In contrast, for a large value of N_{burst} the impact of the interference signal on the MB-OFDM UWB system's BER may become less significant by increasing N_{cpb}. Consequently, our results has shown that choosing proper TH-UWB system's properties may reduce the destructive effect of the INI on the MB-OFDM UWB system's performance. Consequently, our results has shown that choosing proper TH-UWB system's properties may reduce the destructive effect of the INI on the MB-OFDM UWB system's performance. Also, the impact of the interference channel on the interference signal's impulsiveness has been studied. It has been observed that while the least time-dispersive channel (such as LOS farm environment) does not affect the impulsive behavior of the interference signal, a highly time-dispersive channel (such as NLOS-industrial environment) may turn an interference signal into a signal with a Gaussian distribution. Moreover, two distributions, including generalized Gaussian and Symmetrical α-Stable distributions, have been employed to

approximate and model the impulsive and heavy-tailed behavior of the TH-UWB signal. The accuracy of these methods has been investigated via pdf and cdf comparisons of the empirical IPN signal, GG and SαS distributions. Our results have shown that the SαS distribution provides a better fit to empirical IPN compared to the GG distribution for high INR, while for low INR both approximation methods can accurately estimate the performance of the MB-OFDM UWB system. Furthermore, an analytical performance evaluation framework for a MB-OFDM UWB system impaired by a TH-UWB interference signal has been provided. It has been shown that the empirical simulation, approximation result and analytic analysis are in good agreement. The BER simulation results have justified that selecting an appropriate time-hopping parameters may enhance the MB-OFDM UWB's BER from 10^{-1} to 10^{-3}. Additionally, it is worth noting that our analysis can also be used to analyze the impact of the TH-UWB systems on any other OFDM-based systems, such as LTE or WiMAX.

CHAPTER 4

ARTICLE 3: IMPULSIVE NOISE MITIGATION FOR OFDM-BASED SYSTEMS USING ENHANCED BLANKING NONLINEARITY

Farshad Sarabchi, and Chahé Nerguizian
Poly-Grames Research Center, Department of Electrical Engineering,
École Polytechnique de Montréal
Montréal, QC, Canada
Submitted to the Journal of Transactions on Emerging Telecommunications on July 2014

4.1 abstract

Non-Gaussian impulsive interference mitigation is of great interest in robust and reliable communication over wired and wireless channels. One of the most popular impulsive noise cancellation methods used along with the orthogonal frequency division multiplexing (OFDM) is blanking nonlinearity. Although its simplicity and efficiency, the blanking method suffers from inter-carrier interference problem due to its nolinear characteristic which causes inter-carrier interference (ICI). In this paper, enhanced versions of the blanking technique is proposed to cope with the detrimental effects of nonlinear characteristic of blanking method. To do so, an iterative serial interference cancellation technique is proposed to reconstruct ICI and subtract from received signal in frequency domain. Moreover, an ordering metric is proposed to improve the interference mitigation technique. Simulation results show that the proposed enhancement in blanking method significantly decreases the level of the error floors. For instance, a BER of 3×10^{-7} is achievable for highly impulsive environments while conventional OFDM system experience an error floor at 1.8×10^{-2}.

4.2 Introduction

Robust and reliable communication is one of the major issues in wired and wireless communication systems to be performed in the presence of both multiplicative and additive noise. Multiplicative noise or fading which results from communication channel characteristics such as reflection, scattering and diffraction is widely investigated in the literature. Additive noise, on the other hand, usually is associated with the thermal noise and modelled with Gaussian distribution. However, in many realistic communication systems, due to the outliers in noise sample (such as bursty high amplitude signals) the distribution of the noise deviates from

Gaussian distribution which is referred to as a non-Gaussian noise. There are several source of impulsive noises in wired and wireless communication systems which are well documented in the literature including man-made noise [24], co-channel interference[25], time-hopping ultra-wideband interference [26] and noises generated from electric motors, silicon-controlled rectifiers and switching devices in power line communication (PLC) [80].

In such cases, the performance of the conventional systems, which are designed based on the Gaussianity assumption of the environment noise, severely degrades. Therefore, wired and wireless communication systems have to employ interference cancellation techniques in order to deliver promised level of quality of service in presence of non-Gaussian noises. There are several interference cancellation techniques reported in the literature considering various transceiver technologies. For instance, in single carrier communication systems, such as impulse radio ultra wideband systems [29], different adaptive receivers have been proposed that obtained superior performance of multiuser interferences. Optimum adaptive rake structures have been proposed based on an accurate estimation of the probability density function of the MUI and the MUI-plus-noise [38, 40, 41, 42]. On the contrary, multi-carrier systems such as orthogonal frequency division multiplexing (OFDM) are more resilient to the impulsive interference compared to single-carrier systems as they spread out the impulsive noise signal over subcarriers (given moderate impulsive noise power and high numbers of subcarriers). However, in highly impulsive environments, the OFDM receivers cannot cope with impulsive interference and experience severe performance degradation. Therefore, various parametric and non-parametric interference mitigation techniques have been reported in the literature to improve the performance of OFDM-based systems impaired by non-Gaussian impulsive noises.

In parametric methods, a receiver is designed considering an accurate statistical model of the impulsive noise through estimating the parameters of the noise distribution [43, 44]. In [43] a robust L_p-norm decoding metric has been proposed for the bit-interleaved coded modulation based OFDM system where p is the shaping parameter of the generalized Gaussian distribution used to model the impulsive noise. Pre-filtering methods are other mitigation techniques based on the Alpha-Stable-Symmetric distribution which have been proposed in [44]. Although parametric methods improve the performance of the system, the estimation process requires training overheads and inaccurate parameter estimation results in severe performance degradation.

In contrast, non-parametric methods do not rely on the knowledge about statistical parameters of the interference signal [45, 46, 47, 48, 49, 50, 81, 82, 83]. Therefore, these types of impulsive interference mitigation techniques are not sensitive to the parameter estimation error. Caire et al. [45] proposed the application of the compressed sensing to mitigate the

impulsive noise in OFDM systems by estimating the noise from the null tones of the received signal which was subject to a sufficient recovery condition. Another impulsive noise mitigation technique adopting the block-based compressed sensing was proposed in [47] which has tow different modes including suppression mode (recovery of the support of the non-zero impulsive noise samples) and cancellation mode (the actual reconstruction of impulsive noise samples). In [46], sparse Bayesian learning (SBL) methods were proposed to mitigate asynchronous sparse impulsive noise in power line communication systems. In this method, SBL techniques have been used to estimate the impulsive noise and subtract it from the received signal. In [48], a frequency domain interference cancellation technique was employed where the impulsive noise is estimated and subtracted from the received signal after the FFT operation process.

Blanking/cliping nonlinearity [49, 50] represents efficient and simple impulsive non- parametric noise mitigation techniques, in which the received signal is compared with a predefined threshold, T, and noise samples with values higher than T are set to zero (blanking) or replaced with a predefined value (clipping). A joint impulsive noise and multipath fading mitigation technique, which is composed of time domain interleaver and a two-stage blanking nonlinearity, is proposed in [81]. Tseng [82] derived the clipping threshold without assuming the a priori knowledge of the probability density function of impulsive noise. However, due to the nonlinear behaviour of the blanking/clipping technique, the orthogonality between the OFDM subcarriers is destroyed which may cause inter-carrier interference (ICI) after the FFT process. To the best of our knowledge, Yih [83] and [84] are the only investigation that has been reported in the literature addressing this issue by proposing an iterative interference cancellation scheme to reduce the level of ICI. However, the proposed ICI cancellation method relies on the symbol detection before the interference mitigation which may cause a propagation error.

In this paper, an iterative successive interference cancellation technique is proposed to cope with the nonlinear effect of the blanking method. In particular, for each subcarrier the ICI is reconstructed from previously detected symbols and subtracted from received signal. Since the inter-carrier interference is not evenly distributed over all subcarriers, some tones may experience severe ICI while some may be ICI-free. Therefore in order to achieve higher level of performance, the proposed interference cancellation algorithm is started from subcarriers experiencing the least effect from adjacent tones and to do so a novel ordering approach is presented. Simulation results reveal that the proposed method offers significant performance improvement compared to the conventional blanking method and the parallel ICI cancellation approach [83].

The rest of this paper is organized as follows. Section II describes briefly the system model.

In section III, the iterative parallel interference cancellation as well as proposed frequency domain interference mitigation technique called successive interference cancellation method are explained. Section IV presents the simulation results and finally the conclusions are drawn in section V.

4.3 System Model

An OFDM-based communication system with N subcarriers is considered. The input bits, $\mathbf{d} = [d_m | m \in Z_M^+]$, are mapped to symbols, $\mathbf{X} = [X_k | k \in Z_N^+]$, using generic modulators such as MPSK or MQAM. Then, the OFDM subcarriers are modulated by $\mathbf{X}$ using N-points inverse fast Fourier transform (IFFT) module. The OFDM signal in the discrete domain is defined as $\mathbf{x}(l) = [x_n(l) = \frac{1}{\sqrt{N}} \sum_{k=0}^{N-1} X_k(l) e^{(j2\pi \frac{kn}{N})} | n \in Z_N^+]$, where $x_n(l)$ and $X_k(l)$ denote n^{th} sample of the l^{th} transmitted OFDM symbol and the data symbol which modulates the k^{th} subcarrier, respectively. Then, in order to mitigate the inter-symbol-interference, a cyclic prefix is added to the beginning of the l^{th} OFDM symbol.

Assuming a fading channel with L independent multipath components, the received signal is $\mathbf{y}(l) = \mathbb{H}(l)\mathbf{x}(l) + \mathbf{w}(l)$, where $\mathbf{w}(l) \sim N(0, \sigma_w^2)$ represents the AWGN; $\mathbb{H}(l)$ is $N \times N$ circulant matrix given by

$$\mathbb{H}(l) = \begin{pmatrix} h_0 & 0 & 0 & 0 & h_{L-1} & \cdots & h_1 \\ h_1 & h_0 & 0 & \vdots & 0 & 0 & h_2 \\ \vdots & h_1 & \ddots & 0 & \vdots & 0 & \vdots \\ h_{L-1} & \vdots & \ddots & h_0 & 0 & \vdots & h_{L-1} \\ 0 & h_{L-1} & \vdots & h_1 & h_0 & 0 & \vdots \\ \vdots & \vdots & \ddots & \vdots & \vdots & \ddots & 0 \\ 0 & 0 & \cdots & h_{L-1} & h_{L-2} & \cdots & h_0 \end{pmatrix} \tag{4.1}$$

where h_m is the gain for m^{th} multipath component. At the receiver, after discarding the CP, the transmitted symbols are reconstructed by performing FFT as

$$\begin{aligned} Y(k) &= \frac{1}{\sqrt{N}} \sum_{n=0}^{N-1} \sum_{l=0}^{L-1} h(l) x(n-l) e^{-j2\pi \frac{nk}{N}} + \frac{1}{\sqrt{N}} \sum_{n=0}^{N-1} w_n e^{-j2\pi \frac{nk}{N}} \\ &= \frac{1}{N} \sum_{m=0}^{N-1} X_m \sum_{n=0}^{N-1} \sum_{l=0}^{L-1} h(l) e^{j\frac{2\pi}{N}(n(m-k)-ln)} + \frac{1}{\sqrt{N}} \sum_{n=0}^{N-1} w_n e^{-j2\pi \frac{nk}{N}} \end{aligned} \tag{4.2}$$

where $Y(k)$ denotes the k^{th} sample of the received signal. Noting that for the notation

simplicity, the subscript l is removed. (4.2) can be written in a vector-matrix-product as

$$\mathbf{Y} \;=\; \mathbf{HX} + \mathbf{W} \tag{4.3}$$

In the case where the OFDM system is ICI-free, $\mathbf{H}$ is a diagonal matrix whose components are $H_m = \sum_{l=0}^{L-1} h(l) e^{-2\pi jlm/N}$. However, in presence of ICI due to temporal variations of the channel or the carrier frequency offset, $\mathbf{H}$ has non-zero off-diagonal components as well. Therefore, given perfect synchronization and non-time varying channel, employing a frequency-domain channel equalizer, the received signal can be expressed as $\tilde{\mathbf{Y}} = \mathbf{X} + \tilde{\mathbf{W}}$.

4.3.1 Impulsive Noise Model

Non-Gaussian impulsive noises have been analytically or empirically modeled in the literature for the performance analysis or optimum receiver design [29, 34]. Generally, the statistic of impulsive noises have been analytically or empirically modeled in the literature in order to perform system performance analysis or optimum receiver design. The common distribution for modeling impulsive noises in the wired communication systems are gated Bernoulli-Gaussian [34], Gaussian mixture [35] or the Middleton's class A [36]. On the other hand, the impulsive noise in the wireless communication systems are usually modeled with generalized Gaussian (GG) [37], symmetric α-stable (SαS) [32] and Gaussian-Laplacian mixture [38] distributions.

Although Bernoulli-Gaussian (GB) is widely used to analyze the performance of blanking nonlinearity, in this work, the generalized Gaussian distribution (GGD) [29] is adopted. This is due to the fact that GB is not the proper tool to model all realistic impulsive noises, however, GGD can model impulsive and heavy-tailed behaviours of wide range of interference noises such as the inter-network interference between time-hopping and multiband-OFDM ultra-wideband systems [26]. The probability density function of GGD is given by [66]:

$$P_i(i) = \frac{p}{2\Gamma(1/p)A(p,\sigma)} e^{-\left(\frac{|i-\mu|}{A(p,\sigma)}\right)^p} \tag{4.4}$$

where $A(p,\sigma) = \left(\frac{\sigma^2\Gamma(1/p)}{\Gamma(3/p)}\right)^{1/2}$, σ^2 and μ are the scale parameter, the variance and the mean of the GGD, respectively and p denotes the shape parameter. $\Gamma(x)$ is the Gamma function. The value of p determines the degree of impulsiveness of the GGD relative to the Gaussian distribution. The GGD includes standard Gaussian distribution ($p = 2$) and Laplacian distribution ($p = 1$) as two special cases. Therefore, considering the overall noise samples (AWGN

plus impulsive noises), $z_n = w_n + i_n$ $\big(\mathcal{GG}(z_n; 0, (\sigma_w^2 + \sigma_i^2), p_z)\big)$, the GGD is able to model the total noise by properly estimating p, the variance and the mean from the empirical noise samples as in [26].

4.3.2 Blanking Nonlinearity

Since FFT averages received noises over all subcarriers, controlling the amplitude of the received noise samples before applying it to the FFT process is a promising method to mitigate the effect of impulsive noises on the performance of OFDM systems 4.1. Blanking [49, 50] is one of the efficient impulsive noise mitigation techniques, in which the received signal, r_n, is compared with a pre-defined threshold, T, and noise samples with values higher than T are set to zero as follows

$$y_n = \begin{cases} r_n, & |r_n| \leq T \\ \\ 0, & |r_n| > T \end{cases}, \tag{4.5}$$

From (4.5) it can be noted that calculating the optimum threshold plays an important role controlling the false detection probability of the impulsive noise [50]. In other words, given small T, the blanking nonlinearity may increase the system error rate due to the false detection of desired OFDM samples as impulsive noises. However, for large T, OFDM receiver can severely be impaired by impulsive noises. Although the blanking is a simple and practical impulsive noise mitigation technique, it suffers from inter-carrier interference impairment. The reasons for this can be due to the fact that the orthogonality between the subcarriers may be broken down by the blanking nonlinearity. In order to demonstrate this fact, let us consider that N_B samples of the received signal ($\Phi = \{n | y_n = 0, n \in Z_N^+\}$) are blanked with $\Theta = \{n | y_n = r_n, n \in Z_N^*, n \notin \Phi\}$ being a set of samples' indices which are not blanked. Therefore, (4.2) can be modified as

$$Y(k) \;=\; \frac{1}{N}\sum_{l=0}^{N-1} H_l X_l \underbrace{\sum_{n\in\Theta}^{N-1} e^{j\frac{2\pi n}{N}(k-l)}}_{P_{l,k}} + \frac{1}{\sqrt{N}}\sum_{n\in\Theta} z_n e^{-j2\pi\frac{nk}{N}} \tag{4.6}$$

Then, in the vector-matrix-production form, (4.6) can be expressed as $\mathbf{Y} = \hat{\mathbf{P}}\mathbf{H}\mathbf{X} + \hat{\mathbf{Z}}$ where $\hat{\mathbf{P}} = \mathbf{F}\mathbf{\Lambda}\mathbf{F}^H$ denotes the modified FFT-IFFT kernel matrix considering blanked samples and $\hat{\mathbf{Z}}$ represents the FFT of the noise signal including the AWGN and a portion of the impulsive noise passed through blanking. $\mathbf{F} = \big[f_{l,k} = \frac{1}{\sqrt{N}} e^{-2\pi jlk/N} | l \in Z_N^*, k \in Z_N^*\big]$ and $\mathbf{\Lambda} = \big[\lambda_{i,j} =$

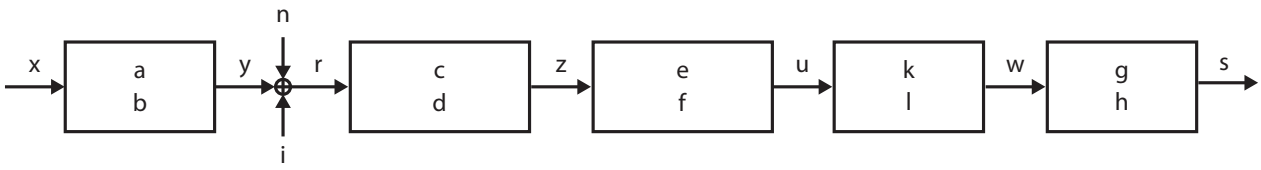

Figure 4.1 Block diagram of an OFDM system with impulsive noise canceller

$\delta_{i,j}|i \in \Theta, j \in Z_N^*\big]$ denote the FFT kernel matrix and the blanking matrix,respectively. $\delta_{i,j}$ is the Kronecker delta. Hence, $\mathbf{Y}$ consists of the desired signal, ICI and aggregated noise components as

$$\mathbf{Y} = \underbrace{\mathbf{P}_1\mathbf{X}}_{\mathbf{H\hat{X}}} + \underbrace{\mathbf{P}_2\mathbf{X}}_{\mathbf{ICI}} + \hat{\mathbf{Z}} \tag{4.7}$$

where $\mathbf{P}_1 = \text{diag}(\hat{\mathbf{P}}\mathbf{H})$ and $\mathbf{P}_2 = \text{off-diag}(\hat{\mathbf{P}}\mathbf{H})$ are diagonal and off-diagonal components of $\hat{\mathbf{P}}\mathbf{H}$, respectively. For sufficiently large number of subcarriers, the noise terms (including ICI, AWGN and remained portion of the impulsive noise) can be modeled by the Gaussian distribution. Hence, the signal to interference and noise ratio after channel equalization can be calculated as

$$SINR_k = \frac{\epsilon^2 E\{|X_k|^2\}}{\sigma^2_{\hat{Z}} + \sigma^2_{ICI_k}} \tag{4.8}$$

where $\sigma^2_{\hat{Z}}$ and σ^2_{ICI} denote the variance of noise term (including the AWGN and the portion of the impulsive noise passed through blanking) and the ICI, respectively, which are obtained in Appendix A. ϵ=$\frac{|\Theta|}{N}$, and $|\Theta|$ represents the length of Θ. Therefore, in order to improve the performance of the blanking method, the ICI resulting from the nonlinearity block has to be cancelled.

4.4 Frequency Domain Interference Canceller

The main idea behind the proposed inter-carrier interference cancellation is to reconstruct the ICI and subtract it from the received signal in frequency domain. On the contrary to the parallel inter-carrier interference cancellation (PIC) technique presented in [83], in this paper, an iterative successive inter-carrier interference cancellation (ISIC) technique is proposed. In the ISIC method, accuracy of the symbol detection and the ICI reconstruction is improved by avoiding the initialization step employed in PIC method.

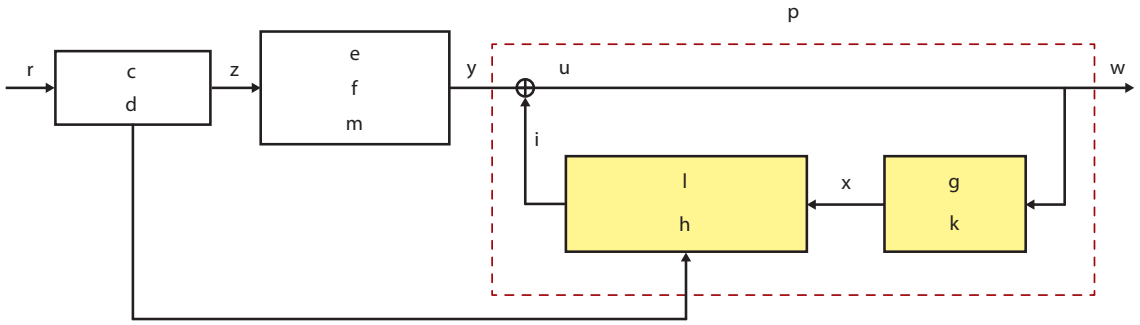

Figure 4.2 Block diagram of an OFDM receiver with the blanking and the IPIC block.

4.4.1 Iterative Parallel Interference Cancellation (IPIC)

The parallel interference mitigation [83] was the only proposed method to tackle the problem of ICI in blanking technique. Therefore, in order to demonstrate the performance improvement of the proposed method, in the following the parallel interference cancellation is explained shortly. Moreover, while the presented method in [83] considered AWGN channel, in this paper, the PIC technique is generalized for frequency selective fading channel. In PIC method, in each iteration, the inter-carrier interference over all subcarriers is reconstructed from temporarily detected symbols and subtracted from received signal in frequency domain (Fig. 4.2). Therefore in each iteration using a decision making function ($f(\cdot)$), the output of the FFT block is forced to the nearest symbol of the modulation alphabet, $\acute{\mathbf{X}}^{(i-1)}$. Then, the ICI is calculated from multiplication of off-orthogonal components of $\hat{\mathbf{P}}$ by detected transmitted symbols as follows

$$\mathbf{I}^{(i)} = \mathbf{P}_2 \mathbf{H} \acute{\mathbf{X}}^{(i)} \tag{4.9}$$

As shown in Fig. 4.2, off-diagonal components of modified kernel matrix are computed based on the indices of the blanked subcarriers which are fed to the ICI reconstruction block. Afterwards, the interference-free received data is calculated as $\hat{\mathbf{Y}}^{(i)} = \mathbf{Y} - \mathbf{I}^{(i)}$, where

$$Y_k^{(i)} \;=\; \epsilon X_k + \frac{H_k^{-1}}{N} \sum_{\substack{l=0 \\ l \neq k}}^{k-1} \hat{p}_{kl} H_l (X_l - \acute{X}_l^{(i)}) + \hat{z}_k \tag{4.10}$$

where $\acute{X}_l^{(i)}$ denotes the temporary detected symbol of the l^{th} subcarrier at the i^{th} iteration. It is noteworthy to mention that in the each iteration, the cancellation algorithm requires to be initialized with an estimation of the transmitted data, $\acute{\mathbf{X}}$, which may cause performance degradation in case of erroneous detection of $\hat{\mathbf{X}}$.

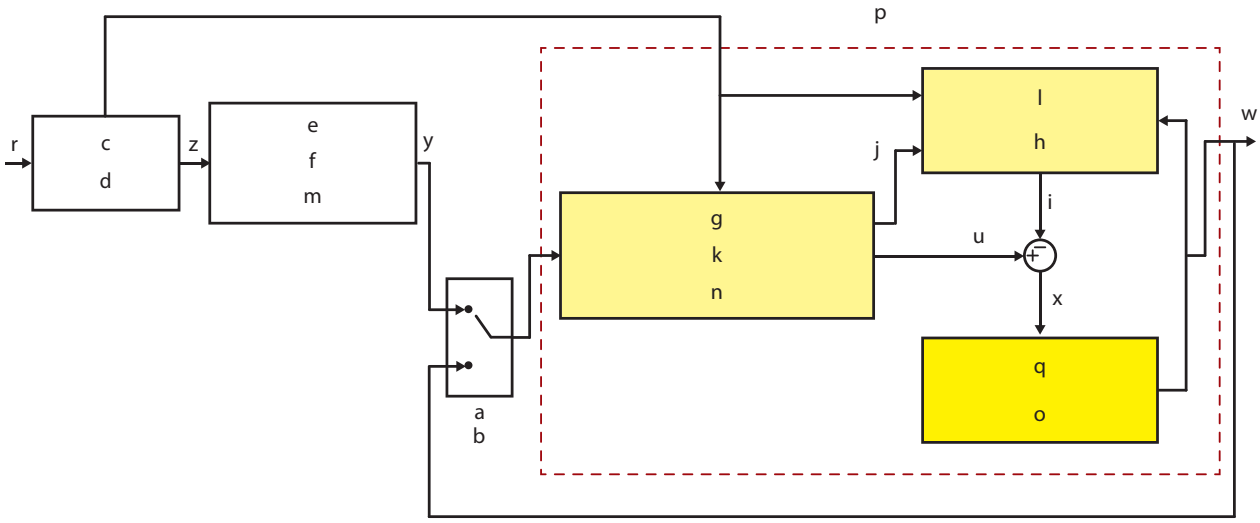

Figure 4.3 Block diagram of an OFDM receiver with the blanking and the proposed ISIC block.

4.4.2 Iterative Serial Interference Cancellation (ISIC)

The main idea behind ISIC method is to improve the symbol detection and ICI reconstruction by avoiding the initialization step in IPIC method. To do so, in each iteration of the ISIC, the symbol detection, ICI reconstruction and subtraction are performed subcarrier-by-subcarrier (Fig. 4.3). Since the inter-carrier interference is not evenly distributed over all subcarriers, some tones may experience severe ICI while others may be ICI-free. Therefore, if received subcarriers are ordered from one with the least effect from adjacent tones, the probability of the erroneous detection decreases. Hence, a new ordering metric is proposed to sort subcarriers based on the detrimental effect of ICI. Generally, subcarriers which experience stronger ICI have higher probability of erroneous detection (in contrast ones with weaker ICI have higher probability of correct detection). However, the amplitude of ICI is not the only fact to be considered (Fig. 4.4-b). It is obvious that, given a high SNR scenario and at the k^{th} subcarrier, a received symbol is detected incorrectly (Fig. 4.4-a) if

$$\begin{cases} |ICI_k| > X_k, & X_k > 0 \quad \text{and} \quad ICI_k < 0 \\ ICI_k > |X_k|, & X_k < 0 \quad \text{and} \quad ICI_k > 0 \end{cases}, \tag{4.11}$$

Clearly, (4.11) illustrates that error occurs more likely when ICI reaches not only its local maximum but also when its sign is different from the transmitted symbol. Therefore, sorting

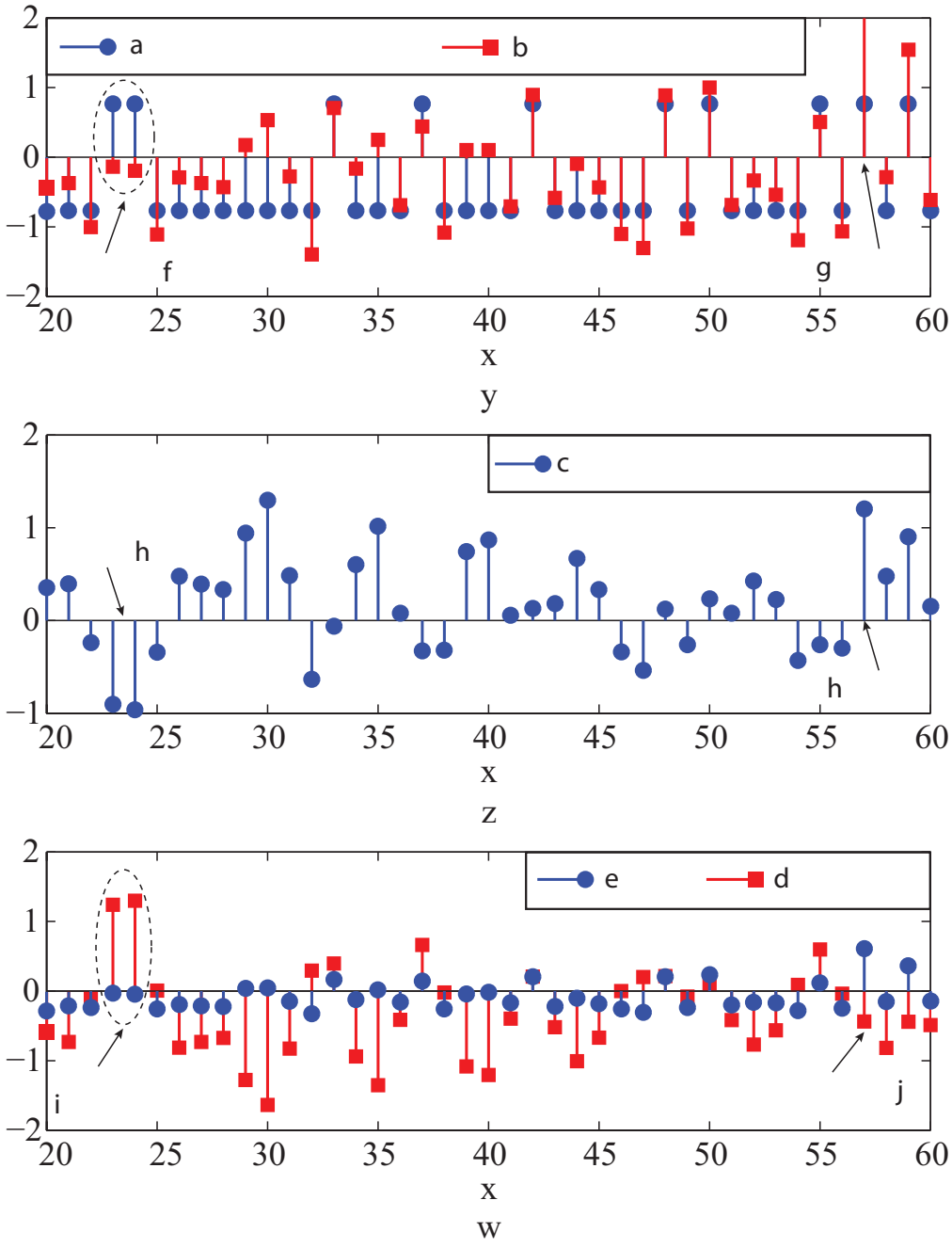

Figure 4.4 Real part of (a) the transmitted and the received modulated symbols, (b) the inter-carrier interference, (c) the two proposed ordering metrics.

subcarriers only based on $\mathbf{ICI} = \mathbf{H}^{-1}\mathbf{P}_2\mathbf{H}\mathbf{X}$, where $\mathbf{H}^{-1} = \text{diag}[(\frac{1}{H_0}, \frac{1}{H_1}, \cdots, \frac{1}{H_{N-1}})]$, is not an effective tool to locate subcarriers with the highest probability of error (Fig. 4.4-b). Hence, new ordering metric is proposed as $\mathcal{M} = \mathbf{P}_2\mathbf{P}_2\mathbf{H}\mathbf{X}$. According to the inherent characteristics of $\mathbf{P}_2$ and after simple mathematical manipulations, the proposed ordering metric can be divided into two parts. The first part is proportional to the transmitted symbols and the second one accounts for the inter-carrier interference resulting from blanking nonlinearity, $\mathcal{M} = \alpha\mathbf{X} - \mathbf{ICI}$. Therefore, exploiting the fact that subcarriers with the maximum absolute value of the proposed metric satisfy the condition of (4.11), the proposed metric can be used to sort subcarriers (Fig. 4.4-c). However, in order to calculate $\mathcal{M}$, one needs to have prior knowledge about transmitted signal, $\mathbf{X}$, which is not available in the receiver. The proposed ordering metric can be re-written by replacing ICI from (4.7) as

$$\begin{aligned} \mathcal{M} &= \mathbf{P}_2\,\mathbf{ICI} \\ &= \mathbf{P}_2\mathbf{Y} - \mathbf{ICI} \end{aligned} \tag{4.12}$$

It has to be noted that the absolute value of $\mathcal{M}$ is maximized when $\mathbf{P}_2\mathbf{Y}$ is minimum. Therefore, subcarriers are ordered by sorting $\mathbf{P}_2\mathbf{Y}$ in descending order (Ω is the set of subcarriers' indices after ordering). Then, considering k^{th} subcarrier, the interference from the previously detected symbols (i.e. previous subcarriers according to Ω) is calculated as follows

$$ICI_k^{(i)} = \frac{H_k^{-1}}{N} \sum_{\substack{l<k \\ l \in \{\text{previously detected symbols according to } \Omega \text{ in the } i^{th} \text{iteration}\}}} \hat{p}_{kl} H_l \acute{X}_l^{(i)} + \frac{H_k^{-1}}{N} \sum_{\substack{l>k \\ l \in \{\text{previously detected symbols according to } \Omega \text{ in the } (i-1)^{th} \text{iteration}\}}} \hat{p}_{kl} H_l \acute{X}_l^{(i-1)} \tag{4.13}$$

where $\hat{p}_{kl}$ and $\acute{X}_l^{(i)}$ are $(k,l)^{th}$ off-diagonal component of the matrix $\hat{\mathbf{P}}$ and previous detected symbols of the l^{th} subcarrier at the i^{th} iteration, respectively. Then, $\acute{X}_k^{(i)} = f(Y_k - ICI_k^{(i)})$ is calculated to be used for reconstructing the ICI that will be exploited for detecting the next subcarrier, with $f(\cdot)$ being a decision making function. Therefore, the k^{th} received subcarrier (according to the ordering set, Ω) after FFT and ICI cancellation is given by

$$
\begin{aligned}
Y_k^{(i)} &= \epsilon X_k + \frac{H_k^{-1}}{N} \sum_{\substack{l=0 \\ l \neq k}}^{N-1} \hat{p}_{kl} H_l X_l - ICI_k^{(i)} + \hat{z}_k \\
&= \epsilon X_k + \frac{H_k^{-1}}{N} \sum_{l=0}^{k-1} \hat{p}_{kl} H_l (X_l - \acute{X}_l^{(i)}) + \frac{H_k^{-1}}{N} \sum_{m=k+1}^{N-1} \hat{p}_{km} H_m \acute{X}_m^{(i-1)} + \hat{z}_k \qquad (4.14)
\end{aligned}
$$

Obviously employing interference mitigation method, the received signal can be divided into four parts, first one is the desired symbol, the second part is the cancelled ICI, the third one is the remained ICI and the last one is the noise. According to the ordering procedure, the ICI cancellation and the symbol detection are stared with subcarriers with the highest probability of correct detection. Hence, second part of (4.14) is equal to zero. However, for the latest subcarriers due to the possible erroneous detection (from previous iteration), the second part may be different than zero but the third part is negligible.

4.5 Simulation Results

To evaluate the performance of the proposed algorithms, an OFDM-based communication system with a FFT size of 1024 is considered. Data symbols are modulated using QPSK modulation. Impulsive noise is modeled with generalized Gaussian distribution, where the impulsiveness of the noise is controlled with the shaping parameter, p. Unless stated otherwise, signal to noise ratio (SNR) and signal to interference ratio (SIR) are set to 15 dB and -20 dB. In the following, B-OFDM [49] , PIC-OFDM and ISIC-OFDM stand for conventional blanking nonlinearity, blanking with PIC (the method presented in [83]) and proposed ISIC techniques, respectively, employed in an OFDM system. It is worth noting that to clearly study the efficiency of the proposed technique and to be capable of comparing the obtained results with previous methods, the channel is considered as AWGN.

Fig. 4.5 compares the performance of B-OFDM, PIC-OFDM and ISIC-OFDM systems in presence of an impulsive noise with $p = 0.8$. The performance of an OFDM system without any interference mitigation technique is outlined as a baseline. While conventional blanking technique leads to an error floor at $\simeq 4 \times 10^{-3}$, the OFDM system employing blanking nonlinearity with inter-carrier interference techniques floors at relatively lower BERs for different numbers of iterations. Obviously, the error floor is still exist for high SNR with the proposed algorithms, which is due to the fact that the proposed blanking techniques can only mitigate impulses which have higher amplitude than the pre-defined threshold. Furthermore, the simulation results show that ISIC-OFDM provides better interference mitigation performance than PIC-OFDM even for high number of iterations due to (a) the initialization step of the

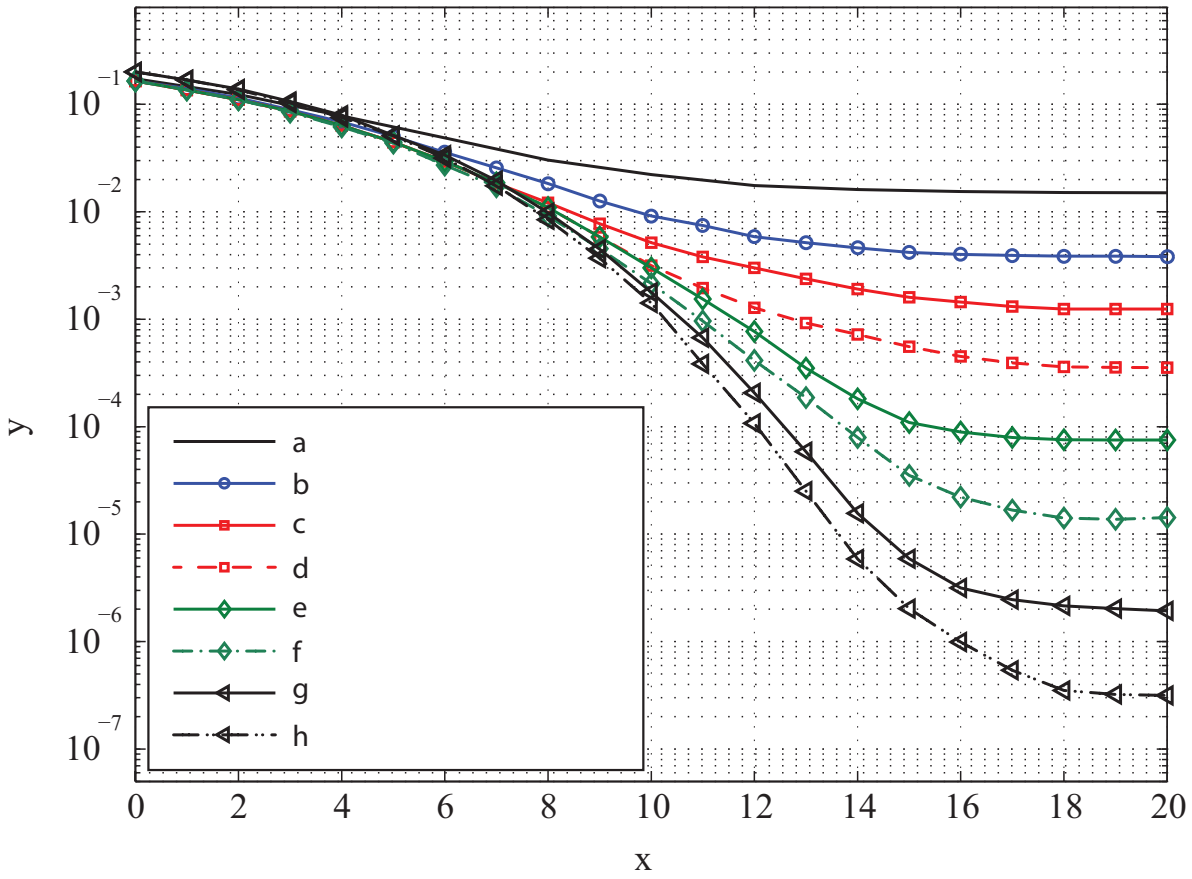

Figure 4.5 Performance comparison of B-OFDM and PIC-OFDM with proposed ISIC-OFDM considering p = 0.8.

PIC-OFDM which results in erroneous detection, and (b)the error propagation inherent in all iterative methods.

Calculating an optimum threshold is critical to successfully detect and mitigate impulsive noise samples. Fig. 4.6 depicts the BER of the OFDM system versus the blanking threshold, where the minimum achievable BER occurs in the optimum threshold. It can be seen that as the number of iteration increases, the optimum threshold decreases owing to higher probability of ICI cancellation in higher iteration. Moreover, the simulation results show that the maximum number of iteration with significant performance improvement is seven. This is a consequence of the fact that the blanking nonlinearity is not able to cancel a portion of the impulsive noise that is below the threshold, raising indeed the noise floor. Although, not shown here due to space constraints, similar performance pattern is observed for IPIC when iteration tends to a large number.

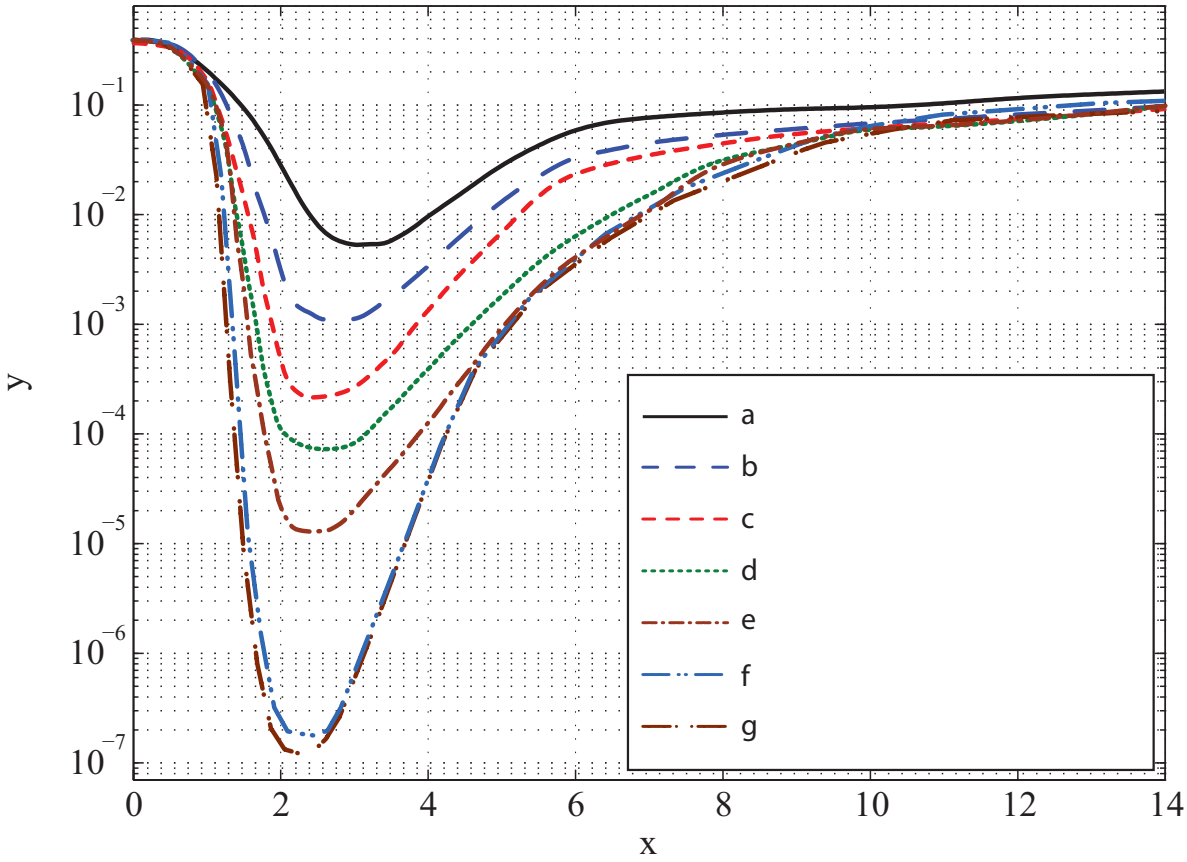

Figure 4.6 BER vs. threshold of PIC-OFDM and ISIC-OFDM for various number of iterations, considering p = 0.8.

Fig 4.7 compares the performance of B-OFDM, PIC-OFDM and ISIC-OFDM impaired by different impulsive noises. It can be observed that both enhanced blanking methods lead to lower BER as shaping parameter of the impulsive noise decreases (i.e highly impulsive interference). This can be attributed to the definition of the non-Gaussian distribution (probability of relatively high magnitude noise samples is extremely higher than the ones with low magnitude). Therefore, when the interference is highly impulsive (for instance p = 0.3 in Fig.4.7), received samples with high magnitude are set to zero and the ones passing through the blanking nonlinearity block have high signal to interference plus noise ratio (SINR) which result in a considerable performance improvement. In contrast, for low impulsive noise (for instance p = 1 in Fig.4.7), the blanking can slightly reduce the variance of the impulsive noise (interference can pass through the blanking nonlinearity) and the received signal after FFT block, according to (4.8), has low SINR. Moreover, considering a BER of 10^{-4} as a target performance criteria, it can be seen that the proposed method achieves 4 dB SNR gain for highly impulsive environment compared to the parallel interference mitigation [83].

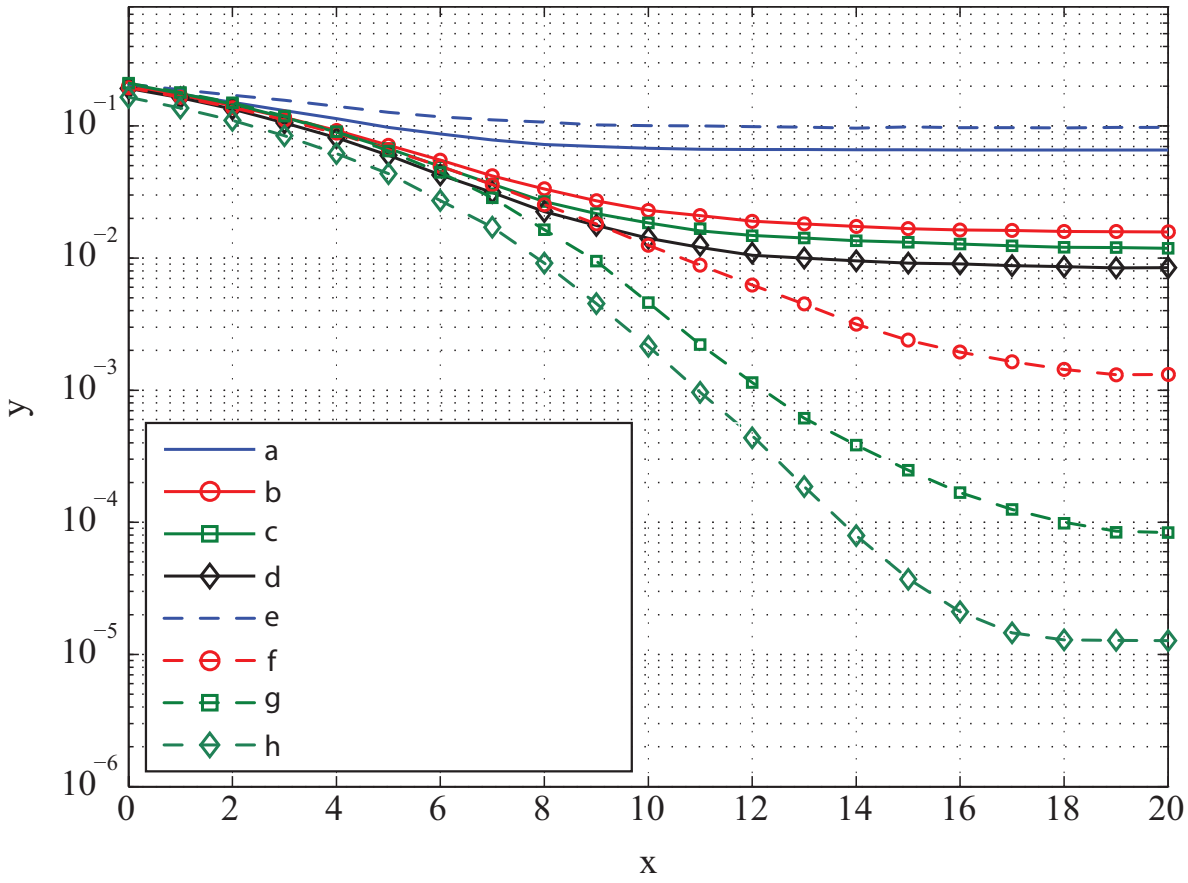

Figure 4.7 Performance comparison of B-OFDM and PIC-OFDM with ISIC-OFDM for various impulsive noises.

In order to investigate the effect of the received noise impulsiveness on the functionality of the proposed method, the performance of ISIC-OFDM system over a wide range of threshold is compared for various noise environments (Fig. 4.8). As mentioned earlier, for higher impulsive noises, lower BER may be achievable using the blanking nonlinearity. However, the optimum threshold for various impulsive noises is different due to the effect of the blanking nonlinearity. For low impulsive noises, lower threshold guarantee minimum achievable error since the probability of relatively high magnitude noise samples is very low. On the contrary, for high impulsive noises, since the received signal has heavy tailed noise distributions, the optimum threshold can be relaxed which may result in lower probability of false detection of impulses (i.e. blanking OFDM symbols instead of impulses) and lead to a lower minimum BER.

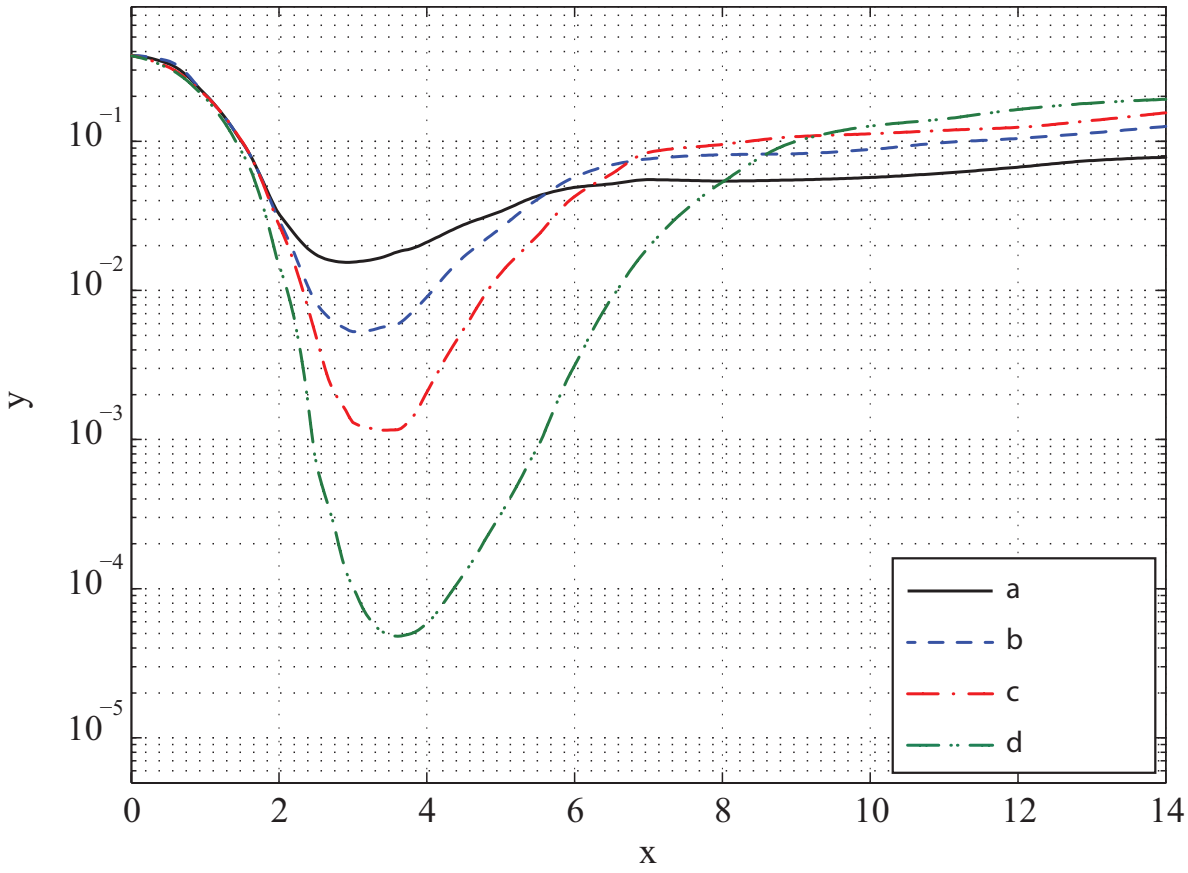

Figure 4.8 BER vs. threshold of ISIC-OFDM for various noise environment.

4.6 Conclusion

In this paper, the problem of the impulsive noise in OFDM-based systems was studied. According to the efficiency and the simplicity of the blanking nonlinearity technique, an iterative successive interference mitigation technique was proposed to be used after FFT block to improve the performance of the blanking method by coping with its nonlinearity effects. To do so, the inter-carrier interference in each subcarrier is reconstructed from previous detected symbols and subtracted from the received signal in frequency domain. In order to enhance the procedure of the ICI reconstruction, a novel subcarrier ordering method was presented. The simulation results showed that the proposed enhancement remarkably improved the performance of OFDM-based communication systems impaired by impulsive noises. It was depicted that, considering a BER of 10^{-4} as a target performance criteria, the proposed method achieves 4 dB SNR gain for highly impulsive environment and 1 dB SNR gain for moderate impulsive environment compared to the parallel interference mitigation [83]. Moreover, it was shown that the employment of ISIC method lowers the error floor by

up to 4 order of magnitude compared to the conventional blanking method.

CHAPTER 5

GENERAL DISCUSSION

In the last few years, we have seen impressive changes in the radio spectrum usage by wireless communication systems and applications which result in the radio spectrum scarcity problem. One of the most promising approach to increase the spectrum usage efficiency is a peaceful reuse of underutilized licensed radio frequencies without generating harmful interference to other systems. On the other hand, radio spectrum reuse approaches and coexistence issues bring major design challenges such as interference analysis, spectrum sharing techniques and robust receiver design. Therefore, this thesis is motivated by the following main factors:

- Potentially, secondary systems may interfere to primary systems, hence, they have to avoid any interference by employing efficient spectrum sharing techniques.
- Lack of sufficient analysis on the potential interference between different technologies sharing the same radio spectrum is evident in the literature.
- Besides higher spectrum efficiency, acceptable system performance and reliability in noisy environment are critical for successful deployment of unlicensed utilization of radio spectrum.

As a consequence of the above mentioned motivations, this thesis mainly focuses on the coexistence issues in spectrum sharing paradigm. In order to implement proposed signal processing algorithms in a practical application, MB-OFDM UWB system which is an underlay system, is considered. Hence, the objectives of the thesis focus on the following aspects:

- Propose spectrum shaping techniques for SISO and MIMO applications in order to mitigate the possible interference from MB-OFDM UWB system to the legacy communication systems.
- Provide an analytical framework to accurately analyze and model the effect of non-Gaussian noises on the performance of a MB-OFDM UWB system.
- Propose a robust MB-OFDM UWB receiver with optimal performance in the presence of non-Gaussian noises.

Generally, the objectives of the thesis can be divided into two main parts dealing with the potential interference to (a) the primary users and (b) to the secondary users. Three papers in previous chapters reveal the development of these two main contributions. In each paper some conclusions have been made, hence in this chapter we review the general aspects of these achievements.

We started our research with tackling the problem of avoiding the potential interference from MB-OFDM UWB system to other legacy wireless communication systems. To do so, we studied various interference mitigation techniques such as time-domain windowing, multiple-choice sequence, subcarrier weighting, adaptive symbol transition and active interference cancellation techniques. Finally, we chose the active interference cancellation technique due to having better performance among other techniques. However, the non-constrained conventional AIC technique suffers from the spectrum overshoot problem and applying single constraint on the total power of the protection tones may result in a notch depth reduction. Hence, the request for an efficient spectrum shaping technique with low complexity, less throughput reduction and respecting the regulatory spectrum masks for single and multiple transmit antennas applications has motivated our research in this section. The contributions of this thesis regarding the issues of spectrum shaping techniques are as follow:

- An enhanced version of the AIC method was proposed by applying individual power constraints to each protection subcarrier in order to tackle the spectrum overshoot problem. This technique leads to a multi-constrained minimization problem (MCMP), which has a solution with high computational complexity. Therefore, in this research an iterative method was proposed to turn MCMP into a set of simple least squares problems with single quadratic inequality constraint.
- The conventional AIC algorithm was modified to add the capability of controlling the depth and the width of the created notch.
- Two novel spectrum shaping methods for OFDM-based cognitive radio systems with multiple transmit antennas were proposed. The main idea behind the bulk and the per-tone transmit antenna selection (TAS) techniques were employed along with the enhanced AIC, to increase the throughput of the CR system. In the proposed techniques, a transmit antenna or a subset of subcarriers over all transmit antennas (in bulk and per-tone TAS techniques, respectively) with the worst interference channel is selected such that the throughput loss of the AIC technique is improved.

After securing a non-interfering transmission for the MB-OFDM UWB system, we stepped towards analyzing and modeling the noise received at the receiver of the MB-OFDM UWB system. Due to the huge bandwidth of UWB systems, interference is one of the most important issues which can be divided into three categories: narrowband interference from legacy wireless systems, multiuser interference and inter-network interference. Since very few investigations have been reported in the literature addressing statistic analysis and modeling of inter-network interference between UWB systems, the request for deriving and validating an accurate model of the interference signal was the main goal of this section of the thesis. This thesis establishes the following contributions and advances regarding spectrum shaping

approach:

- To the best of our knowledge, this research is the first reported theoretical approach proposed to model the impulsive inter-network interference signal from the IR-UWB system to the MB-OFDM system. It provides a comprehensive analytical framework to analyze the statistical characteristics of the INI interference. The accuracy and tractability of the approximation methods were established by means of comparison with the probability and cumulative distribution functions of the empirical signal.
- It widely analyzed the impact of the TH-UWB system's parameters on the BER performance of a MB-OFDM UWB system. It has been shown that the BER of a MB-OFDM UWB system highly depends on time-hopping parameters of the interference signal.
- An analytical BER analysis of a MB-OFDM UWB system impaired by an empirical TH-UWB interference was provided.

The last objective of this thesis is to propose a robust MB-OFDM UWB receiver impaired by an impulsive noise. Since, one of the most important problems in wired and wireless communication systems is addressing the destructing effect of impulsive noise, we aimed at proposing a simple and an effective technique that can be used in any OFDM-based systems. Therefore, we studied various interference mitigation techniques such as L_p-norm decoding, pre-filtering methods and parametric methods. Amongst them, blanking/cliping nonlinearity is notable in that it represents an efficient and simple impulsive noise mitigation approach. However, it suffers from intercarrier interference problem. The contributions of the thesis in the field of impulsive interference cancellation are as follow:

- It presents an iterative method to suppress the intercarrier interference which results from nonlinear characteristics of the blanking technique. It has been shown that the proposed enhancement remarkably improved the performance of OFDM-based communication systems impaired by impulsive noises.
- It provides an analytical approach to calculate the intercarrier interference at the output of the FFT block which can be used to calculate the output SINR for performance evaluation.
- It presents a novel approach of subcarrier ordering according to the contribution of the intercarrier interference on each subcarrier.

CHAPTER 6

CONCLUSIONS AND FUTURE WORKS

In this chapter, we briefly summarize the work done in this thesis and focus on the main achievements during the course of the work. We also suggest topics and open problems for further research.

6.1 Conclusions

In this thesis we have focused on the design of a MB-OFDM transceiver considering several practically relevant aspects, namely: (1) non-interfering underlay transmission, (2) interference analysis and system performance ; and (3) robustness against the impulsive noise. To do so, two different scenarios were considered. In Chapter 2, interference free transmission of an OFDM-based cognitive radio system (such as MB-OFDM system) coexisting with legacy communication systems (such as Wimax or WiFi) was investigated. On the other hand, in Chapter 3 and 4, a MB-OFDM UWB system in presence of a TH-UWB system was considered. First, we provided a comprehensive analysis of a heavy-tailed impulsive interference from TH-UWB systems in Chapter 3, then a robust OFDM-based receiver was proposed in Chapter 4. In the following, a summary of the contributions of the thesis, which discussed in Chapter 1, is presented.

In particular, in Chapter 2, we proposed different interference mitigation techniques for an OFDM-based Cognitive Radio system considering single antenna and multiple antennas applications. Motivated by the fact that the active interference cancellation technique suffers from the spectrum overshoot problem and the complexity issues, we presented a multi-constraint approach to improve the performance of the conventional constrained AIC technique in terms of the achievable interference reduction. Since employing multi-constraint approach turns the optimization problem to a complex multi-constrained minimization problem, we proposed a novel iterative SVD-based algorithm to reduce the complexity of the solution to MCMP. The obtained simulation results showed that applying distinct power constraints to the protection tones results in more efficient interference reduction technique (in terms of notch depth) than applying single constraint to the total power of protection tones. Moreover, we improved the enhanced AIC technique with the ability of controlling the characteristics of the created notch. Based on the simulation results, we showed that the proposed E-AIC technique provides higher performance in terms of sidelobes suppression with 0dB spectrum overshoot, less

computational complexity and less throughput reduction compared to the previous constrained AIC methods. Considering multiple antennas applications, we proposed two novel E-AIC techniques, where the main ideas behind the bulk and the per-tone transmit antenna selection approaches combined with the proposed E-AIC technique for SISO applications. We showed that both presented techniques provide acceptable interference reduction performance and less throughput loss compared to the previous methods.

We studied the BER performance of a MB-OFDM UWB system impaired by a TH-UWB interference signal in Chapter 3. We analytically analyzed statistical characteristics and key features of the TH-UWB interference signal's distribution. We showed that the impulsive behavior of the TH-UWB interference signal highly depends on the time-hopping parameters of the interferer system. The obtained perfromance simulation results have justified that selecting an appropriate time-hopping parameters may enhance the MB-OFDM UWB's BER from 10^{-1} to 10^{-3}. We also investigated the impact of the interference channel on the interference signal's impulsiveness, and showed that the time-dispersiveness of the channel can affect the impulsive behavior of the interference signal. Furthermore, we adopted generalized Gaussian and Symmetrical α-Stable distributions to approximate and model the impulsive and heavy-tailed behavior of the TH-UWB signal. We showed that the SαS distribution provides a better fit to empirical IPN compared to the GG distribution for high INR, while for low INR both approximation methods can accurately estimate the performance of the MB-OFDM UWB system. Finally, we employed an MGF-based approach to obtain the exact BER of a MB-OFDM UWB system impaired by a TH-UWB interference signal. We demonstrated that the empirical simulation, approximation result and analytic analysis are in good agreement. It is worth noting that our analysis can also be used to analyze the impact of the TH-UWB systems on any other OFDM-based systems, such as LTE or WiMAX.

In Chapter 4, we mainly focused on proposing robust OFDM-based receivers in impulsive environments. Among various interference mitigation techniques we chose blanking nonlinearity as signal-processing based solution which shows significant impulsive noise reduction capability and acceptable implementation complexity. In order to tackle its nonlinear effects, we proposed an iterative successive interference mitigation technique to be used after FFT block. In the presented method, in each subcarrier, the inter-carrier interference was reconstructed from previous detected symbols and subtracted from the received signal in the frequency domain. Since the interference cancellation was performed subcarrier-by-subcarrier, we presented a novel subcarrier ordering method to enhance the procedure of the ICI reconstruction. In particular, in each iteration, we ordered all subcarriers according to the contribution of the ICI, then the ICI cancellation and the symbol detection were started with subcarriers with the highest probability of correct detection. We showed that the proposed enhancement

significantly improved the performance of OFDM-based communication systems impaired by impulsive noises. For instance, it was shown that the employment of ISIC method lowers the error floor by up to 4 order of magnitude compared to the conventional blanking method.

6.2 Future Works

Spectrum reuse has been widely considered as one of the promising solutions to address the spectrum scarcity. However, the potential interference between different wireless communication systems sharing radio spectrum, is one of the most challenging issues in spectrum sharing paradigm. We have made an effort to address this issue for different scenarios, nonetheless, there exist extensions to the work presented in this thesis.

1. In chapter 2, we have considered that the victim transmitter (an OFDM-based system) has the perfect interference channel information. However, the effect of the channel estimation error on the performance of the enhanced AIC would be an interesting topic to explore. Furthermore, according to practical limitations of MIMO technologies such as spatial correlation or diversity gain constraints due to the terminal size limitation, distributed MIMO was proposed [85]. Hence, the possible use of the proposed enhanced-AIC to mitigate the interference in cooperated MIMO cognitive radio systems is an open problem of some interest.
2. In chapter 3 the performance of an uncoded MB-OFDM UWB system impaired by non-Gaussian impulsive noise has been studied. It is of interest to investigate the performance of Coded MB-OFDM UWB receivers in the presence of UWB interference and other types of non-Gaussian noise and to extent the framework developed considering different coding schemes.
3. In chapter 4, we have considered that the channel is time-invariant and CP is large enough to avoid intercarrier interference. However, in many practical cases, due to the time-variation of the channel or insufficient length of CP, the orthogonality between subcarriers is destroyed which leads to ICI. Hence, we have to mitigate intercarrier interference signals originating from different sources. Since, the nature of the ICI produced due to the nonlinearity effect of the blanking is different than the one originates from practical issues, the proposed ICI cancellation method is not applicable anymore.Therefore, it is of interest to incorporate such issue in the designing a robust receiver. Furthermore, Since multiple receive antennas can be used to suppress the interference in noisy environment, the proposed interference mitigation technique in chapter 4 can be employed along with multiple receive antennas to improve the performance. In this regard, such an interference mitigation approach can present several challen-

ging design issues such as choosing a proper MIMO-OFDM structure which improves the performance of the interference mitigation considering acceptable computational complexity and calculating optimum threshold.

REFERENCES

[1] I. Güvenç, S. Gezici, S. Sahinoglu, and U. C. Kozat, Eds., *Reliable communications for short-range wireless systems*. Cambridge University Press, 2011.

[2] FCC, "Part 15 - radio frequency devices," Ch 1, Title 47 of the code of Federal Regulation (CFR).

[3] ——, "Revision of Part 15 of the Commissions Rules Regarding Ultra-Wideband Transmission Systems," First Report and Order, ET Docket 98-153, FCC 02-48 ; Adopted: February 14, 2002 ; Released: April 22, 2002.

[4] J. Mitola and J. G. Maguire, "Cognitive radio: making software radios more personal," *IEEE Personal Communications*, vol. vol. 6, no. no. 4, pp. pp. 13–18, 1999.

[5] S. Haykin, "Cognitive radio: Brain-empowered wireless communications," *IEEE J. Select. Areas Commun.*, vol. 23, p. 201Ů220, 2005.

[6] G. Weightman, *Signor Marconis Magic Box: The Most Remarkable Invention Of The 19th Century & The Amateur Inventor Whose Genius Sparked A Revolution*. Da Capo Press, 2003.

[7] "Ieee 802.15 wpan high rate alternative phy task group 3a (tg3a)," [Online]: http://www.ieee802.org/15/pub/TG3a.html.

[8] "Ieee 802.15 wpan low rate alternative phy task group 4a (tg4a)," [Online]: http://www.ieee802.org/15/pub/TG4a.html.

[9] A. B. *et al.*, "Multiband OFDM Physical Layer Proposal for IEEE 802.15 Task Group 3a," IEEE P802.15-03/268r3, Mar. 2004.

[10] R. Fisher, R. Kohno, M. McLaughlin, and M. Welborn, "DS-UWB Physical Layer Submission to 802.15 Task Group 3a," IEEE P802.15-04/0137r4, Jan. 2005.

[11] ECMA, "Standard ECMA-368: High Rate Ultra Wideband PHY and MAC standard," 2005. [Online]. Available: http://www.ecma-international.org/publications/standards/Ecma-368.htm

[12] I. P802.15.4a, "Wireless medium access control (MAC) and physical layer (PHY) specifications for low-rate wireless personal area networks (LR-WPANS): amendment to 802.15.4 for an alternative phy," 2007.

[13] M. Chiani and A. Giorgetti, "Coexistence between uwb and narrow-band wireless communication systems," *Proceedings of The IEEE*, vol. 97, pp. 231–254, 2009.

[14] G. Manzi, M. Feliziani, P. Beeckman, and N. van Dijk, "Coexistence between ultra-wideband radio and narrow-band wireless lan communication systems, part i: Modeling and measurement of uwb radio signals in frequency and time," *IEEE Transactions on Electromagnetic Compatibility*, vol. 51, no. 2, pp. 372–381, 2009.

[15] Z. Li, W. Zou, B. Li, Z. Zhou, and X. Huang, "Analysis on coexistence of ultra wideband with ofdm-based communication systems," *IEEE Transactions on Electromagnetic Compatibility*, vol. 53, no. 3, pp. 823–830, Aug 2011.

[16] A.Nasri, R. Schober, and L. Lampe, "Analysis of narrowband communication systems impaired by mb-ofdm uwb interference," *IEEE Transactions on Wireless Communications,*, vol. 6, no. 11, pp. 4090–4100, November 2007.

[17] P. Tan and N. C. Beaulieu, "Reduced ici in ofdm systems using the "better than" raised-cosine pulse." *IEEE Communications Letters*, vol. 8, no. 3, pp. 135–137, 2004.

[18] I. Cosovic, S. Brandes, and M. Schnell, "Subcarrier weighting: a method for sidelobe suppression in ofdm systems," *IEEE Communications Letters*, vol. 10, no. 6, pp. 444–446, 2006.

[19] . Cosovic and T. Mazzoni, "Suppression of sidelobes in ofdm systems by multiple-choice sequences," *European Trans. Telecommun*, vol. 17, pp. 623–630, 2006.

[20] H. Mahmoud and H. Arslan, "Sidelobe suppression in ofdm-based spectrum sharing systems using adaptive symbol transition," *IEEE Communications Letters*, vol. 12, no. 2, pp. 133–135, 2008.

[21] H. Yamaguchi, "Active interference cancellation technique for mb- ofdm cognitive radio," in *European Microwave Conf.*, vol. 12, 2004, p. 1105âĂŞ1108.

[22] S.-G. Huang and C.-H. Hwang, "Improvement of active interference cancellation: avoidance technique for ofdm cognitive radio," *IEEE Transactions on Wireless Communications*, vol. 8, no. 12, pp. 5928–5937, 2009.

[23] S. Brandes, I. Cosovic, and M. Schnell, "Reduction of out-of-band radiation in ofdm based overlay systems," in *Proc. IEEE International Symposium on Dynamic Spectrum Access Networks (DySPAN)*, 2005, pp. 662–665.

[24] D. Middleton, "Statistical-physical models of man-made radio noise-parts i and ii," 1974 and 1976.

[25] K. Gulati, B. Evans, J. Andrews, and K. Tinsley, "Statistics of co-channel interference in a field of poisson and poisson-poisson clustered interferers," *IEEE Transactions on Signal Processing*, vol. 58, no. 12, pp. 6207–6222, Dec 2010.

[26] A. Nasri, R. Schober, and L. Lampe, "Performance of bicm-ofdm systems in uwb interference," *IEEE Trans. on Wireless Commun.*, vol. 8, no. 9, pp. 4386–4392, Sept. 2009.

[27] C. Snow, L. Lampe, and R. Schober, "Performance analysis and enhancement of multi-band ofdm for uwb communications," *IEEE Trans. on Wireless Commun.*, vol. 6, no. 6, pp. 2182 –2192, june 2007.

[28] X. Cheng and Y. L. Guan, "Narrow-band interference suppression in impulse radio ultra-wideband systems," *IEEE Trans. on Vehicular Tech.*, 2013.

[29] N. Beaulieu and D. Young, "Designing time-hopping ultrawide bandwidth receivers for multiuser interference environments," *Proceedings of the IEEE*, vol. 97, no. 2, pp. 255–284, 2009.

[30] N. Beaulieu and B. Hu, "A soft-limititng receiver structure for time-hopping UWB in multiple access interference," *in Proc. IEEE ISSSTA*, pp. 417–421, 2006.

[31] N. Beaulieu, S. Hua, and J. Fiorina, "P-order metric UWB receiver structures with superior performance," *IEEE Trans. on Commun.*, vol. 56, no. 10, pp. 1666 –1676, oct. 2008.

[32] E. Ghannudi and et al., "α-stable interference modeling and cauchy receiver for an ir-uwb ad hoc network," *IEEE Trans. on Commun.*, vol. 58, no. 6, pp. 1748 –1757, june 2010.

[33] A. Mehbodniya and S. Aissa, "Outage and ber analysis for ultrawideband-based wpan in nakagami- fading channels," *IEEE Trans. on Vehicular Technology*, vol. 60, no. 7, pp. 3515–3520, 2011.

[34] M. Ghosh, "Analysis of the effect of impulse noise on multicarrier and single casrrier qam systems," *IEEE Transactions on Commun.*, vol. 44, pp. 145–147, Feb 1996.

[35] T. Erseghe, V. Cellini, and G. Dona, "On uwb impulse radio receivers derived by modeling mai as a gaussian mixture process," *IEEE Trans. on Wireless Commun.*, vol. 7, no. 6, pp. 2388 –2396, june 2008.

[36] D. Middleton, "Statistical-physical models of electromagnetic interference," *IEEE Transactions on Electromagnetic Compatibility*, vol. EMC-19, no. 3, pp. 106–127, Aug 1977.

[37] D. I. Kim, "Near-optimal and suboptimal receivers for multiuser UWB impulse radio systems in multipath," *IEEE Trans. on Commun.*, vol. 57, no. 10, pp. 3001 –3011, october 2009.

[38] N. Beaulieu and S. Niranjayan, "UWB receiver designs based on a gaussian-laplacian noise-plus-MAI model," *IEEE Trans. on Commun.*, vol. 58, no. 3, pp. 997 – 1006, March 2010.

[39] R. Gonzalo, *Nonlinear Signal Processing: A Statistical Approach.* John Wiley & Sons, 2005.

[40] N. Beaulieu and B. Hu, "Soft-limiting receiver structures for time-hopping uwb in multiple-access interference," *IEEE Transactions on Vehicular Technology*, vol. 57, no. 2, pp. 810–818, March 2008.

[41] S. Wang, Y. Chen, M. Leeson, and N. Beaulieu, "New receivers for generalized uwb transmitted reference systems with improved performances," *IEEE Transactions on Wireless Communications*, vol. 9, no. 6, pp. 1837–1842, June 2010.

[42] H. Shao and N. Beaulieu, "A novel zonal uwb receiver with superior performance," *IEEE Transactions on Communications,*, vol. 57, no. 4, pp. 1197–1206, April 2009.

[43] A. Nasri, R. Schober, and L. Lampe, "Robust l_p-norm decoding for bicm-based secondary user systems," *IEEE Trans. on Communication*, vol. 58, no. 11, pp. 3084–3090, Nov. 2010.

[44] M. Nassar, K. Gulati, M. DeYoung, B. L. Evans, and K. Tinsley, "Mitigating near-field interference in laptop embedded wireless transceivers," *Journal of Signal Proc. Sys.*, p. 1Ű12, 2009.

[45] G. Caire, T. Al-Naffouri, and A. Narayanan, "Impulse noise cancellation in ofdm: an application of compressed sensing," in *in Procc of the IEEE International Symposium on Information Theory*, July 2008, pp. 1293–1297.

[46] J. Lin, M. Nassar, and B. Evans, "Impulsive noise mitigation in powerline communications using sparse bayesian learning," *IEEE Journal on Selected Areas in Communications*, vol. 31, no. 7, pp. 1172–1183, July 2013.

[47] L. Lampe, "Bursty impulse noise detection by compressed sensing," in *International Symposium on Power Line Communications and Its Applications*, April 2011, pp. 29–34.

[48] S. V. Zhidkov, "Impulsive noise suppression in ofdm based communication systems," *IEEE Trans. Consum. Electron.*, vol. 49, pp. 944–948, Nov. 2003.

[49] S. Zhidkov, "Analysis and comparison of several impulsive noise mitigation for ofdm receivers," *IEEE Transactions on Communications*, vol. 56, no. 1, pp. 5–9, Jan 2008.

[50] S. V. Zhidkov, "Performance analysis and optimization of ofdm receiver with blanking nonlinearity in impulsive noise environment," *IEEE Trans. on Vehicular Technology*, vol. 55, no. 1, pp. 234–242, Jan 2006.

[51] A. Molisch, M. Toeltsch, and S. Vermani, "Iterative methods for cancellation of intercarrier interference in ofdm systems," *IEEE Transactions on Vehicular Technology*, vol. 56, no. 4, pp. 2158–2167, July 2007.

[52] E. Alian and P. Mitran, "Improved active interference cancellation for sidelobe suppression in cognitive ofdm systems," in *Proc. IEEE Global Telecomm. Conf. (GLOBECOM)*, 2012, pp. 1460–1465.

[53] E. Alian, H. Saffar, and P. Mitran, "Cross-band interference reduction trade-offs in siso and miso ofdm-based cognitive radios," *IEEE Transactions on Wireless Communications*, vol. 11, no. 7, pp. 2436–2445, 2012.

[54] F. Sarabchi and C. Nerguizian, "Spectrum sharing technique for cognitive uwb systems over indoor uwb channel," in *Proc. IEEE Radio and Wireless Symposium (RWS)*, 2012, pp. 403–406.

[55] J.-M. Wu, T.-F. Yang, and H.-J. Chou, "Mimo active interference alignment for underlay cognitive radio," in *Proc. IEEE Intl. Conf. Comm. (ICC)*, 2010, pp. 1–5.

[56] F. Sarabchi and C. Nerguizian, "Interference cancellation technique for mimo mb-ofdm uwb cognitive radio," in *Wireless and Mobile Communications (ICWMC), 2010 6th International Conference on*, 2010, pp. 472–477.

[57] S.-G. Huang and C.-H. Hwang, "Improvement of active interference cancellation: avoidance technique for ofdm cognitive radio." *IEEE Transactions on Wireless Communications*, vol. 8, no. 12, pp. 5928–5937, 2009.

[58] G. H. Golub and C. F. V. Loan, *Matrix Computations*, 4th ed. The Johns Hopkins University Press, 2012.

[59] Y. Wang and J. Coon, "Active interference cancellation for systems with antenna selection," in *Proc. IEEE Intl. Conf. Comm. (ICC)*, 2008, pp. 3785–3789.

[60] M. Sandell and J. P. Coon, "Performance of combined bulk and per-tone antenna selection precoding in coded ofdm systems." *IEEE Transactions on Communications*, vol. 60, no. 3, pp. 655–660, 2012.

[61] B. Clerckx and C. Oestges, *MIMO Wireless Networks: Channels, Techniques and Standards for Multi-Antenna, Multi-User and Multi-Cell Systems*, 2nd ed. Academic Press, 2013.

[62] A. Saleh and R. Valenzuela, "A statistical model for indoor multipath propagation," *IEEE Journal on Selected Areas in Commun.*, vol. 5, no. 2, pp. 128 –137, Feb. 1987.

[63] P. Pagani, *Ultra-Wideband Radio Propagation Channels*. John Wiley & Sons, 2008.

[64] Y. Xiao and Y. Pan, *Emerging Wireless LANs, Wireless PANs, and Wireless MANs: IEEE 802.11, IEEE 802.15, 802.16 Wireless Standard Family*, 1st ed. Wiley Publishing, 2009.

[65] J. Fiorina and W. Hachem, "On the asymptotic distribution of the correlation receiver output for time-hopped uwb signals," *IEEE Trans. on Signal Processing*, vol. 54, no. 7, pp. 2529 –2545, july 2006.

[66] S. M. Key, *Fundamentals of Statistical Signal Processing, Volume II.* NJ Prentice Hall, 1998.

[67] M. K. Varanasi and B. Aazhang, "Parametric generalized gaussian density estimation," *J. Acoust. Soc. Amer.*, vol. 86, no. 4, pp. 1404–1415, Oct. 1989.

[68] J. Dennis and R. Schnabel, *Numerical Methods for Unconstrained Optimization and Nonlinear Equations (Classics in Applied Mathematics, 16).* Soc for Industrial & Applied Math, 1996.

[69] L. DeCarlo, "On the meaning and use of kurtosis," *Psychological Methods*, vol. 2, no. 3, pp. 292–307, june 1997.

[70] S. Niranjayan and N. Beaulieu, "The BER optimal linear rake receiver for signal detection in symmetric alpha-stable noise," *IEEE Trans. Commun.*, vol. 57, no. 12, pp. 3585–3588, Dec. 2009.

[71] M. Win, P. Pinto, and L. Shepp, "A mathematical theory of network interference and its applications," *Proc. IEEE*, vol. 97, no. 2, pp. 205–230, Feb. 2009.

[72] I. Koutrovelis, "Regression-type estimation of the parameters of stable laws," *Journal of the American Statistical Association*, vol. 75, pp. 918–928, 1980.

[73] M. Novey, T. Adali, and A. Roy, "A complex generalized gaussian distribution-characterization, generation, and estimation," *IEEE Trans. on Signal Processing*, vol. 58, no. 3, pp. 1427 –1433, March 2010.

[74] R. Weron, "On the chambers-mallows-stuck method for simulating skewed stable random variables„" *Statistics and Probability Letters*, vol. 28, pp. 165171„ March 1996.

[75] A. F. Molisch and et. al., "A comprehensive standardized model for ultrawideband propagation channels," *IEEE Trans. on Antennas and Propagation*, vol. 54, no. 11, pp. 3151 – 3166, Nov. 2006.

[76] E. Biglieri, C. Caire, G. Taricco, and J. Ventura-Traveset, "Computing error probabilities over fading channels: A unified approach„" *European Trans. on Telecom.*, vol. 19, pp. 15–23, Jan./Feb. 1998.

[77] G. Taricco and E. Biglieri, "Exact pairwise error probability of space-time codes," *IEEE Trans, on Information Theory*, vol. 48, no. 2, pp. 510–513, Feb 2002.

[78] G. E. Biglieri, Caire, G. Taricco, and J. Ventura-Traveset, "Simple method for evaluating error probabilities," *Electronics Letters*, vol. 32, no. 3, pp. 191–192, Feb 1996.

[79] ECMA, "Standard ECMA-368: High Rate Ultra Wideband PHY and MAC standard," 2005. [Online]. Available: http://www.ecma-international.org/publications/standards/Ecma-368.htm

[80] M. Zimmermann and K. Dostert, "Analysis and modeling of impulsive noise in broadband powerline communications," *IEEE Transactions on Electromagnetic Compatibility,*, vol. 44, no. 1, pp. 249–258, Feb 2002.

[81] M. Mirahmadi, A. Al-Dweik, and A. Shami, "Ber reduction of ofdm based broadband communication systems over multipath channels with impulsive noise," *IEEE Transactions on Communications*, vol. 61, no. 11, pp. 4602–4615, Nov. 2013.

[82] D.-F. Tseng, Y. Han, W. H. Mow, L.-C. Chang, and A. Vinck, "Robust clipping for ofdm transmissions over memoryless impulsive noise channels," *IEEE Communications Letters*, vol. 16, no. 7, pp. 1110–1113, July 2012.

[83] C.-H. Yih, "Iterative interference cancellation for ofdm signals with blanking nonlinearity in impulsive noise channels," *IEEE Signal Processing Letters*, vol. 19, no. 3, pp. 147–150, March 2012.

[84] F. Sarabchi and C. Nerguizian, "Impulsive noise mitigation for ofdm-based systems using enhanced blanking nonlinearity," in *Proc. of IEEE International Symposium on Personal, Indoor and Mobile Radio Communications (PIMRC)*, Sep. 2014.

[85] A. del Coso, U. Spagnolini, and C. Ibars, "Cooperative distributed mimo channels in wireless sensor networks," *IEEE Journal on Selected Areas in Communications*, vol. 25, no. 2, pp. 402–414, February 2007.

Appendix A

NOISE AND ICI VARIANCES CALCULATION

In order to find the variance of noise and ICI terms, let us consider the output of the channel equalizer as follows

$$Y(k) = \frac{|\theta|}{N}X_k + \frac{H_k^{-1}}{N}\sum_{\substack{m=0\\m\neq k}}^{N-1} X_m \sum_{n\in\Theta}^{N-1} e^{j\frac{2\pi n}{N}(m-k)} + \frac{H_k^{-1}}{\sqrt{N}}\sum_{n\in\Theta} z_n e^{-j2\pi\frac{nk}{N}} \tag{A.1}$$

Therefore, the variance of the noise term including the AWGN and remained interference is obtained by

$$\sigma_{\hat{Z}}^2 = E\Big\{\Big|\frac{H_k^{-1}}{\sqrt{N}}\sum_{n\in\Theta} z_n e^{-j2\pi\frac{nk}{N}}\Big|^2\Big\} \tag{A.2}$$

$$= \frac{|\theta|}{N}\frac{(\sigma_w^2+\sigma_i^2)}{H_k^2} \tag{A.3}$$

where σ_w^2 and σ_i^2 denote AWGN and the portion of the interference passed through blanking nonlinearity. Before calculating the variance of the ICI, given that N_B subcarriers from α to β are blanked, the expression of $\sum_{n\in\Theta} e^{\omega nN(k-m)}$, $\omega = \frac{j2\pi}{N}$ is obtained as

$$\sum_{n\in\Theta}^{N-1} e^{\omega n(m-k)} = \underbrace{\sum_{n=0}^{\alpha-1} e^{\omega nN(m-k)}}_{I} + \underbrace{\sum_{n=\beta+1}^{N-1} e^{\omega n(m-k)}}_{II} \tag{A.4}$$

Using geometric series properties and Euler's formula I and II are given by

$$\begin{aligned} I &= \frac{1-e^{\omega(m-k)\alpha}}{1-e^{\omega(m-k)}} \\ &= \frac{e^{-j\pi(m-k)\alpha/N} - e^{j\pi(m-k)\alpha/N}}{e^{-j\pi(m-k)/N} - e^{j\pi(m-k)/N}}\frac{e^{j\pi(m-k)\alpha}}{e^{j\pi(m-k)}} \\ &= \underbrace{\frac{\sin(\pi(m-k)\alpha/N)}{\sin(\pi(m-k)/N)}}_{A(m,k)} e^{j\pi(\alpha-1)(m-k)/N} \end{aligned} \tag{A.5}$$

$$
\begin{aligned}
II &= \frac{e^{\omega(m-k)(\beta+1)} - e^{\omega(m-k)N}}{1-e^{\omega(m-k)}} \\
&= \frac{e^{j\pi(m-k)(\beta+1)/N} - e^{-j\pi(m-k)(\beta+1)/N}}{e^{-j\pi(m-k)/N} - e^{j\pi(m-k)/N}} \frac{e^{j\pi(m-k)(\beta+1)}}{e^{j\pi(m-k)}} \\
&= \underbrace{\frac{\sin(\pi(k-m)(\beta+1)/N)}{\sin(\pi(m-k)/N)}}_{B(m,k)} e^{j\pi\beta(m-k)/N}
\end{aligned} \tag{A.6}
$$

Then, the variance of the ICI is given by

$$
\begin{aligned}
\sigma^2_{ICI} &= E\left\{ \left| \frac{H_k^{-1}}{N} \sum_{\substack{m=0 \\ m\neq k}}^{N-1} H_m X_m \sum_{n\in\Theta} e^{\omega nN(k-m)} \right|^2 \right\} \\
&= E\left\{ \left| \frac{H_k^{-1}}{N} \sum_{\substack{m=0 \\ m\neq k}}^{N-1} H_m X_m \Big[A(m,k) e^{j\pi(\alpha-1)(m-k)/N} + B(m,k) e^{j\pi\beta(m-k)/N} \Big] \right|^2 \right\} \\
&= \frac{|H_k^{-1}|^2}{N^2} E\left\{ \sum_{\substack{m=0 \\ m\neq k}}^{N-1} \sum_{\substack{l=0 \\ l\neq k}}^{N-1} H_m H_l^* X_m X_l^* \Big[A(m,k) e^{j\pi(\alpha-1)(m-k)/N} + B(m,k) e^{j\pi\beta(m-k)/N} \Big] \right. \\
&\qquad \left. \Big[A(m,l) e^{-j\pi(\alpha-1)(m-l)/N} + B(m,l) e^{-j\pi\beta(m-l)/N} \Big] \right\}
\end{aligned} \tag{A.7}
$$

According to i.i.d behaviour of the transmitted samples X_i, and after some tedious but rather straightforward manipulations, (A.7) can be simplified as

$$
\begin{aligned}
\sigma^2_{ICI} &= \frac{|H_k^{-1}|^2 \sigma_X^2}{N^2} \sum_{\substack{m=0 \\ m\neq k}}^{N-1} H_m^2 \Big[A(m,k)^2 + B(m,k)^2 \\
&\qquad + A(m,k)B(m,k) \Big(e^{j\pi(\alpha-\beta-1)(m-k)/N} + e^{-j\pi(\alpha-\beta-1)(m-k)/N} \Big) \Big] \\
&= \frac{|H_k^{-1}|^2 \sigma_X^2}{N^2} \sum_{\substack{m=0 \\ m\neq k}}^{N-1} |H_m|^2 \Big[A(m,k)^2 + B(m,k)^2 \\
&\qquad + 2A(m,k)B(m,k) \cos(\pi(\alpha-\beta-1)(m-k)/N) \Big] \\
&= \frac{|H_k^{-1}|^2 \sigma_X^2}{N^2} \sum_{\substack{m=0 \\ m\neq k}}^{N-1} |H_m|^2 \Big[\cos^2(\Omega_{m,k}(\alpha-\beta-1)) \\
&\qquad - 2\cos(\Omega_{m,k}(\alpha+\beta+1)) \cos(\Omega_{m,k}(\alpha-\beta-1)) + 1 \Big] \times \sin^{-2}(\Omega_{m,k})
\end{aligned} \tag{A.8}
$$

where $\Omega_{m,k} = \frac{\pi}{N}(m-k)$.